

REVIEW

Dynamical phase transitions in the collisionless pre-thermal states of isolated quantum systems: theory and experiments

To cite this article: Jamir Marino *et al* 2022 *Rep. Prog. Phys.* **85** 116001

View the [article online](#) for updates and enhancements.

You may also like

- [Nonequilibrium magnetic features in a mixed spin \(2, 5/2\) Ising system driven by the external oscillating magnetic field by path probability method](#)
Mustafa Gençaslan and Mustafa Keskin
- [Thermalization and prethermalization in isolated quantum systems: a theoretical overview](#)
Takashi Mori, Tatsuhiko N Ikeda, Eriko Kaminishi *et al.*
- [Coupled activity-current fluctuations in open quantum systems under strong symmetries](#)
D Manzano, M A Martínez-García and P I Hurtado



IOP | ebooks™

Bringing together innovative digital publishing with leading authors from the global scientific community.

Start exploring the collection—download the first chapter of every title for free.

Review

Dynamical phase transitions in the collisionless pre-thermal states of isolated quantum systems: theory and experiments

Jamir Marino^{1,*}, Martin Eckstein², Matthew S Foster^{3,4}
and Ana Maria Rey^{5,6}

¹ Institut für Physik, Johannes Gutenberg-Universität Mainz, D-55099 Mainz, Germany

² Department of Physics, University of Erlangen-Nürnberg, 91058 Erlangen, Germany

³ Department of Physics and Astronomy, Rice University, Houston, TX 77005, United States of America

⁴ Rice Center for Quantum Materials, Rice University, Houston, TX 77005, United States of America

⁵ JILA, National Institute of Standards and Technology, and Department of Physics,
University of Colorado, Boulder, CO 80309, United States of America

⁶ Center for Theory of Quantum Matter, University of Colorado, Boulder, CO 80309, United States of
America

E-mail: jamarino@uni-mainz.de

Received 11 February 2022, revised 26 July 2022

Accepted for publication 8 September 2022

Published 19 October 2022



CrossMark

Abstract

We overview the concept of dynamical phase transitions (DPTs) in isolated quantum systems quenched out of equilibrium. We focus on non-equilibrium transitions characterized by an order parameter, which features qualitatively distinct temporal behavior on the two sides of a certain dynamical critical point. DPTs are currently mostly understood as long-lived prethermal phenomena in a regime where inelastic collisions are incapable to thermalize the system. The latter enables the dynamics to sustain phases that explicitly break detailed balance and therefore cannot be encompassed by traditional thermodynamics. Our presentation covers both cold atoms as well as condensed matter systems. We revisit a broad plethora of platforms exhibiting pre-thermal DPTs, which become theoretically tractable in a certain limit, such as for a large number of particles, large number of order parameter components, or large spatial dimension. The systems we explore include, among others, quantum magnets with collective interactions, ϕ^4 quantum field theories, and Fermi–Hubbard models. A section dedicated to experimental explorations of DPTs in condensed matter and AMO systems connects this large variety of theoretical models.

Keywords: dynamical phase transitions, collisionless pre-thermal states, isolated quantum systems

(Some figures may appear in colour only in the online journal)

* Author to whom any correspondence should be addressed.
Corresponding editor: Dr Hui Zhai.

Contents

1. Introduction	2
2. Dynamical phase transitions and the Landau–Ginzburg paradigm	3
2.1. Fully-connected Ising model in transverse field	4
2.2. Long-range interactions	6
2.3. $O(\mathcal{N})$ models in the large \mathcal{N} limit	6
3. Exactly solved dynamics in Richardson–Gaudin models via the Lax spectral method	8
3.1. BCS superfluids and Richardson–Gaudin	9
3.2. The Lax spectral method	10
3.2.1. Isolated roots and phases I, II, III	10
3.3. A simple example	11
3.3.1. Phases I and II	11
3.3.2. Quench-generated Floquet phase III	13
3.4. Fluctuation phenomena	14
3.5. Topological features	14
4. Dynamical phase transitions in infinite dimensions	16
4.1. The Hubbard model in infinite dimensions	16
4.2. DPTs related to non-thermal symmetry breaking	17
4.3. DPTs between pre-thermal phases at short-time	19
5. Experimental observation	20
5.1. DPTs in condensed matter systems	20
5.2. DPTs in cold atom experiments	22
6. Conclusions and perspectives	26
Acknowledgments	26
Data availability statement	26
References	26

1. Introduction

Dynamical phase transitions occur whenever the observables of an isolated quantum system feature distinct qualitative temporal behavior as a function of a control parameter measuring the deviation of the system from equilibrium. In this review, we are interested in a particular class of dynamical phase transitions (DPTs) which are characterized by an order parameter that features non-analytic behavior at the non-equilibrium critical point separating distinct dynamical phases [1]. The DPTs we discuss here manifest during the so called pre-thermal stage of dynamics of a quantum many body system [2–4]. The notion of pre-thermalization is broad, encompassing high energy physics and condensed matter. A system is said to pre-thermalize when its observables approach a long-lived quasi-steady state at intermediate times, before inelastic collisions

set in and the system reaches thermodynamic equilibrium. In this regard, the behavior of the order parameter witnessing the DPT will manifest after a transient where non-universal effects attributed to microscopic details of the model, such as lattice properties or short-time inhomogeneous dephasing, have faded away.

Pre-thermalization is mostly studied in the context of small interaction quenches that can result in a long, perturbative, window of the dynamics where the quasi-particles of some pre-quench integrable model are weakly deformed and still free to scatter elastically [5–11]. Interactions renormalise the energy of these excitations, and only at later times they induce inelastic processes responsible for the redistribution of energy and for the eventual equilibration. Accordingly, we will refer to pre-thermalization as a *collisionless regime*, which is a shorthand to describe that inelastic collisions are still weak and ineffective. From a formal standpoint, this is equivalent to the vanishing of the collisional integral which governs the scattering of excitations in a Boltzmann equation picture. This can manifest over a long time window because the system remains close to an integrable point after an interaction quench, or because the phase space for scattering is compressed in low dimensions, or for a certain choice of initial conditions. After such pre-thermal transient the collisional integral will start to grow sizeably, dragging dynamics toward the thermal state. Although a general criterion for such collisionless prethermal regime is lacking, there are various ways to effectively attain such regime in a large- N limit. Essentially all the models for DPTs which have been systematically studied so far fall in this class, and they constitute the core of this review.

In order to access DPTs, one routinely performs quenches in Hamiltonian parameters. In the recent years this has become accessible in AMO experiments and to some extent also in condensed matter experiments. To date, the main focus has been on DPTs that take place in some limit such that interactions can still be treated non-perturbatively at the expense of solving dynamics which are mean-field like, Gaussian or semi-classical. The study of DPTs in this regime is the central topic of this review. We will revisit a broad plethora of systems exhibiting collisionless behavior within a long lived pre-thermal window, enabled by taking a large intrinsic parameter in the system such as the number of particles (N)—in sections 2.1 or 3.2, and the number of components of a field (\mathcal{N})—in section 2.3. Further, some aspects of DPTs beyond the collisionless regime can be studied in a controlled manner in the limit of infinite dimensions, which is reviewed in section 4.

The focus on a non-equilibrium order parameter, which characterizes the DPT, distinguishes the subject of this review from the notion of dynamical transitions explored in the context of Loschmidt echoes [12–14]. We will also not review the broad topic of non-thermal fixed points in cold atoms [15–19] (see [20] for a review), which although appear akin to a pre-thermal phenomenon, exhibits a different mechanism from the large N , \mathcal{N} , or d pre-thermal states discussed in this review.

Regarding experimental observation, broadly speaking, non-equilibrium dynamical phases are observed in much wider contexts than their equilibrium counterparts. They are relevant for a variety of disciplines beyond AMO and condensed matter physics, including chemistry, biology and even sociology [21]. For example, non-equilibrium critical phenomena have been seen in polymers, colloidal gels, molecular glasses and spin glasses as they are cooled down below a critical temperature, ‘glassy transition point’, at which the system’s evolution slows down so much that it falls out of equilibrium [1]. The mass distribution of the Universe might also be the result of non-equilibrium critical behavior during the Universe formation [22]. Basically just after the ‘Big Bang’ the Universe expands and cools precipitating a sequence of symmetry-breaking phase transitions, the last of which converts quark–gluon plasma into nucleons. These transitions are believed to be genuinely non-equilibrium given the finite time of propagation of information between spatial regions and the extremely slow equilibration time at criticality. Lasers also show dynamical transitions, where the light emitted by an array of atoms changes abruptly from incoherent to extremely coherent when the input power (the control parameter in this case) exceeds a certain threshold [21].

The emergence of spontaneous synchronization in coupled oscillators is also an iconic example of dynamical phase transitions where, depending on the strength of the nonlinear interactions among the oscillators, their amplitude or phases (or both) can get locked throughout the whole system or a part of it [23]. Another example is liquid layers, where the heat transport changes from conduction to convection when the temperature-gradient between the lower and the upper surfaces of the liquid is increased above a critical point [24]. Finally, different dynamical phases occur in the population dynamics or ecology when two interacting ‘kinds’ of species, the predator and the prey, start to feature a perpetual cyclic pattern when the food supply for one species is maintained at or beyond a certain limit [25]. Similar behavior is seen in chemical reactions where a chemical instability triggers oscillatory patterns in which the color of the reactants changes periodically from red to blue and vice versa [26]. Also in cellular biology, for example, it is believed that the normal-to-cancer transition is a dynamical non-equilibrium phenomenon, which depends on both metabolic energy supply and local physiological conditions [27].

Although it is clear that in any of these situations the concepts of temperature, and thermal equilibrium, do not have a clear meaning, all of them share the fact that the familiar notion of the order parameter, introduced by Landau for a description of second order phase transitions, can be used to describe the distinct change of behavior of the system as an external control parameter is varied. This is profitable since it allows one to treat disparate systems at a macroscopic level with similar concepts and mathematical tools, and allows us to make fascinating analogies between them by invoking the concept of universality.

Nevertheless, a key point shared by all the systems described in the above paragraph is that they belong to the realm of non-equilibrium open systems, and therefore

their dynamics are fundamentally irreversible [21]. A more restricted scenario, which is the one discussed in this review, deals with evolution under fully unitary, coherent and reversible dynamics. Under this context experimental observations of non-equilibrium phase transitions have remained more elusive. Only in the recent years have new opportunities in many-body physics been opened up thanks to the increased degree of control and ability to synthesize, manipulate, and detect ultra cold atomic systems as well as new developments in THz pump–probe experiments. The novel experimental capabilities are stimulating new methods to benchmark and understand DPTs in general, and they are leading to exciting investigations of non-equilibrium behaviors.

The review is structured as follows. In sections 2.1 and 3.2 we present the dynamics of exactly solvable fully-connected spin models in the limit of large number of spins, $N \rightarrow \infty$. The associated DPTs include the Ising universality class and Richardson–Gaudin magnets. In section 2.2 we discuss different dynamical behaviors associated with interactions which are not all-to-all, but decay spatially in a power law fashion. In section 2.3, we consider the limit of a large number of components (\mathcal{N}) of a ϕ^4 field theory. This serves as an instructive toy model to show how Gaussian fluctuations can modify the physical picture of sections 2.1 and 3.2. In section 4 we consider DPTs arising in strongly correlated systems in the large dimensionality limit $d \rightarrow \infty$, where an exact solution is possible within dynamical mean field theory (DMFT); interestingly the model studied in this limit exhibits ergodic behavior and eventually thermalizes, allowing one to inspect aspects of DPTs beyond pre-thermalization. Emphasis is placed on the similarities between the DPTs observed in this class of models and those discussed in section 2.1. Finally, section 5 discusses the experimental platforms where DPTs have been observed from solid state to cold atoms. This section serves as a further connection between the other three theory sections.

2. Dynamical phase transitions and the Landau–Ginzburg paradigm

The Landau–Ginzburg description of thermal equilibrium phase transitions is one of the cornerstones of criticality and universality [28] in a vast plethora of systems [29] including soft matter (e.g. liquid–gas critical points), condensed matter (e.g. magnets, superfluidity, and superconductivity), as well as applications to cosmology [30]. Together with a systematic inclusion of thermal or quantum fluctuations via a renormalization group analysis, Landau–Ginzburg theory lays the foundations of critical phenomena in equilibrium statistical mechanics [31–33]. Given its success in explaining equilibrium [34] and relaxational dynamics of classical [35] and open quantum systems [36–38], it was not surprising to witness in the last decade a surge of works exploring dynamical phase transitions after a quench, which can be understood via an effective ϕ^4 -field theory description. Our review will therefore start considering those DPTs which possess an effective description in terms of a double well picture of the energy landscape of the underlying physical model.

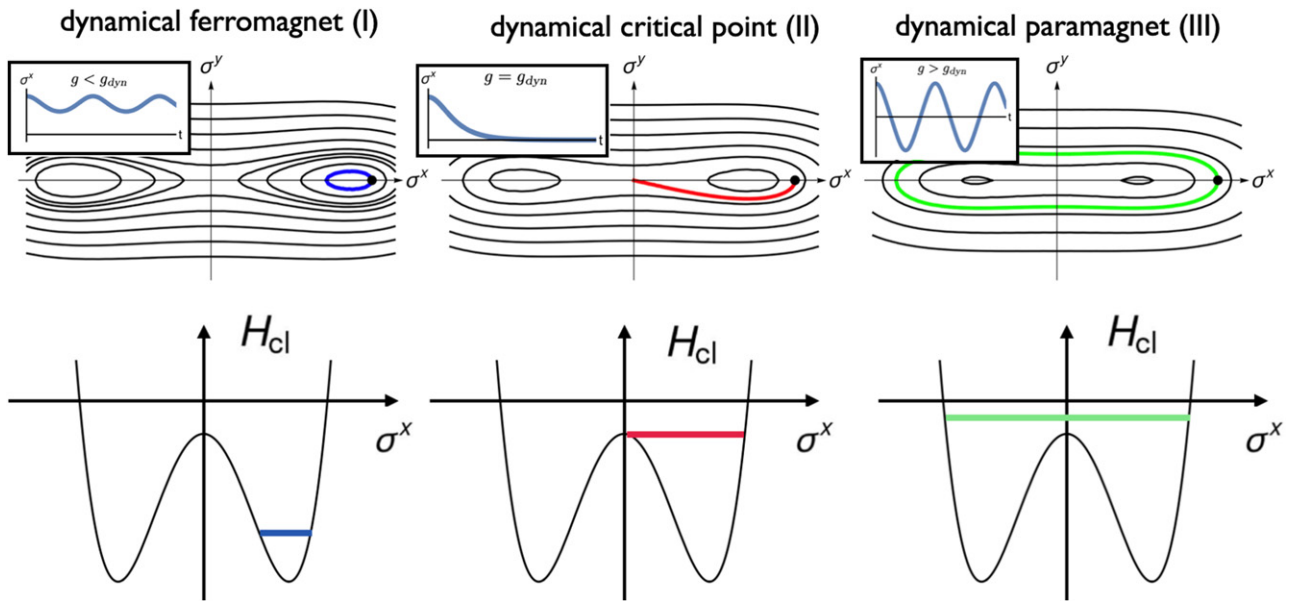


Figure 1. Upper row: quantum quench of the transverse field in the LMG model: dynamical ferromagnetism (I) with oscillations around a non-vanishing value of σ^x ; critical relaxation (II) at the dynamical critical point; dynamical paramagnetism (III) with persistent oscillations around a zero mean value. Lower row: energy H_{cl} of the collective classical spin configuration, $\vec{\sigma}$, as a function of the magnetization σ^x . For the dynamical ferromagnet the energy of the initial state (cf main text) is not sufficiently large to escape the minima of the potential (blue line); for the paramagnetic phase the energy is above the double-well barrier (green line), and therefore the orbit of the magnetization can encircle both minima and average out to zero over long time windows. The figure is adapted from reference [56].

We will first consider a fully connected spin model (the Lipkin–Meshkov–Glick model [39–51]) which is exactly solvable through a mean-field analysis in the thermodynamic limit (section 2.1). Its dynamical phases can be understood using a double well picture, providing the simplest analytically tractable instance of a dynamical critical point.

In section 2.3, we will then consider the dynamics of a field theory with an \mathcal{N} -component scalar order parameter [31], which in the $\mathcal{N} \rightarrow \infty$ limit admits an exact solution in terms of Gaussian fluctuations self-consistently coupled to the motion of the order parameter. The leading $1/\mathcal{N}$ correction controls non-integrable scattering among different modes and therefore the disappearance of the pre-thermal plateau where the DPT of the field theory can occur. This is analogous to the effect of $1/N$ corrections (where now N is the system size) on the DPTs of LMG and Richardson models discussed in sections 2.1 and 3, and it merges with the unifying theme of this review: DPTs occur in collisionless non-equilibrium states of dynamics [3–5, 7, 30, 52–55]. When collisions due to non-linearities set in, these pre-thermal states are destabilized and the system is attracted towards a thermal fixed point where only equilibrium phase transitions can occur (if permitted by dimensionality and symmetries). A further example of this phenomenology will be provided in section 4, where DPTs are obtained in strongly correlated systems through an exact dynamical mean field treatment valid in the $d \rightarrow \infty$ limit (here d are the physical dimensions).

Despite a unifying framework for DPTs is currently missing, we have decided to introduce the reader to this subject relying first on models endowed with an effective description in terms of a double well potential. This should appear as

familiar to the reader from a conventional equilibrium statistical mechanics perspective. Very broadly speaking, the dynamical phase diagrams discussed in this work share a common structure: upon increasing the value of the post quench coupling, the system can transit from a dynamically ‘disordered’ to a dynamically ordered phase. The fact that this constitutes only a bona fide description of the onset of DPTs in the models reviewed in this work, reflects that a solid categorization of DPTs remains an open outstanding question. This is aggravated by the lack of a sufficiently abundant statistics of numerically or analytically tractable models in the thermodynamic limit, as it will become clear in the next sections.

2.1. Fully-connected Ising model in transverse field

In this section, we consider a class of quantum Ising systems with spins s on a d -dimensional lattice, interacting via a ferromagnetic coupling, $J_{|r-r'|}$, and subject to a transverse magnetic field pointing along the z direction

$$H = -\sum_{r,r'} J_{|r-r'|} \hat{\sigma}_r^x \hat{\sigma}_{r'}^x - g \sum_r \hat{\sigma}_r^z. \quad (1)$$

Here the sums run over $r = 1, 2, \dots, N$, with N the total system size. In equation (1), $\hat{\sigma}_r^\alpha$ are the operators corresponding to the normalized spin components in the $\alpha = x, y, z$ direction. For concreteness we consider in the following the $s = 1/2$ case, although most of the results remain qualitatively unchanged for arbitrary spin length s . The parameter g is the Larmor frequency induced by the transverse field. This class of systems is of importance for experimental realizations of DPTs in trapped ions [57], cavity QED systems [58], and neutral atoms arrays [59], as we discuss in section 5.

For all-to-all interactions $J_{|\mathbf{r}-\mathbf{r}'|} = \lambda/N$, for all \mathbf{r}, \mathbf{r}' , the Hamiltonian in equation (1) corresponds to the infinite-range or fully-connected Lipkin–Meshkov–Glick (LMG) model [39–51]

$$\hat{H} = -\frac{\lambda}{N} \sum_{i,j=1}^N \hat{\sigma}_i^x \hat{\sigma}_j^x - g \sum_{i=1}^N \hat{\sigma}_i^z, \quad (2)$$

where each of the N spins interacts with all the others with the same ferromagnetic coupling strength $\propto \lambda$. The $1/N$ scaling of the coupling λ in equation (2) is adopted to make the energy extensive in the thermodynamic limit (notice that this scaling is not always satisfied in experimental implementations, e.g. cavity QED systems, see section 5). As $N \rightarrow \infty$ the mean-field approximation becomes exact for the Hamiltonian (2), and therefore the model is solvable in the thermodynamic limit: the properly normalized commutation relations of these collective spin operators, $\hat{\sigma}^\alpha \equiv \sum_{i=1}^N \hat{\sigma}_i^\alpha / N$, approach the classical limit for $N \rightarrow \infty$. In fact, these operators have a spectrum in $[-1, 1]$ and they satisfy

$$[\hat{\sigma}^\alpha, \hat{\sigma}^\beta] = \frac{1}{Ns} i \epsilon^{\alpha\beta\gamma} \hat{\sigma}^\gamma, \quad (3)$$

which can be used to define an effective Planck's constant $\hbar_{\text{eff}} \equiv (N/2)^{-1}$. This property is instrumental to investigate the corrections to the $N \rightarrow \infty$ limit via a semi-classical expansion in inverse powers of N . Such corrections include [56] wavepacket spreading with deviations from the classical trajectory on Ehrenfest time scales $\propto \mathcal{O}(\sqrt{N})$, recurrences on times $\sim \mathcal{O}(N)$ and tunnelling events between the two ferromagnetic minima on time scales $\propto \mathcal{O}(e^{cN})$.

From equation (3), it results that, for $N \rightarrow \infty$, the model can be exactly solved in terms of a classical, continuous spin $\vec{\sigma}$ of normalized length ρ , by neglecting the above mentioned finite N effects which require exact diagonalization or a semi-classical approximation to be observed [60]. The three-dimensional vector $\vec{\sigma} = \rho(\sin \theta \cos \varphi, \sin \theta \sin \varphi, \cos \theta)$ is a classical spin whose phase space is the surface of a Bloch sphere of radius $0 < \rho \leq 1$, with polar, θ , and azimuth angles, φ . The LMG model then reduces to the classical Hamiltonian

$$\mathcal{H}_{\text{cl}}(\vec{\sigma}) = -\lambda(\sigma^x)^2 - g\sigma^z = -\lambda\rho^2 \sin^2 \theta \cos^2 \varphi - g\rho \cos \theta. \quad (4)$$

For ferromagnetic interactions the system exhibits an equilibrium zero-temperature phase transition from a paramagnetic ground state with $\langle \hat{\sigma}^x \rangle = 0$ for $g > g_{\text{cr}} \equiv 2\lambda$, to a pair of ferromagnetic ground states with $\langle \hat{\sigma}^x \rangle_{\pm} = \pm m \neq 0$ for $g < g_{\text{cr}}$, characterized by the spontaneous breaking of the \mathbb{Z}_2 -symmetry. These two ferromagnetic minima can be derived from the Bloch sphere representation of equation (4) and they are given by $(\theta^*, \varphi = 0)$ and $(\theta^*, \varphi = \pi)$ with $\cos \theta^* = g/g_{\text{cr}}$. Accordingly, the value of the order parameter is $\sigma^x = \pm \rho \sin \theta^* = \pm \rho \sqrt{1 - (g/g_{\text{cr}})^2}$, where we have kept ρ fixed since the total spin length of the system is conserved.

The associated classical energy landscape of the collective spin $\vec{\sigma}$ (along the plane $\sigma^y = 0$) is portrayed in figure 1 as a function of the magnetization σ^x for the ferromagnetic phase $g < g_{\text{cr}} = 2\lambda\rho$. At equilibrium and in the thermodynamic limit, the degenerate ground state wave-functions of

the collective spin are localized at the two classical minima respectively, and $\vec{\sigma}$ behaves like a classical particle at rest at the bottom of one of the two wells.

DPTs in the LMG model have been studied extensively in the last decades [61–68]. We now overview the dynamical phase diagram summarized in figure 1, primarily following reference [56] for the sake of concreteness. The non-equilibrium evolution of $\langle \vec{\sigma}_i(t) \rangle$ is given by the classical equations of motion associated to the Hamiltonian in equation (4), $\dot{\sigma}^\alpha = \{\sigma^\alpha, \mathcal{H}_{\text{cl}}\}$, where the evolution is given in terms of Poisson brackets.

We prepare the spin chain in a ferromagnetic ground state of the Hamiltonian equation (4) with transverse field $g_0 < g_{\text{cr}} = 2\lambda\rho$. This choice of initial state is instrumental to illustrate the archetypal features of the dynamical phase diagram, and it corresponds to a quantum quench of the transverse field g . We prepare the spin chain in the ground state of the Hamiltonian $H(g_0)$ at $t = 0$, and then abruptly vary the transverse field up to the value g so that the evolution at times $t > 0$ would occur under the Hamiltonian $H(g)$.

For a quench, $H(g_0) \rightarrow H(g)$, with $g < g_{\text{dyn}} \equiv (g_0 + g_{\text{cr}})/2$, the energy of the system remains below the barrier that separates the two ferromagnetic sectors. Indeed, the value of g_{dyn} can be determined [64–69] by equating the energy of the initial state with the height of energy ‘hill’ separating the two minima in figure 1. Correspondingly, the spin will precess within the starting ferromagnetic sector (trajectory I in figure 1). As the strength of the quench increases, the precession period increases, until for $g \rightarrow g_{\text{dyn}}$ it takes an infinite time to complete one cycle, and the unstable point at the top of the energy barrier is approached exponentially (trajectory II in figure 1). For deep quenches above this threshold, $g > g_{\text{dyn}}$, the energy of the system is larger than the energy barrier separating the two minima of the double well. The orbit of the collective spin encircles both minima, such that the symmetry is restored after taking time-averages, and the average magnetization, $\overline{\sigma^x}$, vanishes (trajectory III in figure 1). Indeed, the time-average

$$\overline{\sigma^x} = \lim_{T \rightarrow \infty} \frac{1}{T} \int_0^T dt \sigma^x(t), \quad (5)$$

as a function of the post quench value, acts as a dynamical order parameter, and it vanishes abruptly at the dynamical critical value g_{dyn} .

This dynamical critical point therefore separates a *dynamical ferromagnetic phase* with $\overline{\sigma^x} \neq 0$ from a *dynamical paramagnetic phase* with $\overline{\sigma^x} = 0$. The singularity of the equilibrium order parameter upon approaching the critical point is algebraic, $\overline{\sigma^x} \sim (g_{\text{dyn}} - g)^\beta$, with critical exponent $\beta = 1/2$; in contrast, the non-equilibrium order parameter $\overline{\sigma^x}$ discussed here displays a logarithmic singularity at the dynamical critical point.

Similar dynamical mean-field pictures hold also for infinite dimensional Bose–Hubbard systems [64], Jaynes–Cummings Hamiltonians [64], or for the evolution of classical ϕ^4 -field theories [70, 71] (see also the following section 2.3). The DPTs occurring in these models can be all explained with a classical cartoon for their energy landscape after a quench, as done here for the LMG model. In section 2.3, we review a model where

the effects of Gaussian fluctuations on top of the evolution of a classical order parameter are instead crucial to characterize the onset of the DPT.

2.2. Long-range interactions

DPTs beyond the exact mean-field behavior of the LMG model can also be inspected by considering long-range couplings $J_{|\mathbf{r}-\mathbf{r}'|} \propto |\mathbf{r}-\mathbf{r}'|^{-\alpha}$ in equation (1) (see references [72, 73]). For $\alpha \leq 3$, the model describes, for instance, trapped ions simulators (cf section 5 for experimental observations of the DPT in a chain of trapped ions with $0.8 \lesssim \alpha \lesssim 1$). The resulting non-equilibrium phase diagram can be derived using a MPS time-dependent variational principle [74]. Equipped with long-range interactions, the quantum spin model in equation (1) interpolates from the LMG limit ($\alpha = 0$) to the short-range Ising model in transverse field ($\alpha \rightarrow \infty$), and it therefore offers a precious angle to analyze the interplay of dimensionality and interactions range in the formation of a dynamical critical point [75–81] (see also section 4 in this regard). In particular, the authors of reference [72] have considered dynamics in one dimension starting from a fully polarized state along the \hat{x} -direction, unveiling a DPT for all values of $\alpha \leq 2$. This critical value of α is the same for supporting a thermal phase transition in equilibrium long-range interacting spin chains [48, 82–84]. An important difference with the LMG case is that the model is now not integrable neither can its dynamics be mapped to classical equations of motion. As a consequence, the order parameter decays because of inhomogeneous dephasing [85–87] towards a vanishing or non-vanishing expectation value depending on the dynamical phase (paramagnetic or ferromagnetic), rather than exhibiting long-lived orbits as in the LMG model. This is a generic feature expected for quantum many-body systems whose dynamics cannot be simply described with the motion of a collective mode. The model will behave as effectively short-ranged for $\alpha > 2$ (see for instance [48, 82–84]) and it will not sustain order away from the ground state [88], with the result that the order parameter will vanish, in the long time limit, regardless of the post quench value of g .

Furthermore, for $\alpha < 1$, the order parameter acquires again the persistent oscillatory behavior if the thermodynamic limit is taken before the long-time asymptotics. This is again explained by recalling that long-range Ising models with $\alpha < 1$ fall into the universality class of the LMG model [48, 82–84]. It is therefore in the window $1 < \alpha < 2$ that a genuine quantum many body dynamical transition is observed. Upon changing the dimensionality, these two thresholds are expected to change with the qualitative picture remaining unaltered.

Interestingly, dynamical transitions monitored by the cusps of the Loschmidt echo occur at any α (cf reference [72]), showing that these two notions of dynamical criticality describe qualitatively different physics.

This section finds its natural experimental counterpart in section 5 where realizations of DPTs in long-range interacting systems are discussed in detail.

2.3. $O(\mathcal{N})$ models in the large \mathcal{N} limit

In this section we discuss a prototypical example illustrating the richness of non-equilibrium phase transitions of isolated systems beyond mean-field. The model we review allows for an exact treatment of quantum fluctuations. It is furthermore iconic as it deals with the quantum dynamics of a Landau–Ginzburg theory, and it might therefore offer a prototypical model for DPTs in more complex non-integrable quantum many-body systems. We consider a \mathcal{N} -component bosonic order parameter $\hat{\Phi} = (\hat{\phi}_1, \hat{\phi}_2, \dots, \hat{\phi}_{\mathcal{N}})$ in d spatial dimensions, with an $O(\mathcal{N})$ -invariant Hamiltonian [31]

$$\hat{H}(r, u) = \int d^d \mathbf{x} \left[\frac{1}{2} \hat{\Pi}^2 + \frac{1}{2} (c \nabla \hat{\phi})^2 + \frac{r}{2} \hat{\phi}^2 + \frac{u}{4! \mathcal{N}} (\hat{\phi}^2)^2 \right], \quad (6)$$

where $\hat{\Pi} = \partial_t \hat{\Phi}$ is the \mathcal{N} -component momentum canonically conjugated to $\hat{\Phi}$, and r and u parametrise respectively the mass term and the strength of the non-linearity (for quantum quenches of fermionic variants of this model in the context of DPTs, see references [89, 90]). The requirement of invariance under rotations of the $O(\mathcal{N})$ group is the reason for the appearance of scalar products only, $\hat{\Pi}^2$ and $\hat{\phi}^2 = \hat{\Phi} \cdot \hat{\Phi} = \sum_{i=1}^{\mathcal{N}} \hat{\phi}_i^2$, in the Hamiltonian (6). The field theory in equation (6) is customarily taken as an effective continuum description of a microscopic model [88] (with spin, fermionic or bosonic degrees of freedom) and it therefore requires an ultraviolet momentum cutoff Λ , which is usually the inverse of the lattice spacing. Upon varying \mathcal{N} , equation (6) describes the Ising ($\mathcal{N} = 1$) and Heisenberg ($\mathcal{N} = 3$) models, or the Bose–Hubbard at the particle-hole symmetric point ($\mathcal{N} = 2$), to mention a few examples [88].

The success in modeling dynamical phase transitions with the field theory (6) resides in a closure at the Gaussian level of its hierarchy of equations of motion. Specifically, at $\mathcal{N} \rightarrow \infty$ the evolution of the state of the $O(\mathcal{N})$ model is fully characterized by the dynamics of the two point functions self-consistently coupled to the evolution of $\langle \hat{\Phi} \rangle$, with higher order correlation functions parametrically suppressed in powers of $1/\mathcal{N}$. The large- \mathcal{N} limit has allowed the extrapolation of several qualitative features of the equilibrium thermal phase diagram of the $O(\mathcal{N})$ model to finite values of \mathcal{N} and d (see [31, 88]). Specifically, in the limit $\mathcal{N} \rightarrow \infty$, quartic interactions in equation (6) decouple at leading order, which amounts to the formal substitution $(\hat{\phi}^2)^2 \sim \langle \hat{\phi}^2 \rangle \hat{\phi}^2$. In field theoretical language this corresponds to a Hartree–Fock approximation [91, 92]. Here, we have used the fact that, if the $O(\mathcal{N})$ symmetry of the initial state is not broken, the average $\langle \hat{\phi}_a \hat{\phi}_b \rangle$ of two generic components of $\hat{\Phi}$ vanishes unless $a = b$. Its non-vanishing value is independent of a and equal to the fluctuation $\langle \hat{\phi}^2 \rangle$ of a generic component of the field. In diagrammatic language, the large- \mathcal{N} limit amounts to retaining only tadpole corrections to r and ‘candy’ (RPA) diagram corrections to u [93]. The dynamics of the field components are therefore equivalent to a time-dependent quadratic Hamiltonian with an effective mass, $r_{\text{eff}}(t)$, to be self-consistently determined from the expectation value of $\langle \hat{\phi}^2 \rangle$ (see equation (7) below). The model becomes then exactly solvable via a time-dependent self-consistent Gaussian ansatz. The large- \mathcal{N} expansion allowed

the authors of references [70, 91, 92, 94–98] to disregard thermalizing collisions that are effective at times parametrically large in \mathcal{N}/u^2 , and which dictate equilibration. DPTs emerge in such a collisionless pre-thermal regime [3, 4, 30, 99] (cf with section 2), as we will also emphasize later in section 3.

The typical quench protocol used to probe the dynamical phase diagram of this model consists in preparing the system in the ground state of the non-interacting Hamiltonian $\hat{H}(r_0, 0)$, and then letting the dynamics evolve with $\hat{H}(r, u)$ at later times. Exact solvability in the $\mathcal{N} \rightarrow \infty$ limit allows us to elucidate the role of fluctuations in the formation of the dynamical critical point. The time-dependent effective mass, $r_{\text{eff}}(t)$, dressed by Gaussian fluctuations reads

$$r_{\text{eff}}(t) = r + \frac{\mathcal{N} + 2}{6\mathcal{N}} u \int \frac{d^d p}{(2\pi)^d} \langle \hat{\phi}_{\mathbf{p}}(t) \hat{\phi}_{-\mathbf{p}}(t) \rangle \quad (7)$$

with $\hat{\phi}_{\mathbf{p}}$ the Fourier transform of the field. The right-hand side of equation (7) reaches a steady state value as a result of inhomogeneous dephasing of the oscillating factors with frequencies depending on the momenta \mathbf{p} in the integrand. When the post-quench value of the mass r is tuned to a critical value $r_c(r_0, u)$ such that it cancels the contribution from the fluctuations integral in (7), the stationary value of the effective mass $r^* \equiv r_{\text{eff}}(t \rightarrow \infty)$ vanishes and, consequently, the spatial correlation length $\xi = (r^*)^{-1/2}$ diverges, thus signalling the onset of a dynamical critical point. Following reference [96], we can evaluate the behaviour of the effective asymptotic mass r^* for small deviations in the post-quench value, δr , from the dynamical critical point r_c , finding

$$r^* = \delta r - \frac{u}{24} r^* \int_0^\Lambda \frac{p^{d-3} dp (p^2 + r_0)^{1/2}}{(2\pi)^d (p^2 + r^*)}, \quad (8)$$

with Λ the ultraviolet momentum cutoff, typically related to inverse lattice spacing of the microscopic model from which the field theory is derived. For $d > 4$ the integral in equation (8), which encodes the role of fluctuations, converges upon tuning $r^* \rightarrow 0$ (close to criticality). For $2 < d < 4$ the integral is instead the leading term, implying the scaling $r^* \sim (\delta r)^{2/(d-2)}$. This yields a correlation length $1/\xi^* \sim \sqrt{r^*}$, with a static critical exponent $\nu = 1/(d-2)$. For $d \geq 4$ we find the mean field exponent $\nu = 1/2$ since, as we just discussed, fluctuations are RG irrelevant. This upper and lower critical dimension for the DPT of the $O(\mathcal{N} \rightarrow \infty)$ model are the same for thermal equilibrium phase transitions [88, 99]. Although equations (7) and (8) are structurally analogous to equilibrium thermal transitions, the fluctuation corrections to the bare mass are quantitatively different, resulting in a different location for the critical point in the thermal and non-equilibrium cases.

In order to explore the nature of the different dynamical phases, we assume the system is prepared with a given initial mass, r_0 , and consider different post quench values of r . We will focus in the following on the asymptotic $t \rightarrow \infty$ value of the effective mass, r^* , on its real-time scaling features and on momentum-resolved correlation functions. Figure 2 provides a graphical summary of the three dynamical phases and of their

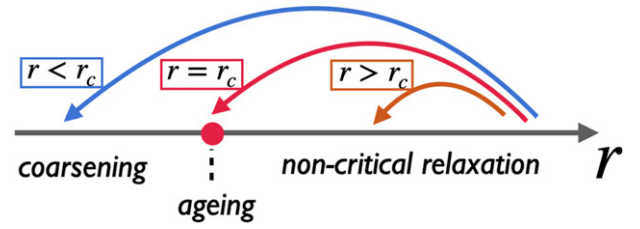


Figure 2. Sketch of the dynamical phases of the $O(\mathcal{N} \rightarrow \infty)$ model resulting from a quench with large initial mass ($r_0 \gg \Lambda^2$). The system is quenched above ($r > r_c$), at ($r = r_c$), or below ($r < r_c$) the dynamical critical point; in the latter case dynamics display ageing. This dynamical critical point separates non-critical relaxation (a dynamically disordered phase) from coarsening (a dynamically ordered phase).

properties. We will be primarily following reference [92] in our exposition.

(i) For $r > r_c(r_0, u)$, the system undergoes a non-critical relaxation characterized by a finite value of the correlation length and correlation time, and by a vanishing value of the order parameter. This is the *dynamically disordered phase*. The symmetric correlation function $C_{\mathbf{p}}(t, t') = -i \langle \{ \hat{\phi}_{\mathbf{p}}(t), \hat{\phi}_{-\mathbf{p}}(t') \} \rangle$ displays oscillations with asymptotic period set by $\sim (r^*)^{-1/2}$.

(ii) For quenches to the *critical point*, $r \rightarrow r_c(r_0, u)$, slow modes are characterized by ageing dynamics, where the symmetric correlation function acquires the scaling form $C_{\mathbf{p}}(t, t') \propto (t/t')^\theta$ for $t \gg t'$ and $p \rightarrow 0$, with a non-equilibrium universal exponent $\theta = d/4$ in $2 < d < 4$ (see references [92, 100]). This is the analog of the ageing exponent occurring in non-equilibrium classical systems quenched close to critical temperature [101, 102]; in contrast, in the case discussed here, the system acts as its own bath because it is isolated from the environment. The phenomenon is called ageing because the characteristic relaxation time-scale is the age of the system itself, i.e. the time, t , elapsed after the quench. As in its classical counterpart, ageing denotes a dynamical regime where correlation functions break time-translational invariance in a universal fashion [97]. Indeed, the exponent θ does not depend on microscopic details, rather it is dictated by dimensionality, symmetries and conservation laws, as in conventional theory of critical phenomena. Remarkably, the value of the exponent θ cannot be related to the equilibrium ones ν, η, z , etc. The absence of a gap and therefore of a characteristic timescale at criticality, implies that each mode has a typical relaxation time scale of order $\sim 1/p$. Therefore the ageing window is expected to extend for each mode within $1/\Lambda \lesssim t \lesssim 1/p$, and for well separated times $t \ll t'$. For $t \lesssim 1/\Lambda$, non-universal effects due to the microscopic details of the model will set in.

Concerning the steady state forming after deep quenches $r_0 \gg \Lambda^2$, the infrared modes equilibrate at the effective temperature $T_{\text{eff}} \simeq \sqrt{r_0}$. Notice however that this does not imply that the system has thermalized to a Gibbs state [91]; on the contrary, higher momenta have occupations that violate equipartition of energy. The fact that in the presence of a finite energy density low momenta modes effectively thermalize, while higher momentum tails do not satisfy detailed balance, is

a general feature of non-equilibrium phase transitions, present also in driven-open systems [38].

For small initial masses $r_0 \ll \Lambda^2$, the system undergoes a dynamical crossover around a time scale $\sim 1/r_0$, from a regime where dynamical scaling is characterized by a ‘quantum’ ageing exponent θ' into a regime ruled by the effectively thermal exponent θ we have just discussed. This additional ageing exponent θ' corresponds to an unstable pre-thermal fixed point [103] whose canonical scaling properties are akin to a zero-temperature quantum critical point (the lower and upper critical dimensions are the same in the equilibrium and non-equilibrium case, $1 < d < 3$).

(iii) Finally, for $r \leq r_c(r_0, u)$, the time-dependent effective mass decays with a universal $\sim 1/t^2$ behaviour on long time scales, as it also happens for quenches at the dynamical critical point (below the upper critical dimension $d < 4$). For $d \geq 4$, this decay turns into $\sim t^{-(d-2)}$, which can be predicted from dimensional analysis. However, in this regime with $r < r_c(c_0, r_0, u)$, the system exhibits coarsening [91, 92, 95], and correlation functions are characterized by a form of dynamical scaling distinct from the ageing typical of the critical point. Coarsening is caused by the formation of growing domains with different values of the order parameter, similarly to the phenomenon of spinodal decomposition [104]. It occurs for quenches starting from a symmetric ground state, $r_0 > r_c$. Physically, one expects that the system globally remains in a symmetric state with vanishing order parameter, however, the symmetry can be broken within spatial domains which appear separated by walls. Within each of them, the order parameter, $\hat{\phi}$, acquires the value of one of the two different Z_2 -symmetry broken phases [104–106]. The average linear extension of the ordered domains increases with time, until a specific domain possibly prevails over the others, establishing the equilibrium state. However, the size of domains grows algebraically and actual equilibrium is reached only asymptotically. This lack of an intrinsic length scale in the system affects the equal-time two-point correlation functions which scale as $C_{p=0}(t, t) \sim t^\gamma$ with $\gamma = d - 1$.

We finally remark that the dynamical phases of the $O(\mathcal{N} \rightarrow \infty)$ model remain qualitatively unaltered [107] when the value of the mass is continuously ramped at a sufficiently fast speed from r_0 to r , rather than suddenly quenched between the same two values. More precisely, when the duration of the ramp is finite, the critical properties associated to the dynamical transition are qualitatively the same as in the sudden quench scenario, whereas if the ramp is infinitely slow the equilibrium quantum phase transition at zero temperature is eventually recovered.

3. Exactly solved dynamics in Richardson–Gaudin models via the Lax spectral method

In this section, we review a class of all-to-all interacting spin exchange models of the Richardson type (equations (12) and (16)) whose evolution under a quantum quench is solved exactly by a version of self-consistent mean field theory [108]. The solution reveals different dynamical phases of an order parameter, which can decay to zero (‘phase I’) [109, 110],

assume a non-equilibrium steady-state value (‘phase II’) [111], or even exhibit persistent oscillations (‘phase III’, a *self-generated* Floquet phase [109]). Although these dynamical phases of matter may carry some resemblance to those resulting from quenches of LMG-type models (cf section 2.1 above), this section aims at emphasising their markedly different origin that results from the classical and quantum integrability of Richardson magnets.

The order parameter for this class of models can be defined via

$$\Delta \equiv -G \sum_i s_i^- . \quad (9)$$

This is an equal-weight sum of spin-1/2 lowering operators in an N -spin system. It plays the role of the BCS pairing gap in applications to quenched superfluids and superconductors (see below).

Figure 3 shows the quench phase diagram for a system exhibiting phases I, II, and III. In this figure, ground-state order-parameter values for the pre- (Δ_i) and post-quench (Δ_f) Hamiltonian label the vertical and horizontal axes, so that any point in the phase diagram away from the diagonal line is a quench. In this particular system (a quenched $p + ip$ superfluid), the ground state exhibits a topological transition at a certain value of the order parameter $\Delta_i = \Delta_f = \Delta_{\text{QCP}}$. This extends to a line in the quench phase diagram, separating nonequilibrium phases characterized by different winding numbers W .

The models described in this section can be realized in a collisionless (prethermalization) regime for a range of physical systems, as will be discussed in section 5, including

- Far-from equilibrium dynamics in solid-state superconductors, following excitation by an intense subgap (terahertz) pulse [116–122],
- Quenches in central-spin type problems (Gaudin magnets), or synthetic spin-1/2 magnets with infinite-range interactions realized in ultracold fermionic atoms in a trap [123] and cavity QED systems [124],
- Ultracold fermionic superfluids, with different pairing symmetries (such as s -wave or p -wave) where a quench corresponds (e.g.) to a change in the strength of the attractive interactions responsible for pairing, as could be accomplished by tuning a Feshbach resonance [109–112, 125–127]. The approach has been extended to multicomponent superconductors with competing orders [128].
- Quenches in topological superfluids, such as a chiral $p + ip$ system that can host circulating Majorana edge modes [112, 113, 129].

All of these systems can be approximately described by a Hamiltonian of Richardson–Gaudin type [130–132], which is both classically and quantum mechanically integrable. Quantum integrability implies that the many-body spectrum can be obtained from the Bethe ansatz [130–138]. Instead, here we focus on the thermodynamic (infinite-system-size) limit, where self-consistent mean field theory can become exact [109, 111, 139, 140]. In this case, the system resides in a pure BCS-type state at all times (with time-dependent coherence factors), and the dynamics of generic observables

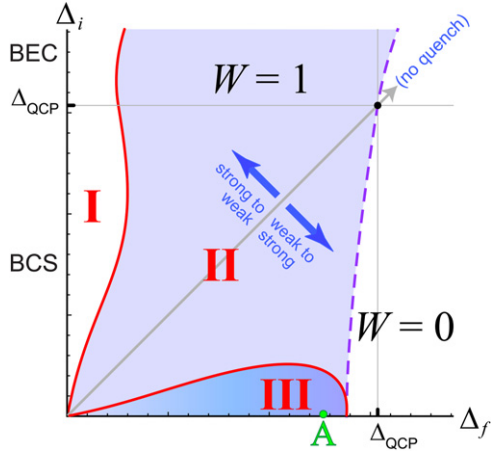


Figure 3. Quench phase diagram for a 2D $p + ip$ fermion superfluid, from references [112, 113]. Here Δ_i (Δ_f) denotes the ground-state BCS order parameter in the pre- (post-)quench Hamiltonian. Any point with $\Delta_i \neq \Delta_f$ corresponds to a quench, while the line $\Delta_i = \Delta_f$ denotes the ground state. Δ_i (Δ_f) is associated to an attractive BCS pairing interaction strength G_i (G_f), assumed to change instantaneously at the time of the quench. The subsequent dynamics of $\Delta(t)$ fall into three different phases I, II, III, described in the text. The phase boundaries are indicated by the heavy red lines; shading instead indicates *topologically nontrivial* dynamical phases. Phase III is a self-generated Floquet phase, which in the case of a $p + ip$ superfluid exhibits topological edge states; dynamics for the quench marked ‘A’ are shown in figure 4. In this figure, $W = 1$ ($W = 0$) indicates topological (trivial) domains of phase II. The region with $W = 1$ hosts Majorana edge states, even for quenches that start from the trivial BEC phase ($\Delta_i > \Delta_{\text{QCP}}$). Δ_{QCP} denotes the ground-state topological quantum phase transition between BCS and BEC phases [114, 115]; the dashed purple line is its nonequilibrium extension.

(Green’s functions) can be computed exactly by exploiting the *classical integrability*.

The integrable models discussed here neglect nonzero center-of-mass momentum for excited Cooper pairs, as well as dissipative processes. Cooper pairs with finite momentum are not expected to play a role in quench dynamics of the collisionless prethermalization regime, for a sample size that is smaller than or of order the superconducting coherence length [141, 142]. Dissipative processes are responsible for thermalization on time scales longer than the collisionless prethermalization plateau captured by the integrable model. The extent to which integrable dynamics can be observed is sensitive to the details of the experimental realization, and is predicted to be different for ultracold superfluids, THz-pumped superconductors, and synthetic atomic-spin model realizations. See sections 3.4, 5.1, and 5.2 for discussions of these various platforms. The solid-state THz experiment [116] exhibited in figure 9 shows an example where quench dynamics have been successfully realized.

This section is organized as follows. First, we will describe how the Richardson–Gaudin spin model emerges from the description of a BCS superfluid. We will then illustrate how the dynamical phase diagram can be obtained using the ‘Lax spectral method’ [111, 112, 125, 139, 140], which exploits the classical integrability and the simplifications that occur

in the thermodynamic limit. For a particularly simple class of initial conditions (different from the usual assumption of a BCS-ground initial state), we show explicitly how the solution method works, giving the dynamical phases I, II, III described above, and we will outline how to compute generic observables. Section 3.4 gives an overview of fluctuation phenomena beyond the scope of mean-field dynamics, including quenches from an initial normal Fermi liquid state [141, 143–149]. Finally, we summarize a few key features of quench-induced dynamical topological phase transitions [112, 113, 129].

We limit the overview in this section to the idealized, thermodynamic limit for integrable Richardson–Gaudin models. Time and length scales for observing this physics in ultracold Fermi gases and THz-driven superconductors are discussed later in section 5.1.

3.1. BCS superfluids and Richardson–Gaudin

Consider a spin-1/2 Fermi gas in d spatial dimensions, with local, attractive interactions. The Hamiltonian is

$$\begin{aligned}
 H &= \sum_{\sigma \in \uparrow, \downarrow} \int d^d \mathbf{r} c_{\sigma}^{\dagger}(\mathbf{r}) \left(-\frac{1}{2m} \nabla^2 \right) c_{\sigma}(\mathbf{r}) \\
 &\quad - G \int d^d \mathbf{r} c_{\uparrow}^{\dagger}(\mathbf{r}) c_{\downarrow}^{\dagger}(\mathbf{r}) c_{\downarrow}(\mathbf{r}) c_{\uparrow}(\mathbf{r}) \\
 &= \sum_{\mathbf{k}, \sigma} \varepsilon_{\mathbf{k}} c_{\mathbf{k}\sigma}^{\dagger} c_{\mathbf{k}\sigma} - G \sum_{\mathbf{k}, \mathbf{k}', \mathbf{q}} c_{\mathbf{k}+\frac{\mathbf{q}}{2}}^{\dagger} c_{-\mathbf{k}+\frac{\mathbf{q}}{2}}^{\dagger} c_{-\mathbf{k}'-\frac{\mathbf{q}}{2}} c_{\mathbf{k}'-\frac{\mathbf{q}}{2}},
 \end{aligned} \tag{10}$$

where the second equality expresses the Hamiltonian in terms of momentum modes in a finite volume. Here $\varepsilon_{\mathbf{k}} = k^2/2m$ is the kinetic energy, and $G > 0$ denotes a local, spin-singlet pairing interaction strength. The fermion creation and annihilation operators satisfy canonical anticommutation relations, $c_{\mathbf{k}\sigma} c_{\mathbf{k}'\sigma'}^{\dagger} + c_{\mathbf{k}'\sigma'}^{\dagger} c_{\mathbf{k}\sigma} = \delta_{\mathbf{k}, \mathbf{k}'} \delta_{\sigma, \sigma'}$, where $\sigma, \sigma' \in \{\uparrow, \downarrow\}$ label the spin.

Inspired by the solution to the Cooper problem that gives a minimal bound-state energy for a two-electron pair with zero center-of-mass momentum, we drop interaction terms in equation (10) with nonzero \mathbf{q} . The resulting ‘reduced BCS Hamiltonian’ [153] can be expressed in terms of Anderson pseudospins [154]

$$\begin{aligned}
 S_{\mathbf{k}}^{+} &\equiv c_{\mathbf{k}\uparrow}^{\dagger} c_{-\mathbf{k}\downarrow}^{\dagger}, \\
 S_{\mathbf{k}}^{-} &\equiv c_{-\mathbf{k}\downarrow} c_{\mathbf{k}\uparrow}, \\
 S_{\mathbf{k}}^z &\equiv \frac{1}{2} (n_{\mathbf{k}\uparrow} + n_{-\mathbf{k}\downarrow} - 1),
 \end{aligned} \tag{11}$$

where $n_{\mathbf{k}\sigma} \equiv c_{\mathbf{k}\sigma}^{\dagger} c_{\mathbf{k}\sigma}$. Simplifying notation by labeling single-particle levels with $i, j \in \{1, \dots, N\}$ instead of momenta, the reduced s -wave BCS Hamiltonian is

$$H = \sum_{i=1}^N 2\varepsilon_i S_i^z - G \sum_{i,j=1}^N S_i^{+} S_j^{-}. \tag{12}$$

This ‘Richardson’ Hamiltonian [130, 131] is similar to the Dicke model, which features all-to-all coupling of the in-plane

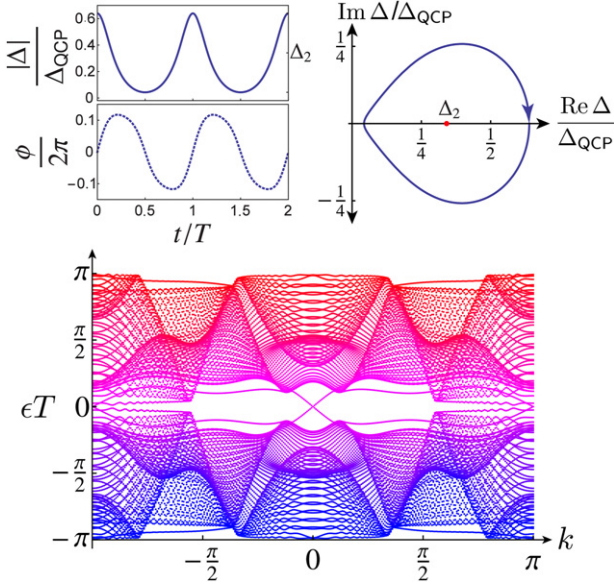


Figure 4. Self-generated Floquet phase III for a sufficiently large weak-to-strong quench in the model described in figure 3 [113, 129]. A Floquet phase is a dynamical state of matter characterized by parameters that oscillate periodically in time [150]. Floquet systems can exhibit topological features [114, 151] such as protected edge states at the sample boundary, even when the undriven system is topologically trivial [152]. The top left shows the periodic (but strongly anharmonic) amplitude and phase of the order parameter $\Delta(t)$, while the top right depicts its orbit in the complex plane. On the bottom, diagonalization of a lattice-regularized strip shows Floquet-Majorana edge states (crossing in the center gap) for this particular quench, marked ‘A’ in figure 3. Majorana edge modes will appear only in a fermionic superfluid or superconductor with a physical boundary. Constraints on observing phase III in quenched superfluids are discussed in section 3.4.

spin components, but here each spin is subject to a potentially different Zeeman field $2\varepsilon_i$. The all-to-all coupling is a necessary, but not sufficient condition for integrability [145]; integrable variants can describe p -wave and other pairings [133–138].

Using the SU(2) algebra of the pseudospins, the Heisenberg equations of motion are

$$\dot{\vec{S}}_i = \vec{S}_i \times \vec{B}(\varepsilon_i), \quad (13a)$$

$$\vec{B}(\varepsilon_i) \equiv -2\varepsilon_i \hat{z} - \Delta(\hat{x} + i\hat{y}) - \Delta^*(\hat{x} - i\hat{y}), \quad (13b)$$

where the BCS order parameter was defined in equation (9).

In the thermodynamic limit $N \rightarrow \infty$, the expectation of Δ in an initial BCS pure state becomes a classical observable (Ehrenfest’s theorem). Then, $\langle \vec{S}(t) \rangle \equiv \vec{s}(t)$ satisfies the equation of motion for a classical spin in an external field. The usual BCS ground-state equation [153] obtains by aligning each spin to its own magnetic field [154]. The total particle number is encoded in the conserved $S^z \equiv \sum_i s_i^z$; its value can be fixed by adding this to the field \vec{B} with a chemical potential.

3.2. The Lax spectral method

3.2.1. Isolated roots and phases I, II, III. The Lax spectral method [111, 112, 125, 139, 140] simplifies the dynamics

for the classical spins generated by the BCS Hamiltonian in equation (12). The idea is that the all-to-all coupling in this model leads to a reduction of the collective dynamics, such that the time evolution of $\Delta(t)$ can be determined by solving an emergent few-spin problem. This can be understood as a sort of exact renormalization group: the effective few-spin problem is governed by a ‘Lax reduced’ Hamiltonian of precisely the same form as equation (12), but with $M < N$ spins and renormalized parameters. The parameters of the reduced model can be determined from the N -spin quench via the integrability. Specifically, these obtain from the roots of a certain spectral polynomial, defined below.

Here, we detail the Lax construction for the s -wave Hamiltonian in equation (12) [111, 125, 139, 140]. A similar construction for a $p + ip$ superconductor can be found in [112]. See references [132–138] for the general classification of Richardson–Gaudin models.

We define the Lax vector and its norm,

$$\vec{L}(u) \equiv \sum_{i=1}^N \frac{\vec{s}_i}{u - \varepsilon_i} - \frac{\hat{z}}{G}, \quad L_2(u) \equiv \vec{L} \cdot \vec{L}(u), \quad (14)$$

where u is an arbitrary parameter. The spins can be taken to satisfy classical Poisson brackets $\{s_i^a, s_j^b\} = \delta_{ij} \epsilon^{abc} s_i^c$. Then equation (12) implies that the Lax vector satisfies the same equation of motion as the spins,

$$\dot{\vec{L}}(u) = \vec{L}(u) \times \vec{B}(u). \quad (15)$$

The Lax norm is conserved. Moreover, it is easy to check that $\{L_2(u), L_2(v)\} = 0$ for any u, v . Using this fact and the explicit expression for the Lax norm, one can identify a set of N independent conserved quantities. These are Hamiltonians of central-spin type (‘Gaudin magnets’),

$$H_i \equiv \vec{s}_i \cdot \left[-\frac{\hat{z}}{G} + \sum_{j \neq i} \frac{\vec{s}_j}{\varepsilon_i - \varepsilon_j} \right], \quad \{H_i, H_j\} = 0 \quad \forall i, j. \quad (16)$$

Up to an additive constant, the BCS Hamiltonian is the particular combination

$$H = -G \sum_i 2\varepsilon_i H_i + G(S^z)^2. \quad (17)$$

From the conserved Lax norm, we define an order $2N$ spectral polynomial in the parameter u ,

$$Q_{2N}(u) \equiv G^2 \prod_{i=1}^N (u - \varepsilon_i)^2 L_2(u). \quad (18)$$

To see how a small number of degrees of freedom can govern the dynamics, we trade the spins for an alternative set of ‘separation variables’, defined as follows. Equations (14) and (9) imply that

$$L^-(u) \equiv L^x(u) - iL^y(u) = -\frac{\Delta \prod_{\alpha=1}^{N-1}(u - u_\alpha)}{G \prod_{j=1}^N(u - \varepsilon_j)}. \quad (19)$$

The $N - 1$ zeroes of this equation $\{u_\alpha\}$ are complicated functions of the $\{s_i^-\}$, the precise form of which we do not need. By considering the $d/dt[L^-(u(t))]$ for a possibly time-dependent $u(t)$, we can derive the equations of motion for these separation variables [139],

$$\dot{u}_\alpha = 2i \frac{\sqrt{Q_{2N}(u_\alpha)}}{\prod_{\beta \neq \alpha} (u_\alpha - u_\beta)}. \quad (20)$$

The reduction to fewer degrees of freedom is best illustrated by an example. Using the spin configuration that solves the BCS equations in the ground state, one can explicitly show that the spectral polynomial in equation (18) possesses $N - 1$ doubly-degenerate zeroes along the real u -axis. Since $L_2(u) = L^+(u)L^-(u) + [L^z(u)]^2$, any such zero u_0 also satisfies $L^-(u_0) = 0$. In other words, the $N - 1$ separation variables $\{u_\alpha\}$ are static, and confined to the real axis (equation (20)). In addition, $Q_{2N}(u)$ possesses a complex-conjugate pair of zeroes $\{u_1, u_1^*\}$ that encode the BCS ground-state order parameter Δ_0 (which we take to be real). For a particle-hole symmetric ε_i spectrum, one simply finds that $u_1 = i\Delta_0$.

Consider the case of a quench, wherein some initial pure state undergoes evolution according to the BCS Hamiltonian in equation (12). The initial state must be expressible as a configuration of the N pseudospins (a pure BCS state), but is otherwise arbitrary [155]. Feeding this initial spin configuration into the spectral polynomial (using the Lax vector in equation (14)), one can characterize the state of the system in terms of the pattern of zeroes for $Q_{2N}(u)$, which is conserved. For finite N and a generic initial state, one finds N complex conjugate pairs of zeroes. In general, these are *not* roots of $L^-(u)$, implying that all separation variables u_α evolve non-trivially according to equation (20). Despite the integrability of these equations, explicit results are only available for small N in terms of hyperelliptic functions [139, 140].

In the thermodynamic $N \rightarrow \infty$ limit, however, for certain classes of initial conditions the situation simplifies dramatically. In particular, for quenches that evolve an initial weakly paired BCS or strongly paired BEC ground state (characterized by coupling G_i) according to a post-quench Hamiltonian with $G \equiv G_f \neq G_i$, one finds that only three possible dynamical phases appear. These are termed phase I, II, and III, and correspond respectively to zero, one, and two isolated pairs of roots of the spectral polynomial [109–111]. Additional pairs isolated roots are possible for more complicated initial conditions, discussed below. The remaining roots merge into a branch cut along the real axis, and thus correspond to a continuum of ‘frozen’ separation variables. The separation between isolated and remaining roots is illustrated for a finite system in figure 5. The physics of phases I–III are as follows (see also the example phase diagrams in figures 3 and 6.)

- In phase I, there are no isolated roots, and $\Delta(t) \rightarrow 0$ in the long-time limit. This occurs for large strong-to-weak quenches, $G_f \ll G_i$ [110], and corresponds to an effective zero-spin problem. In a superconductor quenched to

phase I, the optical conductivity or Meissner response would appear indistinguishable from a normal metal [121]. Anomalous coherences persist however, encoded in the dephased precession of Anderson pseudospins; schemes for detecting these are discussed in [156, 159], see section 4.2. Phase I could be accessed in a solid-state superconductor subject to a sufficiently strong subgap THz pulse, as illustrated in figures 5 and 6.

- In phase II there is one pair of isolated roots, corresponding to an effective one-spin problem. Phase II describes small quenches, and smoothly connects to the ground-state configuration (no quench). $\Delta(t)$ asymptotes to a nonequilibrium, steady-state value Δ_∞ . For quenches entirely in the weak-pairing BCS regime, the approach to this prethermalized value takes a universal form [111, 160],

$$\Delta(t) \simeq \frac{\alpha}{\sqrt{t}} \cos(2\Delta_\infty t + \phi_0) + \Delta_\infty, \quad (21)$$

for some constants α, ϕ_0 . The value of Δ_∞ is precisely determined by the isolated roots of the spectral polynomial for the $N \rightarrow \infty$ spin system. Decaying oscillations at frequency $2\Delta_\infty$ were observed in the THz pump–probe experiment reference [116], see figure 9 and section 5.1.

- In phase III, there are two pairs of isolated roots, corresponding to an effective two-spin problem. This occurs for sufficiently large weak-to-strong quenches, and connects in a somewhat intricate way to a quench starting from a normal (unpaired) Fermi liquid state [108, 143, 144], (see section 3.4, below). The isolated roots of the spectral polynomial in the thermodynamic limit determine the parameters of this two-spin problem, leading to an effective equation of motion for $\Delta(t)$. The solution can always be expressed in terms of elliptic functions, and thus corresponds to a *quench-generated Floquet phase* [109, 125], as illustrated in figure 4 for a $p + ip$ superfluid quench [112, 113, 129]. Heating is a potential difficulty with driven Floquet systems [150], but the quench-induced phase III dynamics could evade this problem. By contrast, a numerical study of quenches in a nodal d -wave superconductor did not exhibit phase III, which is damped out due to excited gapless quasiparticles [161]. This d -wave reduced BCS model is not of Richardson–Gaudin type, due to the form of the interaction coupling.

3.3. A simple example

3.3.1. Phases I and II. In this subsection, we illustrate the Lax spectral method for the model in equation (12). In order to keep the analysis as simple as possible, instead of a BCS (or BEC) initial Anderson pseudospin configuration, we consider a fully x -polarized initial state [162]. In fact, this initial state was used in a recent ultracold fermionic atoms experiment [123] to probe the phase I to phase II DPT (see section 5).

$$\vec{s}_i = (1/2)\hat{x}, \quad \forall i \in \{1, \dots, N\}. \quad (22)$$

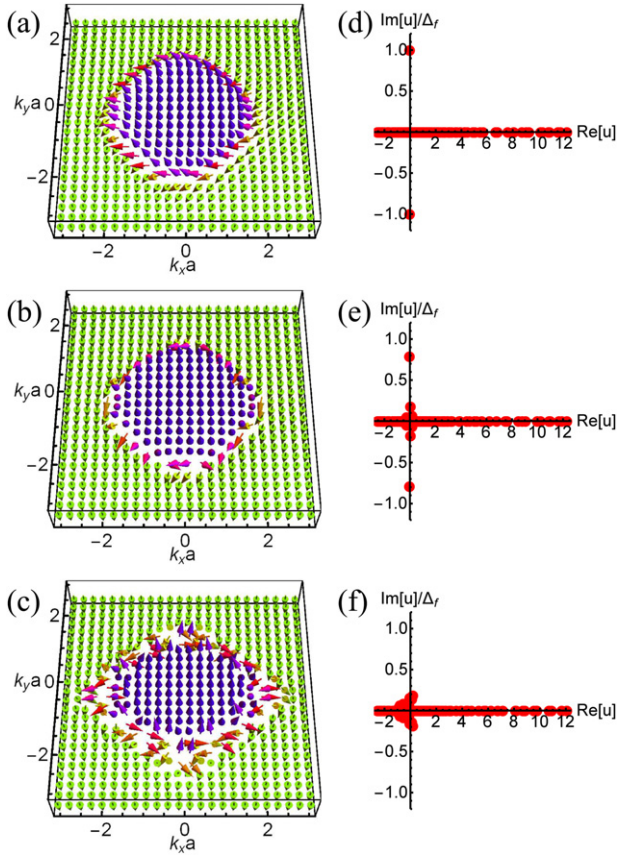


Figure 5. This figure shows the Anderson pseudospin texture for a model 2D s -wave superconductor, following a ‘quench’ induced by a subgap electromagnetic pulse [121], see also references [118–120, 122]. This work was inspired by the results of the experiment by Matsunaga *et al* [116], depicted in figure 9 and reviewed in section 5.1, below. The Anderson pseudospin textures and the Lax roots of the spectral polynomial are depicted immediately after the application of an intense THz pulse. (a)–(c) Are the spin textures after light exposure, corresponding to the roots shown in (d)–(f) respectively. The pair of roots away from the real axis are called isolated roots, and these encode the key properties of the BCS state. The system is a quarter-filled square lattice tight-binding model with 24-by-24 sites (the system is chosen to be small for the purpose of this illustration). Panels (a) and (d) correspond to a very weak pump energy, (b) and (e) to an intermediate pump energy, and (c) and (f) to a strong pump. The isolated roots $u_1^\pm \simeq \pm i\Delta_\infty$ for the deformed spin textures encode the asymptotic value of $\Delta(t \rightarrow \infty) = \Delta_\infty$ in the phase II pre-thermalization plateau. The main effect of the THz field quench is to twist Anderson pseudospins near the Fermi energy in the x - y plane; more intense pulses produce more disordered twist patterns, and push the isolated roots towards the real axis. For strong pulses ((c) and (f)), the isolated roots merge with the real axis and the system enters phase I [109, 110] with $\Delta_\infty = 0$, see figure 6. Phase III cannot be generated by such a single pulse.

The spectral polynomial (equation (18)) is

$$Q_{2N}(u) = \left[\prod_{i=1}^N (u - \varepsilon_i)^2 + \left(\frac{G}{2}\right)^2 P_{N-1}^2(u) \right], \quad (23a)$$

where

$$P_{N-1}(u) \equiv \prod_{i=1}^N (u - \varepsilon_i) \left[\sum_{j=1}^N \frac{1}{u - \varepsilon_j} \right]. \quad (23b)$$

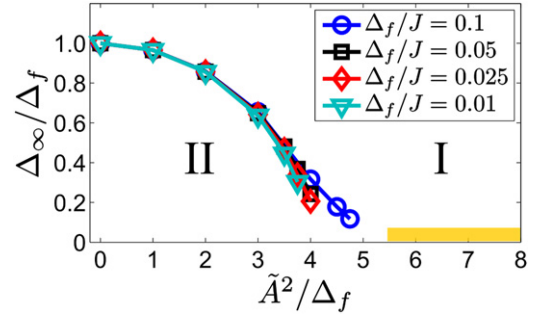


Figure 6. Theoretical prediction for the nonequilibrium phase diagram of an s -wave BCS superconductor subject to an ultrashort (\simeq monocycle) THz pulse with center frequency $\omega \simeq \Delta$, from reference [121], described in figure 5. The 2D square lattice has linear size $L = 1000$ at quarter filling. Values of Δ_∞ are extracted from the isolated Lax roots corresponding to the spin configuration immediately after cessation of the pump pulse. We plot Δ_∞ as a function of the peak pulse intensity \tilde{A}^2 , with different values of Δ/J (J is the hopping strength). As illustrated in figure 5, more intense pulses produce larger deformations of the pseudospins along the Fermi surface, leading to a suppression of the asymptotic BCS gap Δ_∞ .

Assume that the single-particle energies reside in the bounded interval $-2J \leq \varepsilon_i \leq 2J$. Then, for $G \ll 2J$, $Q_{2N}(u)$ possesses $2N$ zeroes that appear in complex conjugate pairs close to each of the N bare real energies $\{\varepsilon_i\}$. On the other hand, for $G \gg 2J$, $2(N-1)$ zeroes appear close to the $N-1$ real zeroes of $P_{N-1}(u)$. Thus there must be an additional, isolated pair.

To take the thermodynamic $N \rightarrow \infty$ limit, we consider a simple 1D cosine band $\varepsilon \rightarrow 2J \cos(k)$, with $|k| \leq \pi$. The Lax norm evaluates to

$$L_2(u) = (L\nu_0)^2 \left[\frac{\pi^2}{(u/J)^2 - 4} + \frac{1}{g^2} \right], \quad g = \nu_0 LG, \quad (24)$$

where $\nu_0 = 1/(2\pi J)$ is the density of states at the band center and L is the linear system size. The roots are $u_1^\pm = \pm J\sqrt{4 - (\pi g)^2}$. There is a dynamical phase boundary at $g_c \equiv 2/\pi$: for $g < g_c$, the isolated roots are real and merge with the continuum branch cut—this is phase I. For $g > g_c$, the isolated roots are purely imaginary, and we have phase II.

For phase II, the Lax reduced problem corresponds to a single collective pseudospin $\vec{\sigma}$, with a one-spin BCS Hamiltonian (compare to equation (12))

$$H_1 = 2\chi\sigma^z - \frac{|\Delta_\infty|^2}{G}, \quad |\Delta_\infty| = -G|\sigma^-|. \quad (25)$$

Here χ , Δ_∞ , and σ^z are all constants that must be determined by the roots of the effective one-spin spectral polynomial,

$$Q_2(u) = (u - u_1^+)(u - u_1^-). \quad (26)$$

Using the isolated roots from the many-body Lax norm in equation (24), we find that

$$\Delta_\infty = |u_1^\pm| = 2J\theta(g - g_c) \sqrt{\left(\frac{g}{g_c}\right)^2 - 1}, \quad (27)$$

where $\theta(x)$ is the unit step function.

It is important to note that not all information about the long-time evolution of the post-quench dynamics is encoded by the isolated roots. In a BCS ground state, each Anderson pseudospin \vec{s}_i is aligned to its magnetic field $\vec{B}(\varepsilon_i)$ (equation (13b)) (possibly modified by a chemical potential term to fix the density). In phase II, the effective magnetic field is determined by the asymptotic value of the gap Δ_∞ ,

$$\vec{B}_\infty(\varepsilon_i) = -2\varepsilon_i\hat{z} - 2\Delta_\infty\hat{x}.$$

However, the steady-state pseudospins will in general exhibit precession around this field at a finite canting angle,

$$\lim_{t \rightarrow \infty} \vec{s}_i(t) = \frac{1}{2} \sqrt{1 - \gamma_i^2} \left\{ \begin{array}{l} \cos[2E_\infty(\varepsilon_i)t] \hat{B}_\infty(\varepsilon_i) \times \hat{y} \\ + \sin[2E_\infty(\varepsilon_i)t] \hat{y} \end{array} \right\} - \frac{\gamma_i}{2} \hat{B}_\infty(\varepsilon_i), \quad (28)$$

where $E_\infty(\varepsilon_i) \equiv \sqrt{\varepsilon_i^2 + \Delta_\infty^2}$ is the asymptotic steady-state BCS quasiparticle energy. The function γ_i can be computed exactly by evaluating the Lax norm for the precessing solution in equation (28), discarding terms that oscillate as $t \rightarrow \infty$, and equating this with Lax norm for the pre-quench initial condition; we omit details here, but see references [110, 112, 125]. In phase II, the function γ_i plays the role of a nonequilibrium distribution function for the quasiparticle spectrum in the asymptotic steady state:

$$-\gamma_i = 1 - 2f_i, \quad (29)$$

where f_i would take the Fermi–Dirac form in terms of the quasiparticle energies for a system in thermal equilibrium.

Once the gap Δ_∞ and the distribution function γ_i are known, generic n -body steady-state Green's functions (retarded, Keldysh, etc) can be computed for the evolving pure BCS state. See e.g. references [112, 129, 163] for examples of one-body functions and observables such as rf spectroscopy, tunneling, and time-resolved ARPES, and references [121, 164] for the current–current correlator that determines the optical conductivity and Meissner response of a quenched solid-state superconductor.

3.3.2. Quench-generated Floquet phase III. Phase III arises for sufficiently large weak-to-strong pairing BCS quenches, see e.g. figures 3 and 4. As we review below in section 3.4, a special case corresponds to turning on attractive interactions for an initially unpaired, noninteracting Fermi gas ground state. Fluctuations (either quantum or thermal) play a crucial role in the real dynamics of such a quench, because the noninteracting ground state (a fully $\pm s^z$ -polarized Anderson pseudospin magnet with a sharp domain wall at the Fermi surface) is a metastable stationary state.

Nevertheless, one can use the Lax spectral method to consider the formal limit of $\Delta_i/\Delta_f \rightarrow 0$, where Δ_i (Δ_f) denotes the prequench (postquench) ground state gap (associated to a pairing strength G_i or G_f , respectively). In this limit, $\Delta(t)$ possesses a soliton solution that grows from zero, reaches a peak, and decays back to zero [108]. The undamped oscillations of

$\Delta(t)$ in phase III can be understood as a train of such solitons [108, 111], and are thus in some sense adiabatically connected to the quench from an initial state with a sharp Fermi step.

Instead of the metastable normal state, here we consider the fully s^x -polarized initial state in equation (22), but now with a pair of sharp domain walls [162]:

$$\vec{s}_i = (1/2)\hat{x} \operatorname{sgn}(\varepsilon_i). \quad (30)$$

As proposed in reference [124] such an initial state can be prepared in a cavity QED system. In that work it is discussed how this state can be used to probe phases I, II and III in a controllable setting. See section 5. For the 1D cosine band employed above, the Lax norm in the continuum limit evaluates to (cf equation (24))

$$L_2(u) = (L\nu_0)^2 \left\{ \frac{[\operatorname{csc}^{-1}(u/2J)]^2}{(u/2J)^2 - 1} + \frac{1}{g^2} \right\}. \quad (31)$$

For $g = 0$, this has only real roots at $u = \pm 2J$. For any $g > 0$, two pairs of conjugate isolated roots nucleate into the complex- u plane. Denote these as $\{u_1, u_1^*, u_2, u_2^*\}$. For this particle-hole symmetric example, $u_2 = -u_1^*$. In the limit of large g , one has

$$\left(\frac{u_1}{2J}\right)^2 \simeq \frac{2g^2}{1 - i\sqrt{4g^2 - 1}}. \quad (32)$$

Two pairs of isolated roots corresponds to an effective two-spin problem, with spectral polynomial

$$Q_4(u) = (u - u_1)(u - u_1^*)(u - u_2)(u - u_2^*). \quad (33)$$

Parameterizing the order parameter $\Delta(t)$ in terms of an amplitude and phase via

$$\Delta \equiv \sqrt{R} \exp(-i\phi), \quad (34)$$

one can solve the two-spin problem to obtain equations of motion in terms of the roots. Details of this calculation can be found elsewhere [108, 112, 125]. The results are

$$\begin{aligned} \dot{R}^2 &= 4(R_+ - R)(R - R_-)(R + \tilde{R}), \\ \dot{\phi} &= c_1 + \frac{c_2}{R}, \end{aligned} \quad (35)$$

where

$$\begin{aligned} R_\pm &\equiv (|\operatorname{Im} u_1| \pm |\operatorname{Im} u_2|)^2, \\ \tilde{R} &\equiv [\operatorname{Re}(u_1 - u_2)]^2, \\ c_1 &\equiv \operatorname{Re}(u_1 + u_2), \\ c_2 &\equiv [\operatorname{Re}(u_1 - u_2)][(\operatorname{Im} u_1)^2 - (\operatorname{Im} u_2)^2]. \end{aligned} \quad (36)$$

In our example (equations (31) and (32)), we define $u_r \equiv \operatorname{Re} u_1$, $u_i \equiv \operatorname{Im} u_1$, and $u_2 = -u_1^*$. Then the amplitude $\Delta(t)$ is given by

$$\Delta(t) = 2u_i \operatorname{dn}\left(2u_i t \middle| M\right) \simeq 2u_i \cos\left(\frac{2\pi t}{T}\right), \quad (37)$$

where

$$M = 1 + u_r^2/u_i^2, \quad (38)$$

$$\mathcal{T} = \frac{1}{2ui}[4K(M) + 4iK(1 - M)].$$

In equation (37), $\text{dn}(z|M)$ is the Jacobi elliptic function, with M the ‘modulo’; the approximate form of $\Delta(t)$ given by the second equality is a very good approximation, except for very large $|u_{r,i}|$. In equation (38), $K(M)$ is the complete elliptic integral of the first kind, and $M = k^2$, with k the elliptic modulus parameter.

We conclude that the x -polarized ‘domain wall’ initial condition in equation (30) gives rise to a self-generated Floquet phase III, where the order parameter is given by the elliptic solution in equation (37). The parameters of this solution are determined by the four isolated roots $\{u_1, u_1^*, -u_1, -u_1^*\}$, where u_1 is given by equation (32) for sufficiently large g .

Finally, we note that more complicated initial conditions with additional discontinuities can excite three or more pairs of isolated roots. These typically give rise to a self-generated, *quasiperiodic Floquet phase* for $\Delta(t)$ in the prethermalized regime [111, 165]. These quasiperiodic phases have so far received little attention, and remain an attractive avenue for future work.

3.4. Fluctuation phenomena

The reduced BCS Hamiltonian in equation (12) is an approximation to the idealized model for a Fermi gas with short-ranged interactions in equation (10). Only Cooper pairs with zero center-of-mass (COM) momentum are retained. This has several consequences. Formally, when this model is coupled to an electric field [121], appropriate for THz driving of a solid-state superconductor, the projection to zero-COM pairs breaks gauge invariance. This can be restored by incorporating the vector potential into the pairs, and still gives an effective classical system that can be efficiently simulated numerically [166].

Two more intricate problems are of particular theoretical and experimental interest. These are (1) a quench from the normal Fermi liquid state, either above T_c or at zero temperature with the pairing interactions turned off, and (2) a quench in a system of size $L \gg \xi$, where ξ is the coherence length. We discuss these in turn.

Quenches in which attractive pairing interactions are switched on from an equilibrium normal state above T_c have been studied in references [146–149]. In this case, the fluctuation dynamics of the pairing amplitude are overdamped and can be treated classically, while the Keldysh method can be employed to evaluate one- and two-fermion observables (such as the optical conductivity [147, 148, 164]).

By contrast, a quench from a normal system with energy density below T_c is an extreme limit of a weak-to-strong pairing quench, and thus would be expected to induce the self-generated Floquet phase III (see e.g. figure 3). A weak-to-strong BCS quench from a finite-temperature initial paired state, in a system with N pseudospins, can exhibit $\mathcal{O}(\sqrt{N})$ oscillation cycles, which can make phase III easily observable for $N \gg 1$. This follows from the central-limit theorem [144]. On the other hand, the quench from the normal state would

exhibit only $\mathcal{O}(\ln N)$ oscillations [144]. This would hardly be distinguishable from phase II (equation (21)) in an ultracold atom experiment (where N is not exponentially large, unlike in solid state systems).

More problematic for ultrafast THz quench experiments in solid-state superconductors (discussed below in section 5.1) is the fact that practical sample sizes typically have linear dimension $L \gg \xi$, where $\xi = \hbar v_F/\pi\Delta$ is the coherence length. It can be shown that phase III is unstable in this case to the spontaneous generation of spatial fluctuations (‘Cooper pair turbulence’) [141, 142]. The mechanism is parametric resonance, and arises from Cooper pairs with nonzero center-of-mass momentum (which are neglected in the Richardson–Gaudin model Hamiltonian equation (12)).

Finally, it must be remembered that even equation (10) is a significant simplification for both real ultracold Fermi gases and solid-state superconductors. In the case of gases, it neglects the internal degrees of freedom that can lead to losses [167–169], while for a superconductor, it neglects the retarded character of the dynamical pairing interaction, as typically mediated by phonons [153, 170].

3.5. Topological features

In an ordinary, s -wave fermionic superfluid or superconductor, the BCS and BEC regimes respectively correspond to weak and strong pairing limits. One speaks of the BCS-to-BEC crossover in the zero-temperature quantum phase diagram, as a function of the pairing interaction strength (G in equation (12)) [115]. The BCS regime can be pictured as a gas of weakly bound, strongly overlapping Cooper pairs, while the cartoon for the BEC is a bosonic condensate of tightly bound two-fermion molecules. Since the zero temperature system is fully gapped for any nonzero pairing strength, the BCS and BEC regimes are limits of the same phase.

By contrast, for non- s -wave pairing, there is typically a genuine quantum phase transition separating the BCS and BEC regimes. In particular, for 2D $p + ip$ superfluid, the weak-pairing BCS phase is topologically nontrivial. It means there exists a quantized integer-value winding number W , which characterizes the phase, that takes a nonzero value. The most important physical consequence of $W \neq 0$ is the presence of gapless, chiral edge states that circulate around a 2D sample of finite extent [114]. This is a superconducting analog of the quantum Hall effect, except that the circulating edge fermions (called ‘Majorana fermions’) carry only energy instead of charge. A $p + ip$ BCS superconductor can also host so-called ‘Majorana zero modes’ in vortex cores; these are non-abelian anyons that could be exploited for topological quantum computation [114, 171].

On the other hand, the strongly paired BEC regime of a 2D $p + ip$ superfluid is topologically trivial; there are no gapless edge states, and it cannot host Majorana zero modes. This is because topology is encoded in the effective bandstructure for the fermionic quasiparticles of the superfluid, but in the strongly paired BEC, the only low-lying excitations are bosonic molecules. The quantum phase transition separating the BCS and BEC regimes involves a closing of the excitation

gap, such that gapless bulk quasiparticles appear precisely at the transition.

Other topologically nontrivial superconductors and superfluids are possible in three dimensions, analogous to the distinct p -wave paired ^3He B and A phases [172, 173]. The former (latter) is a fully gapped, time-reversal invariant (gapless Weyl, time-reversal breaking) topological superfluid; both are predicted to host gapless two-dimensional Majorana fermion surface fluids.

Because topology and its consequences (e.g., gapless edge and surface states) are *global features* of a quantum phase of matter [151], these are expected to be immune to weak symmetry-preserving perturbations. It is therefore natural to ask which features survive under a *global* quantum quench.

Quench and Floquet dynamics in topological bandstructures is already a vast subject, see e.g. references [150, 152, 174–184]. Here we confine our attention to topological features that emerge in a self-consistent quench, studied for a p -wave Richardson–Gaudin model in [112, 113, 129], see also [145, 185, 186].

The dynamical phase diagram for quenches in the 2D $p + ip$ Richardson–Gaudin model is shown in figure 3. It possesses the same three dynamical phases I, II, III for the order parameter $\Delta(t)$ discussed above. In this case, the self-generated Floquet phase III is topological, and features chiral Majorana edge states, shown in figure 4. These are similar to edge states obtained in equilibrium [114] or under external Floquet driving [152], except that they are induced here by a sufficiently large weak-to-strong pairing quench. It was argued in reference [113] that phase III might be realizable in an ultracold Fermi gas, by quenching from an undetectably small (but nonzero) initial gap strength Δ_i to an intermediate strength $\Delta_f \gg \Delta_i$. Although the latter regime is associated to strong parasitic three-body losses [167–169] that prevent the adiabatic cooling to an equilibrium topological state, a parameter window with $\mathcal{T} \ll t_3$ could possibly allow experimental observation of phase III. Here \mathcal{T} is the period of the Floquet phase, and t_3 is the three-body loss lifetime.

Another key feature of the phase diagram in figure 3 is the winding number W , which takes different values in two regions of phase II. The $W = 1$ ($W = 0$) region is a topological (trivial) phase II regime. The topological version would host chiral gapless Majorana edge states for a realization in terms of paired fermions, with a sample boundary.

There are different notions of winding numbers that are equivalent in equilibrium, but which must be distinguished for a quench. The winding number W (Volovik invariant) is defined via [112, 172]

$$W \equiv \frac{\epsilon_{\alpha\beta\gamma}}{3!} \int_{-\infty}^{\infty} d\omega \int \frac{d^2\mathbf{k}}{(2\pi)^2} \text{Tr} \times \left[\hat{\mathcal{G}}^{-1}(\partial_\alpha \hat{\mathcal{G}}) \hat{\mathcal{G}}^{-1}(\partial_\beta \hat{\mathcal{G}}) \hat{\mathcal{G}}^{-1}(\partial_\gamma \hat{\mathcal{G}}) \right]. \quad (39)$$

Here $\alpha, \beta, \gamma \in \{\omega, k_x, k_y\}$ and repeated indices are summed. The matrix $\hat{\mathcal{G}}(\omega, \mathbf{k}) \equiv \hat{G}_R(i\omega, \mathbf{k})$; the latter is the analytic continuation of the Fourier transform for the retarded, Bogoliubov–de Gennes Green’s function $\hat{G}_R(t - t', \mathbf{k})$. In

the long-time steady state of phase II, this Green’s function is time-translationally invariant and independent of the distribution function γ_i (defined in equations (28) and (29), above). Because the retarded Green’s function encodes information about the *spectrum of excitations* in the phase II steady-state, it is the appropriate topological index to determine the post-quench topology and its consequences (presence or absence of edge states). In figure 3, Δ_{QCP} denotes the ground-state topological phase transition between the BCS and BEC regimes; the dashed purple line is its nonequilibrium extension.

By contrast, a different winding number defined to characterize the many-body state of the system does *not* change following a quench in the collisionless, prethermalized regime [112, 174, 175]. This winding number can be defined as [112]

$$Q \equiv 8\pi \epsilon_{abc} \int \frac{d^2\mathbf{k}}{(2\pi)^2} \frac{1}{k} s_{\mathbf{k}}^a \partial_k s_{\mathbf{k}}^b \partial_{\phi_k} s_{\mathbf{k}}^c, \quad (40)$$

where k, ϕ_k are polar coordinates for the momentum plane, and $a, b, c \in \{1, 2, 3\}$ (again with repeated indices summed). The winding number Q characterizes the pseudospin texture of the many-body state. For an equilibrium topological BCS state, this is a skyrmion texture with $Q = W = 1$ [112, 114]. In the BEC state $Q = W = 0$, and the texture can instead be deformed to a trivial ferromagnetic one. The unitary evolution under the Richardson–Gaudin Hamiltonian (which neglects center-of-mass spatial fluctuations for the order parameter $\Delta(t)$) prevents a change in Q for any quench.

In summary, W measures the winding number of the spectrum realized in the asymptotic prethermalization plateau, while Q characterizes the invariant winding of the many-body state. The latter is defined in terms of a translationally invariant system with periodic boundary conditions, and therefore does not encode information about edge states. Instead, edge states are spectral features encoded by W .

The most interesting consequence of the dual winding numbers (W, Q) out-of-equilibrium appears for phase II quenches across the topological quantum phase transition, such that $W \neq Q$. Then, one can show that consistency between equations (39) and (40) requires a *population inversion* in the occupation of steady-state quasiparticle states. I.e., the distribution function $-\gamma = 1 - 2f$ (equations (28) and (29)), which has $\gamma_{\mathbf{k}} = -1$ for all quasiparticle states in either the BCS or BEC ground state, necessarily ‘winds’ to $\gamma_{\mathbf{k}} = +1$ for $\mathbf{k} \rightarrow 0$ (the bottom of the parabolic band without pairing). This population inversion has detectable consequences for far-from-equilibrium phase II observables, such as rf spectroscopy or time-resolved ARPES [112, 129]. The takeaway is that, in a far-from equilibrium situation, a topological change ($W \neq Q$) can be encoded in real *bulk* observables, due to the induced quasiparticle population inversion [112, 187]. This predicted bulk population inversion was very recently proposed as an experimental signature for the topological transition in a trapped ion magnet [188].

Finally, we note that the quenches studied of $p + ip$ superfluids in references [112, 113, 129] always assumed an initial nonzero $p + ip$ order ($\Delta_i \neq 0$ in figure 3). As discussed in section 3.4, a quench from the normal state requires an

analysis of thermal and or quantum fluctuations. However, even in the superconducting phase it is possible to have an initial combination of both $p + ip$ (Δ_+) and $p - ip$ (Δ_-) orders, given that the natural p -wave pairing interaction is time-reversal invariant. A very recent study [189] demonstrates that the coherent, topological phase III is replaced by a *chaotic* non-Floquet phase III', for a quench in such a p -wave system from any simultaneously initial nonzero combination of $\{\Delta_+, \Delta_-\}$. On the other hand, the topological Floquet phase III is recovered for arbitrarily weak time-reversal symmetry breaking in the Hamiltonian, which favors (e.g.) the development (suppression) of $p + ip$ ($p - ip$) order [189].

4. Dynamical phase transitions in infinite dimensions

For systems which follow a collisionless time evolution, non-thermal dynamical phases can be distinguished in terms of the asymptotic behavior at long times. Beyond this paradigm, a universal understanding of DPTs has yet to emerge. A generic interacting quantum system is expected to thermalize [190], in which case DPTs, such as between phases I to III in the collective spin models of section 3, turn into a crossover within the pre-thermal regime. To progress in an understanding of DPTs in non-integrable systems, we can therefore put forward the following questions: (i) how sharp are crossover phenomena which derive from exact mean-field DPTs under experimentally accessible conditions? Are they well-defined even in a realistic solid state setting, and can they be engineered on quantum simulation platforms? (ii) Can one identify different dynamical transitions which are entirely characterized in terms of the short-time dynamics? (iii) Can thermalization be inhibited even in non-integrable systems, so that sharp dynamical transitions exist in the long time behavior?

A challenge in investigating these questions is that the time evolution in non-integrable quantum systems is typically exponentially hard to compute. One limit in which many-body systems can be studied in a numerically controlled way is the limit of infinite dimensions, or infinite lattice connectivity $Z \rightarrow \infty$ [191]. In contrast to spin models for which mean-field theory becomes exact in this limit (cf DPTs in sections 2.1 and 3.2), the dynamics of fermionic or bosonic lattice models generally remains non-integrable and ergodic. The limit of infinite dimensions therefore provides a useful setting to investigate the fate of DPTs when the dynamics is no longer collisionless. In the following section we will briefly comment on the solution of lattice models, in particular the Hubbard model, in this limit, and then review two types of DPTs: (i) a crossover in the pre-thermal evolution of symmetry-broken states (section 4.2), which is closely related to the mean-field DPTs discussed in the first part of this review, and (ii) DPTs in the short-time evolution (section 4.3) which either separate distinct pre-thermal regimes or are related to Bloch oscillations in a time-independent potential gradient.

As a remark we emphasize that the study of non-integrable quantum dynamics is a very active field of research also in the opposite numerically accessible limit, i.e., one-dimensional and finite systems. In particular, many-body localized phases

in disordered systems show non-ergodic behavior [192–194], and the separation between non-ergodic many-body localized phases and thermal phases [195] can give rise to dynamical phase transitions. Weak ergodicity breaking with unusually long relaxation times has also been observed in translationally invariant systems due to dynamical bottlenecks and constraints, somewhat analogous to arrest in glassy dynamics [196–203], and many-body dynamics can remain constrained to atypical eigenstates [204, 205], or quantum many-body scars [206–208]. These settings are naturally interesting for a study of DPTs, but a detailed review of this field of research is beyond the scope of the present work (cf discussion in section 5).

4.1. The Hubbard model in infinite dimensions

A paradigmatic model for strongly interacting fermions is the Hubbard model, given by the Hamiltonian

$$H_{\text{Hub}} = -J \sum_{\langle i,j \rangle, \sigma} c_{i\sigma}^\dagger c_{j\sigma} + U \sum_j n_{j\uparrow} n_{j\downarrow}. \quad (41)$$

Here $c_{j\sigma}$ ($c_{j\sigma}^\dagger$) is the annihilation (creation) operator for a fermion with spin $\sigma \in \uparrow, \downarrow$ on a lattice site j , and $n_{j\sigma} = c_{j\sigma}^\dagger c_{j\sigma}$ is the onsite number operator. The model describes tunnelling of particles between neighbouring sites $\langle i, j \rangle$ on a lattice, with a local interaction U . Depending on interaction and filling, the Hubbard model gives rise to Mott-insulating, magnetically-ordered, and superconducting phases in equilibrium, making it a suitable platform to explore DPTs. A nontrivial solvable limit of the Hubbard model is that of infinite lattice connectivity $Z \rightarrow \infty$. For example, the connectivity can be systematically varied on the Bethe lattice, or on the D -dimensional hypercubic lattice with $Z = 2D$. When the tunnelling matrix elements are rescaled like $J = J_0/\sqrt{Z}$, with fixed J_0 , interaction and kinetic energy for a system with given nonzero filling fraction (e.g. half filling) remain of the same order, resulting in a meaningful competition of various phases [191]. At the same time, the many-body self-energy $\Sigma(\mathbf{k}, \omega)$ becomes local in space (independent of momentum \mathbf{k}) [209], and the model can be solved exactly within dynamical mean-field theory (DMFT) [210]. Within DMFT, the local self-energy $\Sigma(\omega)$ is obtained from a quantum impurity model in which one site of the lattice is embedded in a self-consistently determined particle reservoir [211]. Using Keldysh Green's functions, DMFT can be formulated to study lattice models in different non-equilibrium settings [212–214], including the transient dynamics of isolated lattice systems, non-equilibrium steady states of dissipative driven systems [215–217], and periodically driven systems (Floquet DMFT) [218]. The quantum impurity model for the Hubbard model can be solved numerically exactly for short times using real time quantum Monte Carlo (QMC) [219], or matrix product state (MPS) simulations [220]. Long-time simulations are still exponentially hard due to the dynamical sign problem in the case of QMC, and due to the unbounded growth of the entanglement typical for global quenches in many-body systems in the case of MPS. Nevertheless, diagrammatic expansions on the level of the impurity model both at weak coupling [221] and at strong coupling

[222] allow for a solution at long times, and thus provide a unique possibility to achieve a non-perturbative description of the many-body dynamics in a high-dimensional system.

4.2. DPTs related to non-thermal symmetry breaking

The half-filled Hubbard model on a bipartite lattice supports antiferromagnetic (AFM) order in the repulsive case $U > 0$, and superconductivity as well as charge density wave order in the attractive case $U < 0$. In the following, we focus mainly on the repulsive model; the attractive model can be mapped onto the repulsive one by a particle hole transformation. At weak-coupling ($U \ll J_0$), the normal (non symmetry broken) state is metallic and the AFM phase can be understood within mean-field theory. For $U \gg J_0$, on the other hand, the normal state is a Mott insulator, and the ordered phase is described by a low-energy Heisenberg model. For $U < 0$, the two limits correspond to BCS superconductivity at weak interactions, and a condensate of preformed pairs (BEC) in the Mott regime, respectively. The transition temperature is maximal at the crossover, where U is comparable to the non-interacting bandwidth W (which is proportional to the tunneling J_0).

The dynamics of the ordered phase after quenches of the interaction has been studied both at weak and at strong interactions. The weak-coupling limit is hereby closely linked to the mean-field models discussed in the first part of this review. To see this, one can choose a unit cell with two sites (corresponding to the two sub-lattices A and B) and define momentum-space spinors $\hat{\psi}_{\mathbf{k}\sigma} = (c_{\mathbf{k}A\sigma}, c_{\mathbf{k}B\sigma})^T$; here \mathbf{k} is a quasi-momentum in the Brillouin zone of the symmetry-broken state, which has a doubled unit cell with respect to the normal state due to the antiferromagnetic ordering. With this, one can introduce Anderson pseudo-spins $S_{\mathbf{k}\sigma}^x = \frac{1}{2} \sum_{\sigma} \hat{\psi}_{\mathbf{k}\sigma}^\dagger \hat{\tau}_x \hat{\psi}_{\mathbf{k}\sigma}$, $S_{\mathbf{k}\sigma}^y = \frac{1}{2} \sum_{\sigma} \sigma \hat{\psi}_{\mathbf{k}\sigma}^\dagger \hat{\tau}_y \hat{\psi}_{\mathbf{k}\sigma}$, and $S_{\mathbf{k}\sigma}^z = \frac{1}{2} \sum_{\sigma} \sigma \hat{\psi}_{\mathbf{k}\sigma}^\dagger \hat{\tau}_z \hat{\psi}_{\mathbf{k}\sigma}$, with the Pauli matrices $\hat{\tau}_\alpha$. The Néel order parameter is the sub-lattice magnetization, $m = \langle n_{A\uparrow} \rangle - \langle n_{B\uparrow} \rangle = \langle n_{B\downarrow} \rangle - \langle n_{A\downarrow} \rangle$, which becomes $m = \frac{1}{N_k} \sum_{\mathbf{k}} \langle S_{\mathbf{k}}^z \rangle$ in terms of the pseudo-spins. The mean-field Hamiltonian reads (up to terms which are absorbed in the chemical potential)

$$H_{\text{mf}} = \sum_{\mathbf{k}} \vec{B}_{\mathbf{k}}(t) \cdot \vec{S}_{\mathbf{k}}, \quad (42)$$

with the self-consistent pseudo-magnetic field $\vec{B}_{\mathbf{k}}(t) = (2\epsilon_{\mathbf{k}}, 0, -Um(t))^T$; $\epsilon_{\mathbf{k}}$ is the dispersion. Equation (42) is a spin model with all-to-all interaction as discussed in section 3. Upon a particle-hole transformation it is equivalent to the mean-field models studied for BCS superconductors [109], see also equation (12). After an interaction quench starting from the symmetry-broken state, the order parameter m will therefore either show damped collective oscillations (phase II), an exponential decay (phase I), or self-sustained oscillations (phase III). The solution of the Hubbard model beyond mean field theory allows one to investigate the fate of these DPTs outside the collisionless regime.

To study quenches at weak coupling, one can prepare the system in the AFM phase at a given interaction U_i , and suddenly decrease U to a smaller value U_f . Figure 7 shows the results for a simulation on the infinitely coordinated

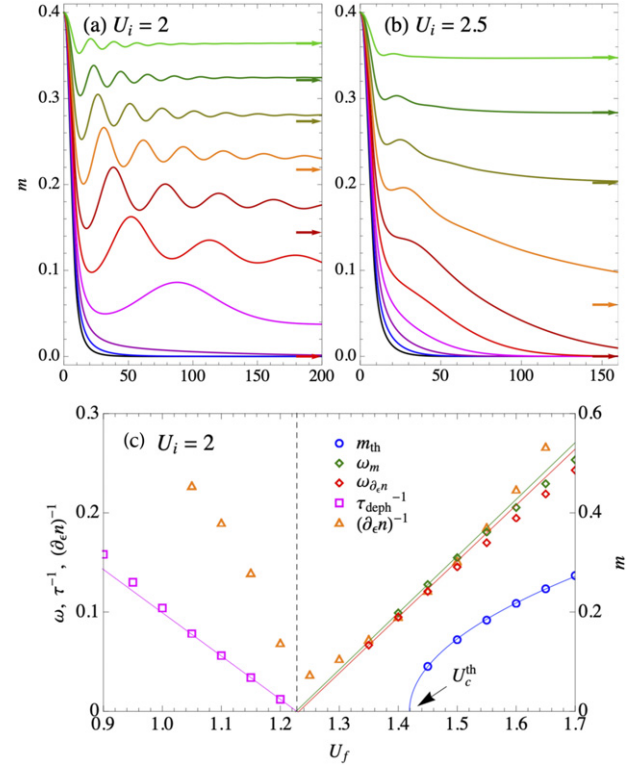


Figure 7. (a) Antiferromagnetic order m after an interaction quench in the Hubbard model on the infinitely connected Bethe lattice. All energies (times) are measured in terms of the (inverse) tunneling J_0 , the noninteracting bandwidth is $W = 4$. Different curves correspond to different final interactions $U_f = 1.9, 1.8, \dots, 0.9$ from top to bottom. The arrow indicates the value of the order parameter after thermalization. (b) Analogous to (a), but for a larger initial value of the interaction, and $U_f = 2.4, 2.3, \dots, 1.4$. (c) Energy and time scales related to the transition (see text) for the initial interaction $U_i = 2$, as function of the quench amplitude U_f . Figure adapted with permission from reference [223].

Bethe lattice. For the smaller value of the initial interaction ($U_i = 2J_0$), one can clearly distinguish two dynamical regimes (figure 7(a)): after weak quenches ($U_f > 1.2J_0$), the order parameter shows a damped oscillatory decay towards a finite value at the longest simulation times (phase II), while for larger quenches, it follows a monotonous exponential decay (phase I). Similar dynamical transitions related to symmetry broken states in infinite dimensional systems are found in a time-dependent Gutzwiller solution of the Hubbard model [224], and for quenches in an $O(\mathcal{N})$ model including fluctuations beyond mean field [95], though both approaches cannot describe thermalization. In the DMFT solution, interactions lead to thermalization, and for quenches close to the dynamical critical point U_c between the two regimes, the order parameter will eventually decay to zero both in phase I and in phase II. However, for sufficiently weak interactions the crossover between the two phases remains remarkably well-defined, and one can even extract the critical behavior close to $U = U_c$: the decay time τ_{def} of the order parameter in phase I diverges like $\tau_{\text{def}} \sim |U - U_c|^{-1}$ and the oscillation frequency ω_m in phase II vanishes like $\omega_m \sim |U - U_c|$. Even for interactions U which are half the bandwidth W , this critical behavior can be observed over an order of magnitude in time (figure 7(c)).

Because of thermalization, the dynamical crossover becomes less well-defined at larger interactions (figure 7(b)). A relevant question is therefore whether one can experimentally distinguish the decay of the order parameter related to phase I from thermalization, although both eventually lead to a vanishing of the order parameter. An indirect evidence would be a crossover in the relaxation time as the system proceeds from the dephasing dynamics to thermalization. More interesting would be a direct measure of the individual momentum-resolved pseudo-spins $S_{\mathbf{k}}$: in the dephasing scenario (phase I), the magnitude of $\langle \vec{S}_{\mathbf{k}} \rangle$ remains nonzero for all \mathbf{k} , but individual spins oscillate out of phase. In the thermal evolution, in contrast, the magnitude of $\langle \vec{S}_{\mathbf{k}} \rangle$ for momenta at the Fermi surface decays to zero. Information on the individual pseudo-spins may be obtained by measuring correlations in the momentum occupations $\langle n_{\mathbf{k}\sigma} n_{\mathbf{k}+\mathbf{Q}\sigma'} \rangle - \langle n_{\mathbf{k}\sigma} \rangle \langle n_{\mathbf{k}+\mathbf{Q}\sigma'} \rangle$ between momenta \mathbf{k} and $\mathbf{k} + \mathbf{Q}$ separated by the antiferromagnetic nesting vector \mathbf{Q} . For cold atoms, such quantities could be addressed using noise correlations in time of flight measurements [156–158], while in the solid-state setting intensity correlations in time-resolved photoemission spectroscopy may provide similar access to such higher order correlations in the momentum distribution and thus distinguish the phase I dephasing from thermalization [159].

The findings for weak quenches in the Hubbard model are reminiscent of non-thermal fixed points in bosonic models [4, 225–228]. Non-thermal critical behavior in this case has been linked to an emergent universal form of the momentum distribution function with a steady flow of energy between short and long length scales. To what extent DPTs between phases I and II in mean-field models give rise to non-thermal critical behavior when interactions beyond mean-field are taken into account is still an open question. For the Fermi–Hubbard model, one could look for universal power laws in the momentum-dependent spin structure factor (antiferromagnetic case) or pair distribution function (superconducting case). A close passage of the non-thermal critical point may moreover lead to a delay in thermalization. For the DMFT simulations, however, the dynamical crossover and subsequent thermalization have so far been seen within the same simulation only for larger interactions, where thermalization is fast, but at the same time the crossover is already relatively broad.

Recent simulations of the long-time dynamics using self-consistent second-order perturbation theory for the $Z \rightarrow \infty$ Bethe lattice have focused on the thermalization of the order parameter in phase II after the decay of the collective oscillation [229]. The system remains in the non-thermal symmetry broken state for a long period of time, with a slow decay of the order, and a gap separating a valence and conduction band. The transient state in this regime is approximately described by a quasi-steady state with separate chemical potentials in the valence and conduction band. At some point, however, the dynamics speeds up, and the system rapidly approaches the disordered state. This highly non-monotonous decay contrasts the conventional evolution of pre-thermal states, which is expected to be a single exponential relaxation of slow variables (almost conserved quantities) [4, 52, 230, 232]. The

initial bottleneck against thermalization in the ordered phase may be linked to the gap in the electronic spectrum, so that the non-thermal symmetry-broken phase is somehow self-sustained. Whether such self-sustained relaxation bottlenecks are robust beyond the second order perturbation theory and beyond the infinite dimensional limit is yet to be seen; if so, the prolonged pre-thermal regime would make the dynamical crossover between phase I and II more well-defined.

Next, one can ask for the existence of phase III, i.e., self-sustained oscillations of the order parameter, in the interacting Hubbard model. In the mean-field model (42), phase III would require quenches to larger interaction, for which the mean-field description of the Hubbard model is probably no longer valid. It is nevertheless interesting to see whether phase III can appear in large quenches of the Hubbard model, such as quenches from the Mott AFM to intermediate coupling, where the AFM order is strongest. Even within DMFT, there is at present no approach which provides an unbiased solution to the long-time evolution in both the weak and strong coupling regime. However, one can obtain a numerically exact solution for short times within an MPS-based solution of the DMFT equations, when the initial state of the model is prepared as a perfect Néel AFM, i.e., the mean-field state of the strong-coupling Heisenberg model [233]. In this case, no indications of phase III are found for quenches to arbitrary interactions [233]. For quenches to small U one finds instead a prompt decay of the order parameter within a few hopping times. The experimental realization of this scenario would be the analog of quantum simulation experiments that analyzed the decay of charge order in a Bose–Hubbard model in one dimension [234].

Quantum quenches in the symmetry broken states have also been performed at large U , within the Mott phase. In this case, the Mott gap itself provides a dynamical constraint which leads to slow thermalization of the interaction energy (double occupancy $d = \langle n_{j\uparrow} n_{j\downarrow} \rangle$) and the kinetic energy [235, 236]. Relaxation times are found to be exponentially long in the ratio U/J_0 [237, 238], closely related to the slow decay of doublons in cold atom experiments [239, 240]. A quenched state can therefore relax into non-thermal phases in which the density of doublons is fixed as a quasi-conserved quantity. In particular, the repulsive single-band Hubbard model favors superconductivity in the η -pairing channel [241] if the doublon density is sufficiently increased with respect to the equilibrium state at the same effective temperature [236, 242, 243]. Such non-thermal phases in Mott insulators have been discussed in connection to possible light-induced superconductivity [242–246]. Because of the exponentially slow thermalization, dynamical phases which correspond to a relaxation to different ordered or disordered non-thermal states can be well-defined, with a non-thermal critical behavior [247]. However, as long as the non-thermal states are protected by a single or few quasi-conserved quantities, dynamical transitions related to these non-thermal phases should be close to dynamical transitions related to the relaxation to different equilibrium phases in a model which incorporates the constraints. For the Hubbard model at large U , where the doubly occupancy is the quasi-conserved quantity, the resulting model

is a generalized $t - J$ model, which describes two species of fermions (holes and doubly occupied sites) moving on the background of quantum spins that interact via an antiferromagnetic Heisenberg exchange. The phase diagram of this model has been studied as an approximation of the non-equilibrium phase diagram of the photo-excited Hubbard model for both the infinite-dimensional [242] and the one-dimensional case [243].

4.3. DPTs between pre-thermal phases at short-time

A non-perturbative solution of the short time dynamics after an interaction quench in the Hubbard model from the non-interacting Fermi sea has been obtained using DMFT and QMC [248]. The system is initially prepared in the noninteracting Fermi sea, and at time $t = 0$, the interaction is suddenly quenched to a value $U_f > 0$. The subsequent dynamics can be monitored in terms of various observables, most importantly the momentum occupation $n_{\mathbf{k}}(t) = \langle c_{\mathbf{k},\sigma}^\dagger c_{\mathbf{k},\sigma} \rangle$ and the doubly occupancy $d(t) = \langle n_{j\uparrow} n_{j\downarrow} \rangle$. In the initial state, $n_{\mathbf{k}}$ shows a unit size discontinuity $\Delta n_F = n_{\mathbf{k}_F^-} - n_{\mathbf{k}_F^+}$ across the Fermi surface; \mathbf{k}_F^\pm denotes a momentum infinitesimally above (below) the Fermi momentum. In thermal equilibrium, the discontinuity in the momentum distribution of a Fermi liquid exists only at zero temperature. Because a quenched system is excited with respect to the ground state, the existence of a finite jump Δn_F indicates that the system is not yet thermalized. Moreover, one can show that the jump discontinuity is robust: while the magnitude Δn_F can change at $t > 0$, there remains an exact step-singularity in the momentum distribution, and the location of the discontinuity is precisely given by the noninteracting Fermi surface [249]. Hence, Δn_F can be taken as an order parameter to distinguish different dynamical regimes.

After the quench, one observes two distinct dynamical regimes, see figure 8: for small quenches below a value $U = U_{fc}$ ($U_{fc} = 3.3J_0$ for the infinitely connected Bethe lattice), the Fermi surface singularity rapidly decreases to a value $\Delta n_F > 0$. The subsequent slower decay toward the thermal value $\Delta n_F = 0$ is not resolved within the short time simulations. For quenches above $U_f = U_{fc}$, the dynamics features damped oscillations, with zero-crossings of Δn_F . For quenches to an interaction between the two dynamical regimes, the whole momentum distribution thermalizes rapidly. Thermalization is also verified by the fluctuation dissipation relation in dynamical correlation functions [251].

The dynamical transition in the short time evolution is not directly related to the equilibrium Mott transition: U_{fc} is about a factor two smaller than the equilibrium Mott transition at temperature $T = 0$, and the final state, after thermalization to a given temperature T^* , is in a bad metallic regime far from any known transition in the equilibrium phase diagram. Intriguingly, a singularity in the equilibrium two-particle vertex, which is related to multi-valuedness of self-consistent perturbation theory [252], has been found right at the point (U_{cf}, T^*) [253]. Whether this is coincidental, or whether such vertex singularities in general are related to DPTs is an open question.

It is useful to note that the two dynamical regimes reflect distinct pre-thermal behavior which can be understood in

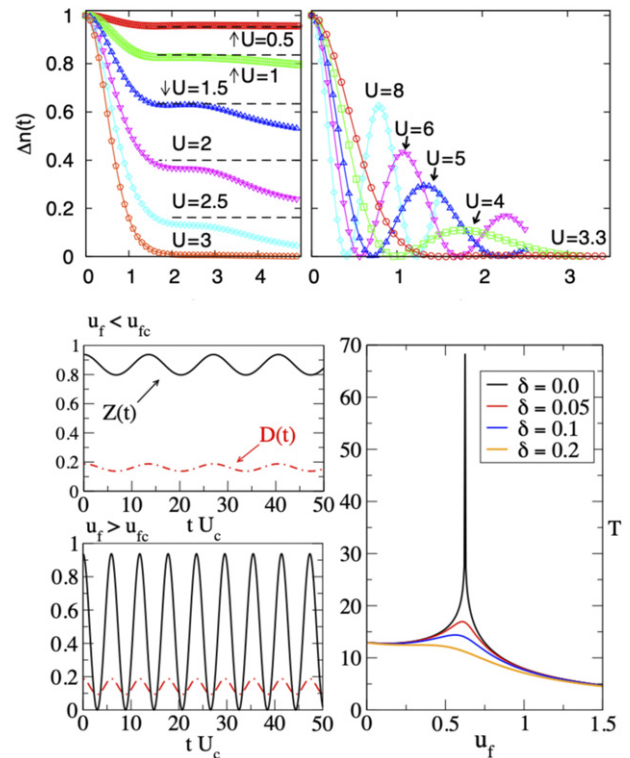


Figure 8. Upper panels: Fermi surface discontinuity $\Delta n_F(t)$ for an interaction quench in the Hubbard model on the Bethe lattice (noninteracting bandwidth $W = 4$), from the noninteracting state to interactions U as indicated. The left and right panel correspond to the different dynamical regimes below and above $U_{fc} = 3.3$. Adapted with permission from [248]. Lower panels: solution of the same model using the time-dependent Gutzwiller approach: left is the quasiparticle weight (Z) and the double occupancy (D) for quenches below ($U_f < U_{fc}$) and above ($U_f > U_{fc}$) the DPT, right the period of oscillations for different values of the doping δ away from half filling, as function of U_f . A sharp DPT is observed for $\delta = 0$ with a divergence of the period. Adapted with permission from [250].

opposite perturbative limits (although these perturbative limits cannot give a description of the transition itself): quenches from $U = 0$ to weak coupling have been studied using perturbative unitary transformations [52] which are accurate for quenches $U \ll J_0$, on a timescale $t \ll J_0/U^2$. The unitary perturbation theory maps the Hubbard model on a system of non-interacting renormalized quasiparticles; the quasiparticle occupations $\tilde{n}_{\mathbf{k}}$ are conserved, providing a constraint on the dynamics which prevents the system from reaching a thermal state. For quenches to $U \gg J_0$, the effective model that describes the dynamics at least on timescales up to U/J_0^2 can be obtained by unitary perturbation theory, treating J_0 as a small parameter: it is the generalized $t - J$ model mentioned at the end of section 4.2, where the number of doubly occupied sites and holes provides a constraint on the dynamics. The oscillations are well understood in the limit $J_0 = 0$, where the dynamics of the system would be $2\pi/U$ -periodic, because the many-body spectrum is perfectly equidistant (analogous to the collapse and revival oscillations in the bosonic Hubbard model [254, 255]).

While the two dynamical regimes can be understood in a respective perturbative limit, an analytical model of the

dynamical transition itself has been observed within time-dependent Gutzwiller theory [250, 256]. The time-dependent Gutzwiller provides a variational approach to the dynamics; for the Hubbard model, one starts from a variational ansatz wave function

$$|\Psi(t)\rangle = \prod_j e^{-iS_j(t)} P_{j,n}(t) |\Phi(t)\rangle, \quad (43)$$

where $|\Phi(t)\rangle$ is a time-dependent Slater determinant, $P_j(t) = \sum_{n=0,1,2} \lambda_{j,n}(t) P_{j,n}$, and $S_j(t) = \sum_n \phi_{j,n}(t) P_{j,n}$ are operators written in terms of variational parameters $\lambda_{j,n}(t)$ and $\phi_{j,n}(t)$ and the local projectors $P_{j,n}$ on the occupation $n = 0, 1, 2$ on site j . The time-dependent variational principle $\delta\langle\Phi(t)|i\partial_t - H|\Phi(t)\rangle = 0$ leads to a set of nonlinearly coupled differential equations for the variational parameters. Within the Gutzwiller approach, an exact dynamical transition is observed, which shares many features with the DMFT results (see figure 8, lower panels): for small quenches, the quasiparticle weight $Z(t)$, which is proportional to the jump Δn_F defined above, oscillates around a nonzero value. Its time average \bar{Z} tends to zero as U_f approaches the dynamical transition. For quenches to the dynamical critical point, $Z(t)$ exponentially relaxes to its thermal value $Z = 0$. The value \bar{Z} follows the pre-thermal plateau obtained by DMFT with quantitative accuracy [250]. For quenches beyond U_c , $Z(t)$ oscillates with a zero crossing. In contrast to the full solution, the Gutzwiller approach does not describe thermalization, and the dynamical transition therefore distinguishes the dynamics at all times.

Being computationally inexpensive, the Gutzwiller approach has allowed one to study the DPT in a wider range of parameters: (i) by varying the initial $U = U_i$, one can map out a dynamical phase diagram which connects the dynamical phase transition to the equilibrium Mott transition U_c^{eq} : for $U_i = 0$, the dynamical point U_{fc} is below U_c^{eq} , while it approaches U_c^{eq} as U_i is increased [250]. (ii) Moreover, the dynamical transition persists if the interaction is ramped up with a nonzero ramp time τ instead of a quench [257, 258]. The dynamics after the ramp still distinguishes different dynamical regimes, and the DPT evolves towards the equilibrium phase transition for larger τ , as expected for an adiabatic dynamics. (iii) When the system is doped away from half filling, where there is no Mott transition in equilibrium, the dynamical transition turns into a crossover. In particular, time averages of the double occupancy and of Z evolve smoothly as a function of U_f . Finally, (iv), time-dependent Gutzwiller simulations have been performed for a multi-orbital Hubbard model [259], which turns out to be different from single-band case due to inter-orbital fluctuations. The dynamical transition is replaced by a broad regime in which the different occupations evolve irregularly, which may be interpreted in terms of long-lived fluctuations between metallic and insulating states.

Unfortunately, DMFT simulations have so far been performed neither away from half filling nor at nonzero U_i , due to a more severe dynamical sign problem. Hence there are so far no numerically unbiased simulations to support these intriguing observations from the Gutzwiller approach, and a complete picture of the dynamical transition in the Hubbard

model is yet to be developed. Another question is the extension of the transition to lower-dimensional systems. In one dimension, the dynamics has been calculated using a systematic solution of the equation of motion for the field operators $c_{i\sigma}$ in terms of higher order operator products [260]. It is found that the non-equilibrium time-evolution after interaction quenches exhibits a similar dynamical transition as in the half-filled case, while the transition becomes a crossover upon doping. This may suggest that the dynamical transitions is a general feature of quenches in such models [260]. On the other hand the prethermalization is typically less pronounced in lower dimensions [260, 261].

Finally, a DPT has been found in the Bose–Hubbard model on an infinitely connected lattice [262], for quenches from the superfluid phase toward to Mott phase. A solution of the Bose Hubbard model within the non-equilibrium generalization of bosonic DMFT [263] can be done at least for the short time evolution. In this case a single DPT is replaced by a richer dynamical phase diagram, including a non-thermal symmetry broken phase for weak quenches, an extended regime in which the system rapidly for intermediate quenches, and oscillations of the order parameter for quenches deep into the Mott phase.

Alternative to quenches of the interaction, dynamical phase transitions in infinite-dimensional lattice models have also been observed after a sudden switch-on of a potential gradient. In the non-interacting case, this leads to perfect Bloch oscillations if the gradient is aligned with a high-symmetry direction of the lattice. In interacting models, these oscillations will be damped, as the system approaches an infinite temperature state (for ergodic systems) or a non-thermal steady state if the system does not behave ergodic. In infinite dimensions, the latter case is represented by the Falikov–Kimball model, which allows for an exact solution in DMFT [264, 265]. The Falikov–Kimball model describes a Hubbard model in which one species of fermions is frozen. Regarding the mobile species, the dynamics obtained by DMFT in the normal (non-symmetry broken) phase is identical to that of fermions with quenched binary alloy disorder. The model does not thermalize after a quench of the interaction, but instead reaches a non-equilibrium steady state at infinite time [266]. The study of Bloch oscillations in the Hubbard and Falikov Kimball model in infinite dimensions gives a rich dynamical phase diagram [213, 267, 268], with transitions between oscillatory and non-oscillatory regimes.

5. Experimental observation

This section overviews a broad number of platforms which are currently employed as quantum simulators for the evolution of interacting many-particle systems where DPTs can be hosted. For continuity with the two previous theory sections, we start by discussing the state of the art in experiments realizing dynamical phases in solid state platforms, and then move to cold atoms experiments.

5.1. DPTs in condensed matter systems

The DPT in the integrable BCS model discussed in section 3 neglects the retarded character of the dynamical pairing

interaction, which is typically mediated by phonons [153, 170]. Nevertheless, under specific conditions superconducting materials could be described by the integrable BCS model and display the three distinct dynamical phases I, II, and III discussed in section 3.2. For that to happen, the asymptotically exact long-time results obtained from the Richardson–Gaudin model can be relevant to experiments which can access a long prethermalization plateau. For a system of many particles $N \gg 1$, this requires that the minimum inelastic lifetime due e.g. to pair-breaking collisions or inelastic electron–phonon scattering in a superconductor must be much larger than $t_{\text{dyn}} \simeq 1/\Delta_\infty$. Here t_{dyn} is the timescale for transitioning to the asymptotic regime and Δ_∞ is the steady-state value of the order parameter in the prethermalization plateau (phase II) [125].

In the case of two-particle collisions for a quench entirely confined to the weak-pairing BCS regime, the two-particle scattering time can be estimated using Fermi liquid theory [125, 269] $t_{\text{in}} \sim (\varepsilon_F/\Delta_\infty)t_{\text{dyn}} \gg t_{\text{dyn}}$, where ε_F is the ground-state Fermi energy. This is consistent with simulations for the Hubbard model in infinite dimensions (section 4.2), which find a well-defined separation of phase I and phase II even when inelastic collisions are taken into account.

To observe phase III, the period \mathcal{T} of the quench-induced Floquet oscillation should be much shorter than the minimum inelastic lifetime. For a quench from an initial BCS state with small (but nonzero) Δ_i , the Floquet period is of order $\mathcal{T} = \frac{2}{\Delta_f} \ln\left(\frac{\Delta_f}{\Delta_i}\right) \ll \tau_{\text{in}}$, where now $\tau_{\text{in}} \sim (\varepsilon_F/\Delta_f^2)$, and Δ_f denotes the ground-state pairing gap for the post-quench system [108, 109, 113].

In addition to the above requirement, the quench that brings the superconductor out-of-equilibrium must occur on time-scales shorter than the inverse of the quasi-particle gap, to ensure the quasiparticle distribution does not adiabatically follow the variation of the system parameters. At the same time the perturbation has to be weak enough to avoid disrupting the system. The latter has been the most important limitation. Near-visible femtosecond optical pulses, which are used as a non-adiabatic excitation of solid state systems are not compliant since excitations with a frequency higher than the BCS gap can break Cooper pairs into hot quasiparticles, and these can serve as an efficient mechanism for rapid dissipation and thermalization. Nevertheless recent developments in THz technology are allowing now the injection of near monocycle pulses with center frequency close to the BCS gap, opening a window to investigate the coherent transient dynamics of superconductors in the nonadiabatic excitation regime over a window of about 10 picoseconds (ps), well before thermalization occurs on a time scale of 100 ps.

In particular the experiment done by Matsunaga *et al* injected an intense, short-duration THz pulse with center frequency $\omega \simeq \Delta_0$ into a low-temperature NbN thin film *s*-wave superconductor [116, 117]. Since most of the spectral weight of the pulse was below the optical gap edge $2\Delta_0$, a weak pulse would not be expected to couple to the system [170]. However, because of the strong character of the injected pulse, it coupled in a nonlinearly fashion and was able to excite the ‘Higgs’

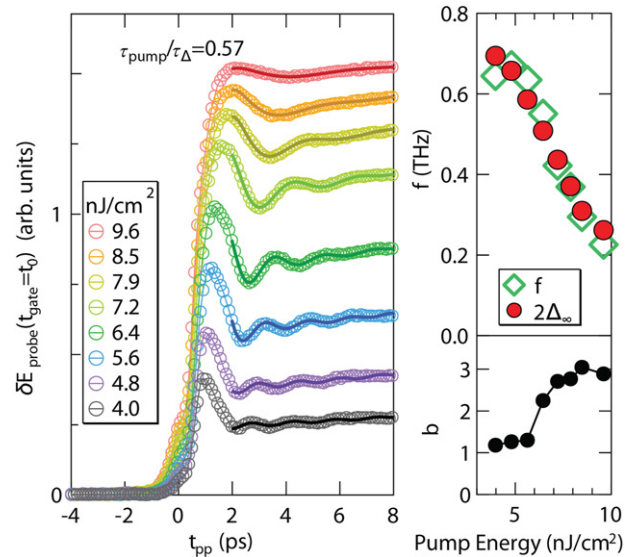


Figure 9. A possible experimental realization of a phase II quench in a solid-state superconductor by Matsunaga *et al*, from reference [116], see also [117]. This figure shows pump–probe THz spectroscopy data on thin film $\text{Nb}_{1-x}\text{Ti}_x\text{N}$. The left panel shows the probe signal oscillations of $\Delta(t)$, and implies the approach to a nonequilibrium value $\Delta_\infty < \Delta_i$ (weak phase II quench). The approach of $\Delta(t) \rightarrow \Delta_\infty$ is characterized by decaying oscillations with frequency $2\Delta_\infty$ (top right), consistent with the theory (equation (21)) [111, 160].

(amplitude) mode of the superconductor. After the application of the pulse, the subsequent free evolution of $\Delta(t)$ was expected to be described by the *s*-wave Richardson–Gaudin model. The experiment [116] measured the system over a window long enough to observe decaying oscillations as predicted by the Lax method in equation (21), as shown in figure 9. Despite the different method of initial state preparation (THz pulse versus instantaneous interaction quench), the phase II dynamics was apparently observed.

A THz electric field pulse can be incorporated into the self-consistent solution for the BCS (Bogoliubov–de Gennes) equations. In order to induce a nontrivial evolution of the system, it is necessary to either account for the finite (but very small) photon momentum [118–120, 122], or to include non-quadratic corrections to the band dispersion [121]. Moreover, in order to model the experiment in reference [116], a short-duration Gaussian electric pulse $\mathbf{E}(t)$, with frequency content mostly below the equilibrium optical gap $2\Delta_0$, needs to be fed into the equations of motion for the Anderson pseudospins. The field twists the pseudospins in the *x*–*y* plane, scrambling the ground state order as shown in figure 5. Importantly, the driving of the Higgs mode arises from nonlinear coupling to the field [117, 121]. After the cessation of the pulse, the system is expected to evolve freely according to the Richardson–Gaudin Hamiltonian.

The Richardson–Gaudin calculation [121] predicts a transition to the gapless phase I for sufficiently strong pump energy, as shown in figure 6. Indeed a putative gapless phase (with suppressed reactive component of the optical conductivity $\sigma_2(\omega)$)

was observed for sufficiently strong pump powers in reference [270], potentially consistent with phase I. Strikingly, this experiment also observed extremely slow relaxational dynamics following the quench, on the order of 1000 ps. A subsequent experiment utilizing asymmetric, multicycle pulses exhibited an intervening ‘gapless’ phase with $\Delta_\infty \neq 0$ [271].

A discrepancy between the collisionless phase II prediction in equation (21) and the data in reference [116] is the more rapid decay of the oscillating envelope than $t^{-1/2}$. This is also consistent with the simulations for the interacting Hubbard model in section 4.1. A better theoretical fit can be obtained by employing a phenomenological ‘ T_2 ’ dephasing time [272]. Another key question is whether spatial fluctuations (‘Cooper pair turbulence’ [141]) play an important role in these solid-state experiments [116, 117, 270, 271]. See discussion in section 3.4.

We finish this section by noting that we have not surveyed here work involving the steady-state of driven solid-state materials [150]. In particular, we do not review multipulse THz driving [272] or continuous-wave mid-infrared laser excitation of superconductors. The latter has attracted significant interest as a possible mechanism for enhancing pairing or T_c far from equilibrium [146–149, 273–280]. Continuous driving has also been discussed in the context of third-harmonic generation via the Higgs mode [117, 281–283]. Although these are certainly interesting developments, our focus here is on the collisionless dynamics of an effectively isolated system, free from external driving (following the quench).

5.2. DPTs in cold atom experiments

DPT in the long-range Ising model. The first observation and quantitative characterization of a DPT was done in a trapped ion quantum simulator consisting of a chain of up to $N = 53$, $^{171}\text{Yb}^+$ ions trapped in a linear radio-frequency Paul trap [57] (see figure 10(a)). Two relevant hyperfine levels were used as a spin 1/2 degree of freedom. Note here we are not accounting for experimental observations of DPTs described in terms of non-analytic behaviors of the Loschmidt echo amplitude which were observed at a similar time [13, 284]. A discussion of these type of experiments can be found in reference [14].

In reference [57] pairs of laser beams were used to generate an optical dipole force that off resonantly excited vibrational modes of the ion chain. The virtually excited phonon modes in turn mediate tunable spin–spin interactions which lead to long-range Ising couplings in the form of equation (1). Explicitly, the engineered Hamiltonian is given by

$$\frac{1}{2} \sum_{i>j} \chi_{ij} \hat{\sigma}_i^x \hat{\sigma}_j^x + \frac{B}{2} \sum_i \hat{\sigma}_i^z, \quad (44)$$

with coupling constants that fall off as $\chi_{ij} \approx J_0/|i-j|^\alpha$, i.e., approximately algebraically with the distance between ions in the chain. The power-law exponent α was set to be between 0.8 and 1.0 in the experiment. Here $\hat{\sigma}_i^{x,y,z}$ are Pauli matrices acting on the i th ion. The competing transverse field proportional to B was generated in the experiment by a controllable Stark shift on the spins from the same laser field that generated the optical dipole force. The transverse field B was used as the control

parameter for crossing the DPT. At time $t = 0$, the system was initialized in the state with all the spins pointing along the x direction of the Bloch sphere and the system was let to evolve under the combined Ising plus transverse field Hamiltonian for some time t after which the collective magnetization

$$\langle \hat{\sigma}^x(t) \rangle = \frac{1}{N} \sum_i \langle \hat{\sigma}_i^x(t) \rangle, \quad (45)$$

and the corresponding time averaged value were measured

$$\overline{\langle \hat{\sigma}^x \rangle}(T) = \frac{1}{T} \int_0^T \langle \hat{\sigma}^x(t) \rangle dt, \quad (46)$$

equivalent to equation (5). At the mean field level the time average magnetization $\overline{\langle \hat{\sigma}^x \rangle}$ is expected to change, as discussed in section 2.1, from a finite value to zero as the system crosses between a dynamical ferromagnetic phase ($B < B^c$) to a dynamical paramagnetic phase ($B > B^c$). Nevertheless, as explained in section 2.2 the quantum nature of the model resulted in a direct decay of the order parameter towards a vanishing or non-vanishing expectation value depending on the dynamical phase considered, without the need of long-time averages to classify phases.

To obtain further signatures of the DPT the experiment measured the spatially averaged two-spin correlator

$$C_2(t) = \frac{1}{N^2} \sum_{i,j} \langle \hat{\sigma}_i^x(t) \hat{\sigma}_j^x(t) \rangle. \quad (47)$$

This quantity was used as a second order parameter for the DPT. It should cross from 1 (at small B) to 1/2 (at large B) with a dip at B^c . However, given the logarithmic scaling of C_2 with N at the critical point and the limited system size of the systems under consideration, the experiment did not observe sharp signatures in C_2 at the critical point. Nevertheless, measurements of the distribution of domain sizes in the chain (a direct measurement of higher-order correlations) accessible in the experiment allowed it to observe a sharp change of behavior at the critical point.

DPT in the Lipkin?Meshkov?Glick model. After this work a similar type of DPT was observed in two different platforms, more specifically the one in the so called Lipkin?Meshkov?Glick (LMG) model (equation (2) in section 2.1), which corresponds the $\alpha = 0$ limit of the system described above with an additional longitudinal field, i.e.

$$\hat{H} = \chi \hat{S}^+ \hat{S}^- + B \hat{S}^x - \delta \hat{S}^z. \quad (48)$$

Here we have introduced the collective spin operators $\hat{S}^\alpha = \sum_j \hat{\sigma}_j^\alpha / 2$ and $\hat{S}^\pm = \hat{S}^x \pm i \hat{S}^y$. The summation runs over the individual spins $j = 1, \dots, N$ and the parameter χ sets the strength of an infinite-range exchange interaction. To connect with the Hamiltonian, equation (2), note that up to $1/N$ corrections $\chi \hat{S}^+ \hat{S}^- \approx \chi (\hat{S} \cdot \hat{S} - (\hat{S}^z)^2)$. Since the first term $\hat{S} \cdot \hat{S}$ is a constant when restricted to the fully symmetric spin manifold, which is the case of interest, the Hamiltonian simplifies to $\hat{H} \rightarrow -\chi \hat{S}_z^2 + B \hat{S}_x - \delta \hat{S}_z$, which up to an overall $\pi/2$ rotation along the y axis of the Bloch sphere, coincides with the one

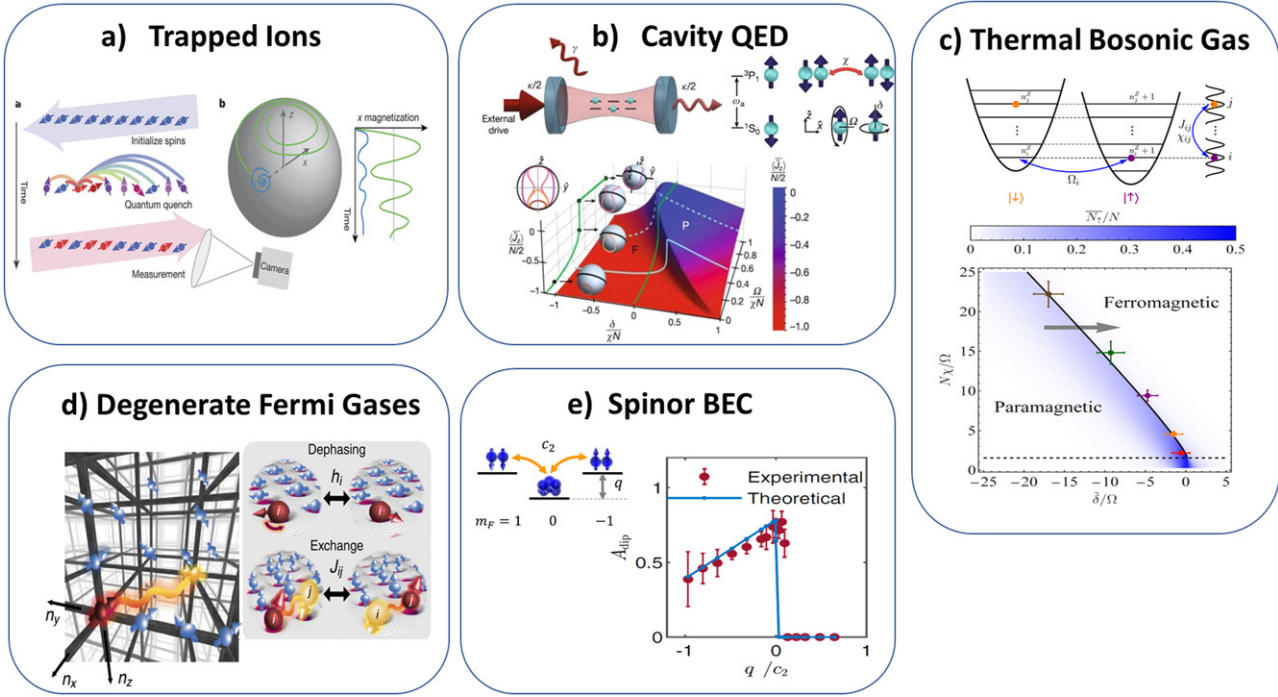


Figure 10. Dynamical phase transitions (DPTs) observed in ultra-cold atomic gases: (a) the first DPT was observed in a trapped ion quantum simulator of the long range Ising model plus transverse field, with up to 53 $^{171}\text{Yb}^+$ ions [57]. (b) A similar type of DPT, but in the collective Ising limit plus an additional longitudinal fields (so called LMG model), was also observed in a cavity QED simulator with $N \approx 10^5 - 10^6$ ^{88}Sr atoms [58], followed up by the observation of a similar DPT in a thermal gas of $N = 10^4 - 10^5$ bosonic ^{87}Rb atoms using a sideband transition [59]. (d) Using a quantum degenerate trapped Fermi gas of $N = 10^4$ ^{40}K atoms the DPT between phase I and phase II predicted to exist in BCS superconductors was observed in reference [123]. (e) Using three internal levels of ^{23}Na atoms prepared in a Bose Einstein condensate (BEC) with $N \sim 10^5$ atoms a DPT was observed as the ratio between collective exchange interactions and an effective quadratic magnetic field was tuned from positive to negative [293, 294].

realized in reference [57] with an extra term proportional to δ which sets the longitudinal field (see figure 10(b)).

The observation of a DPT in the Lipkin-Meshkov-Glick model was first achieved in a cavity-QED simulator using ensembles of $N \approx 10^5 - 10^6$ atoms [58]. We note that in the context of cavity QED a great deal of experimental progress has been done in the observation of non-equilibrium phases characterized by different steady states which therefore depend on parameters such as pump or loss rates but are independent of the initial conditions [285–292]. We will not further discuss these experiments in the following, as in this review we exclusively focus on DPTs related to the unitary time evolution.

In reference [58] the internal spin degree of freedom was encoded in a long lived optical transition (linewidth $\gamma/2\pi = 7.5$ kHz) between the $|\downarrow\rangle$ [1S_0 ($m_J = 0$)] and $|\uparrow\rangle$ [3P_1 ($m_J = 0$)] states of ^{88}Sr atoms. The atoms were confined in a 1D optical lattice and coupled to a single common mode of the optical cavity far detuned from the atomic transition. In this regime the photons can be adiabatically eliminated. As a result their role is reduced to mediate infinite range elastic spin exchange interactions between the atoms, with strength set by χ . The transverse field was engineered by pumping the cavity with a laser that generated, at resonance, Rabi flopping at frequency B . The longitudinal field was simultaneously introduced by detuning the pump laser by a frequency δ from the atomic transition.

For this system the time-averaged collective magnetization along \hat{z} in this case $\overline{\langle \hat{S}^z \rangle} \equiv \lim_{T \rightarrow \infty} (1/T) \int_0^T \langle \hat{S}^z(t) \rangle dt$ serves as an ideal order parameter as discussed in section 2.1. This is equivalent to equation (5) up to an overall unitary rotation that maps $S^x \leftrightarrow S^z$. However, in the experiment additional inhomogeneities and other technical imperfections damped the oscillation in the paramagnetic phase. Under these conditions the magnetization $\langle \hat{S}^z \rangle$ after $4 \mu\text{s}$ of time evolution served as a proxy of the long-term time-averaged magnetization. The experiment observed the DPT in $\langle \hat{S}^z \rangle$ at $\delta = 0$ using B as the control parameter and demonstrated the expected scaling with atom number. The DPT was also probed by varying the longitudinal field for a fixed value of the drive strength B and by observing a sharp change of behavior of the order parameter at the critical point. The robustness of the DPT was demonstrated by the symmetric response of the magnetization for interaction shift $\chi N \leftrightarrow -\chi N$. The experiment also explored the DPT as a function of the initial state. It tracked the variation of the critical point as the system was initialized in a coherent spin state pointing along different directions.

The same LMG Hamiltonian was implemented in an experiment operating with a thermal gas of $N = 10^4 - 10^5$ bosonic ^{87}Rb atoms in a 3D harmonic trap using two hyperfine states to set a spin-1/2 degree of freedom [59]. The two internal states were coupled by laser fields tuned to one of the blue side transitions, i.e. the laser not only generated a spin flip

but at the same time increased one of the motional quantum numbers in the trap by one unit. As a consequence the two coupled states had different motional eigenstates. Even though the interactions in this system are contact interactions during s -wave collisions, effective long range interactions can emerge in the system due to the delocalized nature of the single particle orbitals when operating in the collisionless regime. This is achieved when the trapping potential is much larger than the interaction strength [295, 296]. In this regime it can be assumed, to an excellent approximation, that each atom is fixed in a mode-space lattice with sites set by the single-particle eigenstates of the 3D harmonic trap. The only relevant process between two colliding atoms is to either remain in the same internal states or to exchange them. Even when dealing with bosonic samples restricting the Hilbert space to include only empty or singly-occupied lattice sites is appropriate when the gas temperature is above quantum degeneracy. Under these conditions the contact interaction term can be mapped to a spin-1/2 long-range XXZ spin model where the indices i, j run over the occupied mode-space lattice sites,

$$H_{\text{int}} = \frac{1}{4} \sum_{ij} J_{ij} \vec{\sigma}_i \cdot \vec{\sigma}_j + \frac{1}{4} \sum_{ij} \chi_{ij} \hat{\sigma}_i^z \hat{\sigma}_j^z + \sum_i B_i \hat{\sigma}_i^z. \quad (49)$$

The XXZ couplings depend on the different scattering lengths of the atoms and on the overlap integral of the corresponding 3D harmonic oscillator wave functions. The use of a blue sideband transition that generate mismatched motional states of the coupled internal levels allowed the experiment to generate a finite χ_{ij} . Otherwise it would have been negligible for Rb if the experiment had used a carrier transition (when the laser only flips the spin). In addition to the interaction term, the interrogating laser generated transverse and longitudinal fields with strengths set by the Rabi frequency, and the laser detuning from the blue sideband transition.

To observe the DPT the atoms were initialized in the $|\downarrow\rangle$ state. For this initial state, the exchange interaction term not only becomes a constant of motion but also locks the atoms into the fully collective spin manifold reducing the XXZ Hamiltonian to a LMG model with coupling constants replaced by their averaged value. Similar to the cavity experiment, instead of direct measurements of the long-time-averaged excitation which is inevitably limited by technical issues, the order parameter was set to be the excitation fraction at a probe time 0.5 s. The entire phase diagram was obtained by scanning the two-photon detuning δ for fixed transverse field B and by varying interactions using different atomic densities (see figure 10(c)).

We note that there is a direct connection between the DPT in the LMG model and the phenomena of macroscopic self-trapping and Josephson tunneling observed in coupled atomic condensates [297–300] and in solid state polariton condensates [301]. In this context the ferromagnetic and paramagnetic dynamical phases can be related to the self-trapped and tunneling phases respectively in the corresponding systems. Under this correspondence one can say that self-trapping experiments done years back did observe indications of the

distinct dynamical behaviors. However, they did not provide a full characterization of the DPTs.

DPT in Richardson–Gaudin models. A similar mapping of the single-particle eigenstates of the harmonic trap onto a lattice in mode space was used in a trapped gas of 10^4 ultracold fermionic potassium atoms. In this case the experiment observed a DPT predicted to exist in quenched s -wave superconductors described by Richardson–Gaudin models as explained in section 3. As we will discuss below this DPT has only been indirectly observed in real superconductors (see section 5.1). The model that was simulated in the experiment [123] was a collective Heisenberg model, in which the non-local spin–spin couplings J_{ij} compete with an inhomogeneous axial field set by h_i :

$$\hat{H} = \sum_i h_i \hat{S}_i^z - \sum_{i,j} J_{ij} \vec{S}_i \cdot \vec{S}_j. \quad (50)$$

The inhomogeneous axial field in mode space was generated by different harmonic confinement potentials experienced by the two internal hyperfine levels of ^{40}K . The strength of the inhomogeneity was tuned in two ways. Using the polarization of one of the laser beams forming the optical trap one change the trapping frequency in a spin dependent manner. One can also change the temperature and therefore the distribution of the modes occupied by the atoms. Interatomic collisions were used to generate the exchange term. Due to the extended nature of the motional wave functions, the J_{ij} were again long-ranged. The mode-dependent coupling factor J_{ij} was controlled by tuning the s -wave scattering length of the colliding atoms using a magnetic Feshbach resonance [302]. The expected critical behavior was observed in the experiment as a function of the mean and thermally averaged interaction strength $J = \langle \sum_{i,j} J_{ij} / N^2 \rangle_T$ and the axial field inhomogeneity $\tilde{h} = \langle \sqrt{\sum_i h_i^2 / N - (\sum_i h_i / N)^2} \rangle_T$ where the indices i, j run over N populated modes (see figure 10(d)).

In the ‘all-to-all’ limit, in which coupling constants are replaced by their mean value, $J_{ij} \rightarrow J$, the Hamiltonian becomes integrable and maps to the Bardeen–Cooper–Schrieffer Hamiltonian for fermionic superconductors expressed in terms of Anderson pseudospins discussed in equation (12) with $h_i \rightarrow 2\varepsilon_i$ and $J \rightarrow G$. Note that at the level of mean field the extra term $(\hat{S}^z) \rightarrow 2\hat{S}^z \langle \hat{S}^z \rangle$ acts as a simple collective rotation along z which does not modify the dynamics since $\langle \hat{S}^z \rangle$ is conserved. Moreover this term can be removed by choosing an initial condition with $\langle \hat{S}^z \rangle = 0$.

Using the Lax analysis explained in section 3.2, it is possible to obtain the dynamical phases of this model, characterized by the total transverse magnetization $S(t) = 2\sqrt{\langle \hat{S}^x \rangle^2 + \langle \hat{S}^y \rangle^2} / N$. The initial conditions accessible in experiment, corresponding to a spin polarized state pointing along the x direction of the Bloch sphere is very similar to the simple example discussed in section 3.3, but in 3D and with a different dispersion. In this case there is a DPT between the so called ‘phase I’ below a critical coupling strength J_c where the order parameter quick decays to zero and ‘phase II’ above J_c where the order parameter $S(t)$ exhibits transient oscillations

at the frequency $2|J|S(\infty)$, which slowly damp as $S(t)$ reaches $S(\infty)$ (see equation (21)). The oscillation frequency goes to zero at J_c in a non-analytic manner.

The experimental work described in reference [123] not only fully characterized the phase diagram but in addition determined the parameter regime where the spin model was valid. The latter was explicitly demonstrated via a many-body echo sequence that fully reversed the spin Hamiltonian. Terms in the Hamiltonian such as the kinetic energy, assumed to play no role in the frozen mode approximation, were not reversed. The experiment indeed observed full reversibility of the dynamics in the collisionless regime where the spin model is expected to be valid, and non-reversibility otherwise.

Although the phase diagram was characterized for the first time in reference [123], the understanding that exchange interactions can stabilize coherence in a very useful way had been demonstrated experimentally years before. The experiments were carried out using thermal Rb atoms, which feature a very similar Hamiltonian to the potassium fermionic gas. Deep in phase II (dense sample) a coherence time up to 58 s was observed, while in phase I (dilute conditions) the coherence time decreased to at most 3 s [303–305]. We point out that while the Toronto experiment reference [123] was able to observe the DPT between phase I and phase II, by simulating a spin model, phase III has not been observed yet.

Fermionic ultracold atomic gas experiments that can actually take advantage of the Fermi statistics of the atoms instead of an indirect mapping to Anderson pseudospins in principle are an ideal platform for the observation of the full dynamical phase diagram. However, unfortunately it has remained a challenge in cold atom experiments to reach conditions required to see BCS pairing. This is because both thermal and quantum fluctuations play a crucial role for quenches from the normal state for systems with a finite number N of Anderson pseudospins. Moreover, the control and manipulation of interactions in these systems, specially for the p -wave case, typically require Feshbach resonances. The latter unfortunately introduce strong three-body processes which make the gas unstable and destroy the desired pairing processes [113, 167–169].

Future progress on cooling these systems might allow new opportunities in that direction. An alternative option is the use of an ensemble of cold atoms trapped in an optical cavity. In this case effective Cooper pairs can be encoded in internal states of the atoms and attractive interactions between the internal levels can be realized via the exchange of virtual photons in the cavity. The control of the interaction strength via the parameters of the optical cavity combined with the tunability of the dispersion relation of the effective Cooper pairs via Stark shifts should allow for the near term exploration of the full dynamical phase diagram of the BCS model, as a function of system parameters and the prepared initial state. Reference [124] discusses a way to prepare the simple toy model discussed in section 3.3 in a cavity setup.

DPT in multi-level systems. Beyond two-level systems, DPTs have been also observed in spinor Bose–Einstein condensates (BEC) made of $N \sim 10^5$ ^{23}Na atoms using the three Zeeman states of the lowest hyperfine level, $m_F = 1, 0, -1$ [293, 294] (see figure 10(e)). The experiment operated in the

regime where to an excellent approximation atoms remained frozen in their single particle motional levels. Motional relaxation was only an issue at long times. Because all atoms in the BEC share the same motional level, in this limit the bosonic statistics enforces atoms to remain in the fully symmetric spin manifold. The Hamiltonian that describes the internal dynamics in the experiment therefore becomes a fully collective spin model:

$$H = \frac{c_2}{2N} \hat{S} \cdot \hat{S} + q \sum_i (\hat{S}_{z,i}^2). \quad (51)$$

The first term encapsulates the spin dependent interactions, which are infinite-range in mode space even though the atomic collision interaction by itself is fully local. The second term describes a quadratic Zeeman field q experienced by the atoms from a real magnetic field plus a microwave dressing field. Here $\hat{S}_{z,i}$ is the spin-1 operator for the i th particle along the z component of the Bloch sphere.

To observe the DPT, the experiment prepared the majority of the atoms in the $m_F = 0$ level and then monitored the number of atoms remaining in that level $N_0(t)$ as a function of time for different values of the control parameter q . The order parameter used in the experiment was the a quantity $A_{\text{dip}} \equiv 1 - N_0(t_{\text{dip}})$, with $N_0(t_{\text{dip}})$ being the value of $N_0(t)$ at the first dip of the spin oscillations. For positive $q > 0$, A_{dip} was observed to remain almost at 0. Across the DPT transition point of $q_c = 0$, A_{dip} was seen to jump to finite value which decreased linearly with $|q|$ when $q < 0$ (see figure 10(e)). Further work in this system was able to connect the DPT to an equilibrium phase transition not for the ground state but for the highest energy level in a subspace with zero spin magnetization [294].

Besides observations of DPT which happened at relatively short times, a follow-up experiment using Rb atoms instead of Na atoms observed another complementary type of universal non-equilibrium behavior associated with the emergence of non-thermal fixed points [227]. This type of behavior was observed at intermediate times satisfying two conditions: (i) times that are long enough to allow the frozen mode approximation used to observe the DPT to become invalid. In this case the system loses the information about the initial conditions due to motional relaxation. (ii) Times that are not so long that lead the system to reach a quasi-stationary or an equilibrium situation. In this intermediate regime it was observed that the system develops a universal scaling behavior in time and space. Physically the emergence of non-thermal fixed points have been attributed to the transport of an emergent collective conserved quantity toward low momentum scales. A similar behavior has been observed by another experiment in a single-component Bose gas [4, 228]. In both of these experiments it was experimentally confirmed (by preparing different initial conditions and obtaining the same scaling behavior) that the observed non-thermal scaling phenomenon involved no fine-tuning of parameters.

It is clear from all the discussion presented above that ultra-cold atomic system are opening fantastic opportunities to probe DPTs and even more general non-equilibrium universal phenomena in controllable settings. While most of the observations so far have been guided by theory in conditions

where either a mean field analysis is sufficient, or when exact calculations are possible, soon experiments will enter regimes intractable to theory. This may lead to the discovery of new forms of non-equilibrium phenomena not yet predicted by theory, pushing the field into even more exciting directions.

6. Conclusions and perspectives

In this work we reviewed DPTs occurring in the large N , \mathcal{N} , or d limit of a broad variety of models ranging from statistical mechanics (Ising models, ϕ^4 field theories) to condensed matter (Richardson–Gaudin magnets, strongly correlated fermions). We have also discussed numerous experimental platforms where the dynamics of these models can be realized (section 5). We have illustrated those regimes where experiments are well fitted by the theory presented in sections 2 and 3, as well as the limits where descriptions beyond collision-less regimes may instead be required to describe experiments. Such platforms include trapped ions, cavity QED systems, and ultracold Bose and Fermi systems. They can be employed to demonstrate a broad variety of universality classes of DPTs in isolated quantum systems, and possibly study in the near future operational regimes where DPTs require a full quantum mechanical treatment and cannot be captured by an effective semi-classical description.

There are promising avenues for the future of pre-thermal collisionless DPTs. For instance, Rydberg simulators have been recently shown to be capable to access long-lived athermal states beyond the conventional pre-thermal paradigm [306, 307], referred to as quantum scars [308] and defying the eigenstate thermalization hypothesis. This could be potentially employed in the near future to study forms of DPTs which cannot be characterized within a simple semi-classical description. Recent implementations of models with a fragmented Hilbert space using ultracold fermions [309] and Rydberg atoms [310] suggest similar lines of investigation in that context.

Another exciting direction is the understanding of the fate of the DPTs in systems where quantum fluctuations cannot be ignored. At the theoretical level, it will be crucial to derive new types of order parameters that can describe the distinct dynamical behavior even when quantum effects start to play a role. The order parameters discussed in this review will decay in the ordered phase whenever quantum effects start to play a significant role. Can a properly defined order parameter genuinely characterize the underlying phases associated with a DPT? It is likely there is an affirmative answer to this question. Feasible candidates are observables that measure the interaction energy of the evolving system and therefore involve at the least two-body correlators, as illustrated by the case of the $O(\mathcal{N} \rightarrow \infty)$ model in section 2.3. Closely connected with this question is the robustness of the topological order in non-trivial phases in the presence of quantum effects. Is there a redefinition of the winding number that remains nonzero even in the presence of strong quantum fluctuations?

One of the most important goals of modern quantum science is to learn how to control and entangle many-body systems, and how to use it as a resource in quantum technologies,

such as for the development of improved quantum sensors, materials and technologies. A big limitation in this direction comes from the fact that entangled states are difficult to prepare and maintain, since noise and decoherence rapidly collapse them into classical statistical mixtures. In the context of DPTs it is likely that the same parameter regime where interactions stabilize a finite order parameter is also promising for a generation of robust entanglement. In fact, recent investigations have pointed out the generation of robust spin squeezing in phase II [311]. Understanding the dynamics of entanglement across a DPT is a fascinating new direction [312, 313]. Is entanglement maximum at the critical point? What is the best entanglement witness for the state across the DPT?

While all these questions are theoretically extremely challenging, recent experimental advances in synthesizing, manipulating and detecting quantum many-body systems are bringing quantum control into a new paradigm [307, 314]. It is likely that near term experiments will stimulate new theoretical methods, which may provide unprecedented insight into novel classes of DPTs where strong quantum fluctuations play a key role in shaping the dynamical phases. We hope this review will encourage future work and investigations in this direction.

Acknowledgments

This project has been supported by the Deutsche Forschungsgemeinschaft (DFG, German Research Foundation) - TRR 288 - 422213477 (project B09), TRR 306 QuCoLiMa ('Quantum Cooperativity of Light and Matter'), Project-ID 429529648 (project D04), ERC (starting Grant No. 716648), AFOSR (FA9550-18-1-0319, FA9550-19-1-027), NSF QLCI OMA-2016244, NSF Phys-1734006, DOE National Quantum Information Science Research Centers (Quantum Systems Accelerator), and NIST.

Data availability statement

No new data were created or analysed in this study.

References

- [1] Henkel M, Hinrichsen H and Lübeck S 2008 *Non-Equilibrium Phase Transitions* vol 1 and 2 (Berlin: Springer)
- [2] Berges J 2005 Introduction to nonequilibrium quantum field theory *AIP Conf. Proc.* **739** 3–62
- [3] Gring M *et al* 2012 Relaxation and prethermalization in an isolated quantum system *Science* **337** 1318–22
- [4] Langen T, Gasenzer T and Schmiedmayer J 2016 Prethermalization and universal dynamics in near-integrable quantum systems *J. Stat. Mech.* **064009**
- [5] Kollar M, Alexander Wolf F and Eckstein M 2011 Generalized Gibbs ensemble prediction of prethermalization plateaus and their relation to nonthermal steady states in integrable systems *Phys. Rev. B* **84** 054304
- [6] Essler F H L, Kehrein S, Manmana S R and Robinson N J 2014 Quench dynamics in a model with tuneable integrability breaking *Phys. Rev. B* **89** 165104
- [7] Bertini B, Essler F H L, Groha S and Robinson N J 2015 Prethermalization and thermalization in models with weak integrability breaking *Phys. Rev. Lett.* **115** 180601

- [8] Marcuzzi M, Marino J, Gambassi A and Silva A 2016 Prethermalization from a low-density Holstein–Primakoff expansion *Phys. Rev. B* **94** 214304
- [9] Bertini B, Essler F H L, Groha S and Robinson N J 2016 Thermalization and light cones in a model with weak integrability breaking *Phys. Rev. B* **94** 245117
- [10] Durnin J, Bhaseen M J and Doyon B 2021 Nonequilibrium dynamics and weakly broken integrability *Phys. Rev. Lett.* **127** 130601
- [11] Lin C-J and Motrunich O I 2017 Quasiparticle explanation of the weak-thermalization regime under quench in a nonintegrable quantum spin chain *Phys. Rev. A* **95** 023621
- [12] Heyl M, Polkovnikov A and Kehrein S 2013 Dynamical quantum phase transitions in the transverse-field Ising model *Phys. Rev. Lett.* **110** 135704
- [13] Jurcevic P *et al* 2017 Direct observation of dynamical quantum phase transitions in an interacting many-body system *Phys. Rev. Lett.* **119** 080501
- [14] Heyl M 2019 Dynamical quantum phase transitions: a brief survey *Europhys. Lett.* **125** 26001
- [15] Berges J, Rothkopf A and Schmidt J 2008 Nonthermal fixed points: effective weak coupling for strongly correlated systems far from equilibrium *Phys. Rev. Lett.* **101** 041603
- [16] Nowak B, Sexty D and Gasenzer T 2011 Superfluid turbulence: nonthermal fixed point in an ultracold Bose gas *Phys. Rev. B* **84** 020506
- [17] Prüfer M, Kunkel P, Strobel H, Lannig S, Linnemann D, Schmied C-M, Berges J, Gasenzer T and Oberthaler M K 2018 Observation of universal dynamics in a spinor Bose gas far from equilibrium *Nature* **563** 217–20
- [18] Erne S, Bücken R, Gasenzer T, Berges J and Schmiedmayer J 2018 Universal dynamics in an isolated one-dimensional Bose gas far from equilibrium *Nature* **563** 225–9
- [19] Eigen C, Glidden J A P, Lopes R, Cornell E A, Smith R P and Hadzibabic Z 2018 Universal prethermal dynamics of Bose gases quenched to unitarity *Nature* **563** 221–4
- [20] Schmied C-M, Mikheev A N and Gasenzer T 2019 Non-thermal fixed points: universal dynamics far from equilibrium *Int. J. Mod. Phys. A* **34** 1941006
- [21] Haken H 1975 Cooperative phenomena in systems far from thermal equilibrium and in nonphysical systems *Rev. Mod. Phys.* **47** 67–121
- [22] Zurek W H 1996 Cosmological experiments in condensed matter systems *Phys. Rep.* **276** 177–221
- [23] Strogatz S 2003 *Sync: The Emerging Science of Spontaneous Order* (New York: Hyperion)
- [24] Chandrasekhar S 1968 *Hydrodynamic and Hydromagnetic Stability* (Oxford: Clarendon)
- [25] Chakrabarti C G, Ghosh S and Bhadra S 1995 Non-equilibrium thermodynamics of Lotka–Volterra ecosystems: stability and evolution *J. Biol. Phys.* **21** 273–84
- [26] Glansdorff P and Prigogine I 1971 *Thermodynamic Theory of Structure, Stability and Fluctuations* (New York: Wiley)
- [27] Davies P C W, Demetrius L and Tuszynski J A 2011 Cancer as a dynamical phase transition *Theor. Biol. Med. Model.* **8** 30
- [28] Landau L D and Lifshitz E M 1969 *Statistical Physics* pp 237–41
- [29] Hohenberg P C and Krehov A P 2015 An introduction to the Ginzburg–Landau theory of phase transitions and nonequilibrium patterns *Phys. Rep.* **572** 1–42
- [30] Berges J, Borsányi S and Wetterich C 2004 Prethermalization *Phys. Rev. Lett.* **93** 142002
- [31] Zinn-Justin J 1989 *Quantum Field Theory and Critical Phenomena* (Oxford: Clarendon)
- [32] Amit D J and Martin-Mayor V 2005 *Field Theory, the Renormalization Group, and Critical Phenomena* 3rd edn (Singapore: World Scientific)
- [33] Cardy J and Täuber U C 1996 Theory of branching and annihilating random walks *Phys. Rev. Lett.* **77** 4780–3
- [34] Hohenberg P C and Halperin B I 1977 Theory of dynamic critical phenomena *Rev. Mod. Phys.* **49** 435–79
- [35] Täuber U C 2014 *Critical Dynamics: A Field Theory Approach to Equilibrium and Non-Equilibrium Scaling Behavior* (Cambridge: Cambridge University Press)
- [36] Kamenev A 2011 *Field Theory of Non-Equilibrium Systems* (Cambridge: Cambridge University Press)
- [37] Gagel P, Orth P P and Schmalian J 2014 Universal postquench prethermalization at a quantum critical point *Phys. Rev. Lett.* **113** 220401
- [38] Sieberer L M, Buchhold M and Diehl S 2016 Keldysh field theory for driven open quantum systems *Rep. Prog. Phys.* **79** 096001
- [39] Glick A J, Lipkin H J and Meshkov N 1965 Validity of many-body approximation methods for a solvable model: III. Diagram summations *Nucl. Phys.* **62** 211–24
- [40] Lipkin H J, Meshkov N and Glick A J 1965 Validity of many-body approximation methods for a solvable model: I. Exact solutions and perturbation theory *Nucl. Phys.* **62** 188–98
- [41] Meshkov N, Glick A J and Lipkin H J 1965 Validity of many-body approximation methods for a solvable model: II. Linearization procedures *Nucl. Phys.* **62** 199–210
- [42] Pan F and Draayer J P 1999 Analytical solutions for the LMG model *Phys. Lett. B* **451** 1–10
- [43] Dukelsky J, Pittel S and Sierra G 2004 Colloquium: exactly solvable Richardson–Gaudin models for many-body quantum systems *Rev. Mod. Phys.* **76** 643–62
- [44] Botet R and Jullien R 1983 Large-size critical behavior of infinitely coordinated systems *Phys. Rev. B* **28** 3955–67
- [45] Dusuel S and Vidal J 2005 Finite-size scaling exponents and entanglement in the two-level BCS model *Phys. Rev. A* **71** 060304
- [46] Ribeiro P, Vidal J and Mosseri R 2007 Thermodynamical limit of the Lipkin–Meshkov–Glick model *Phys. Rev. Lett.* **99** 050402
- [47] Ribeiro P, Vidal J and Mosseri R 2008 Exact spectrum of the Lipkin–Meshkov–Glick model in the thermodynamic limit and finite-size corrections *Phys. Rev. E* **78** 021106
- [48] Defenu N, Donner T, Macri T, Pagano G, Ruffo S and Trombettoni A 2021 Long-range interacting quantum systems (arXiv:2109.01063)
- [49] Latorre J I, Orús R, Rico E and Vidal J 2005 Entanglement entropy in the Lipkin–Meshkov–Glick model *Phys. Rev. A* **71** 064101
- [50] Orús R, Dusuel S and Vidal J 2008 Equivalence of critical scaling laws for many-body entanglement in the Lipkin–Meshkov–Glick model *Phys. Rev. Lett.* **101** 025701
- [51] Maity S, Bhattacharya U and Dutta A 2020 One-dimensional quantum many body systems with long-range interactions *J. Phys. A: Math. Gen.* **53** 013001
- [52] Moeckel M and Kehrein S 2008 Interaction quench in the Hubbard model *Phys. Rev. Lett.* **100** 175702
- [53] Marcuzzi M, Marino J, Gambassi A and Silva A 2013 Prethermalization in a nonintegrable quantum spin chain after a quench *Phys. Rev. Lett.* **111** 197203
- [54] Nessi N, Iucci A and Cazalilla M A 2014 Quantum quench and prethermalization dynamics in a two-dimensional Fermi gas with long-range interactions *Phys. Rev. Lett.* **113** 210402
- [55] Mallayya K, Rigol M and De Roeck W 2019 Prethermalization and thermalization in isolated quantum systems *Phys. Rev. X* **9** 021027
- [56] Leroze A, Žunkovič B, Marino J, Gambassi A and Silva A 2019 Impact of nonequilibrium fluctuations on prethermal dynamical phase transitions in long-range interacting spin chains *Phys. Rev. B* **99** 045128
- [57] Zhang J, Pagano G, Hess P W, Kyprianidis A, Becker P, Kaplan H, Gorshkov A V, Gong Z X and Monroe C 2017 Observation of a many-body dynamical phase transition with a 53-qubit quantum simulator *Nature* **551** 601–4

- [58] Muniz J A, Barberena D, Lewis-Swan R J, Young D J, Cline J R K, Rey A M and Thompson J K 2020 Exploring dynamical phase transitions with cold atoms in an optical cavity *Nature* **580** 602–7
- [59] Chu A, Will J, Arlt J, Klempt C and Rey A M 2020 Simulation of xxz spin models using sideband transitions in trapped bosonic gases *Phys. Rev. Lett.* **125** 240504
- [60] Polkovnikov A 2010 Phase space representation of quantum dynamics *Ann. Phys., NY* **325** 1790–852
- [61] Das A, Sengupta K, Sen D and Chakrabarti B K 2006 Infinite-range Ising ferromagnet in a time-dependent transverse magnetic field: quench and ac dynamics near the quantum critical point *Phys. Rev. B* **74** 144423
- [62] Kelly S P, Timmermans E and Tsai S-W 2019 Detecting macroscopic indefiniteness of cat states in bosonic interferometers *Phys. Rev. A* **100** 032117
- [63] Kelly S P, Timmermans E and Tsai S-W 2020 Thermalization and its breakdown for a large nonlinear spin *Phys. Rev. A* **102** 052210
- [64] Sciolla B and Biroli G 2011 Dynamical transitions and quantum quenches in mean-field models *J. Stat. Mech.* **P11003**
- [65] Defenu N, Enss T, Kastner M and Morigi G 2018 Dynamical critical scaling of long-range interacting quantum magnets *Phys. Rev. Lett.* **121** 240403
- [66] Caneva T, Fazio R and Santoro G E 2008 Adiabatic quantum dynamics of the Lipkin–Meshkov–Glick model *Phys. Rev. B* **78** 104426
- [67] Leroose A, Marino J, Žunkovič B, Gambassi A and Silva A 2018 Chaotic dynamical ferromagnetic phase induced by nonequilibrium quantum fluctuations *Phys. Rev. Lett.* **120** 130603
- [68] Leroose A, Marino J, Gambassi A and Silva A 2019 Prethermal quantum many-body Kapitza phases of periodically driven spin systems *Phys. Rev. B* **100** 104306
- [69] Žunkovič B, Silva A and Fabrizio M 2016 Dynamical phase transitions and Loschmidt echo in the infinite-range XY model *Phil. Trans. R. Soc. A* **374** 20150160
- [70] Gambassi A and Calabrese P 2011 Quantum quenches as classical critical films *Europhys. Lett.* **95** 66007
- [71] Sartori A, Marino J, Stringari S and Recati A 2015 Spin-dipole oscillation and relaxation of coherently coupled Bose–Einstein condensates *New J. Phys.* **17** 093036
- [72] Žunkovič B, Heyl M, Knap M and Silva A 2018 Dynamical quantum phase transitions in spin chains with long-range interactions: merging different concepts of nonequilibrium criticality *Phys. Rev. Lett.* **120** 130601
- [73] Halimeh J C, Zauner-Stauber V, McCulloch I P, De Vega I, Schollwöck U and Kastner M 2017 Prethermalization and persistent order in the absence of a thermal phase transition *Phys. Rev. B* **95** 024302
- [74] Haegeman J, Lubich C, Oseledets I, Vandereycken B and Verstraete F 2016 Unifying time evolution and optimization with matrix product states *Phys. Rev. B* **94** 165116
- [75] Lang J, Frank B and Halimeh J C 2018 Concurrence of dynamical phase transitions at finite temperature in the fully connected transverse-field Ising model *Phys. Rev. B* **97** 174401
- [76] Titum P and Maghrebi M F 2020 Nonequilibrium criticality in quench dynamics of long-range spin models *Phys. Rev. Lett.* **125** 040602
- [77] Leroose A and Pappalardi S 2020 Origin of the slow growth of entanglement entropy in long-range interacting spin systems *Phys. Rev. Res.* **2** 012041
- [78] Halimeh J C, Van Damme M, Guo L, Lang J and Hauke P 2021 Dynamical phase transitions in quantum spin models with antiferromagnetic long-range interactions *Phys. Rev. B* **104** 115133
- [79] Piccitto G and Silva A 2019 Crossover from fast to slow dynamics in a long range interacting Ising chain *J. Stat. Mech.* **094017**
- [80] Defenu N, Enss T and Halimeh J C 2019 Dynamical criticality and domain-wall coupling in long-range Hamiltonians *Phys. Rev. B* **100** 014434
- [81] Campbell S 2016 Criticality revealed through quench dynamics in the Lipkin–Meshkov–Glick model *Phys. Rev. B* **94** 184403
- [82] Dutta A and Bhattacharjee J K 2001 Phase transitions in the quantum Ising and rotor models with a long-range interaction *Phys. Rev. B* **64** 184106
- [83] Campa A, Dauxois T and Ruffo S 2009 Statistical mechanics and dynamics of solvable models with long-range interactions *Phys. Rep.* **480** 57–159
- [84] Maghrebi M F, Gong Z-X, Foss-Feig M and Gorshkov A V 2016 Causality and quantum criticality in long-range lattice models *Phys. Rev. B* **93** 125128
- [85] Polkovnikov A, Sengupta K, Silva A and Vengalattore M 2011 Colloquium: nonequilibrium dynamics of closed interacting quantum systems *Rev. Mod. Phys.* **83** 863–83
- [86] Barthel T and Schollwöck U 2008 Dephasing and the steady state in quantum many-particle systems *Phys. Rev. Lett.* **100** 100601
- [87] Rigol M, Dunjko V and Olshanii M 2008 Thermalization and its mechanism for generic isolated quantum systems *Nature* **452** 854–8
- [88] Sachdev S 2011 *Quantum Phase Transitions* (Cambridge: Cambridge University Press)
- [89] Yin S and Jian S-K 2021 Fermion-induced dynamical critical point *Phys. Rev. B* **103** 125116
- [90] Jian S-K, Yin S and Swingle B 2019 Universal prethermal dynamics in Gross–Neveu–Yukawa criticality *Phys. Rev. Lett.* **123** 170606
- [91] Chandran A, Nandori A, Gubser S S and Sondhi S L 2013 Equilibration and coarsening in the quantum $o(n)$ model at infinite n *Phys. Rev. B* **88** 024306
- [92] Maraga A, Chiochetta A, Mitra A and Gambassi A 2015 Aging and coarsening in isolated quantum systems after a quench: exact results for the quantum $O(n)$ model with $n \rightarrow \infty$ *Phys. Rev. E* **92** 042151
- [93] Berges J, Tetradis N and Wetterich C 2002 Non-perturbative renormalization flow in quantum field theory and statistical physics *Phys. Rep.* **363** 223–386
- [94] Sotiriadis S and Cardy J 2010 Quantum quench in interacting field theory: a self-consistent approximation *Phys. Rev. B* **81** 134305
- [95] Sciolla B and Biroli G 2013 Quantum quenches, dynamical transitions, and off-equilibrium quantum criticality *Phys. Rev. B* **88** 201110
- [96] Smacchia P, Knap M, Demler E and Silva A 2015 Exploring dynamical phase transitions and prethermalization with quantum noise of excitations *Phys. Rev. B* **91** 205136
- [97] Chiochetta A, Tavora M, Gambassi A and Mitra A 2016 Short-time universal scaling and light-cone dynamics after a quench in an isolated quantum system in d spatial dimensions *Phys. Rev. B* **94** 134311
- [98] Halimeh J C and Maghrebi M F 2021 Quantum aging and dynamical universality in the long-range o model *Phys. Rev. E* **103** 052142
- [99] Aarts G, Bonini G F and Wetterich C 2000 Exact and truncated dynamics in nonequilibrium field theory *Phys. Rev. D* **63** 025012
- Sondhi S L, Girvin S M, Carini J P and Shahar D 1997 Continuous quantum phase transitions *Rev. Mod. Phys.* **69** 315–33
- Vojta M 2003 Quantum phase transitions *Rep. Prog. Phys.* **66** 2069

- [100] Chiocchetta A, Tavora M, Gambassi A and Mitra A 2015 Short-time universal scaling in an isolated quantum system after a quench *Phys. Rev. B* **91** 220302
- [101] Janssen H-K, Schaub B and Schmittmann B 1989 New universal short-time scaling behaviour of critical relaxation processes *Z. Phys. B* **73** 539–49
- [102] Calabrese P and Gambassi A 2005 Ageing properties of critical systems *J. Phys. A: Math. Gen.* **38** R133
- [103] Chiocchetta A, Gambassi A, Diehl S and Marino J 2017 Dynamical crossovers in prethermal critical states *Phys. Rev. Lett.* **118** 135701
- [104] Bray A J 1994 Theory of phase-ordering kinetics *Adv. Phys.* **43** 357–459
- [105] Biroli G 2015 Slow relaxations and non-equilibrium dynamics in classical and quantum systems (arXiv:1507.05858)
- [106] Cugliandolo L F 2015 Coarsening phenomena *C. R. Phys.* **16** 257–66
- [107] Maraga A, Smacchia P and Silva A 2016 Linear ramps of the mass in the $O(N)$ model: dynamical transition and quantum noise of excitations *Phys. Rev. B* **94** 245122
- [108] Barankov R A, Levitov L S and Spivak B Z 2004 Collective Rabi oscillations and solitons in a time-dependent BCS pairing problem *Phys. Rev. Lett.* **93** 160401
- [109] Barankov R A and Levitov L S 2006 Synchronization in the BCS pairing dynamics as a critical phenomenon *Phys. Rev. Lett.* **96** 230403
- [110] Yuzbashyan E A and Dzero M 2006 Dynamical vanishing of the order parameter in a fermionic condensate *Phys. Rev. Lett.* **96** 230404
- [111] Yuzbashyan E A, Tsyplatyev O and Altshuler B L 2006 Relaxation and persistent oscillations of the order parameter in fermionic condensates *Phys. Rev. Lett.* **96** 097005
- [112] Foster M S, Dzero M, Gurarie V and Yuzbashyan E A 2013 Quantum quench in a $p + ip$ superfluid: winding numbers and topological states far from equilibrium *Phys. Rev. B* **88** 104511
- [113] Foster M S, Gurarie V, Dzero M and Yuzbashyan E A 2014 Quench-induced Floquet topological p -wave superfluids *Phys. Rev. Lett.* **113** 076403
- [114] Alicea J 2012 New directions in the pursuit of Majorana fermions in solid state systems *Rep. Prog. Phys.* **75** 076501
- [115] Chen Q, Stajic J, Tan S and Levin K 2005 BCS–BEC crossover: from high temperature superconductors to ultracold superfluids *Phys. Rep.* **412** 1–88
- [116] Matsunaga R, Hamada Y I, Makise K, Uzawa Y, Terai H, Wang Z and Shimano R 2013 Higgs amplitude mode in the BCS superconductors $\text{Nb}_{1-x}\text{Ti}_x\text{N}$ induced by terahertz pulse excitation *Phys. Rev. Lett.* **111** 057002
- [117] Shimano R and Tsuji N 2020 Higgs mode in superconductors *Annu. Rev. Condens. Matter Phys.* **11** 103–24
- [118] Papenkort T, Axt V M and Kuhn T 2007 Coherent dynamics and pump–probe spectra of BCS superconductors *Phys. Rev. B* **76** 224522
- [119] Papenkort T, Kuhn T and Axt V M 2008 Coherent control of the gap dynamics of BCS superconductors in the nonadiabatic regime *Phys. Rev. B* **78** 132505
- [120] Krull H, Manske D, Uhrig G S and Schnyder A P 2014 Signatures of nonadiabatic BCS state dynamics in pump–probe conductivity *Phys. Rev. B* **90** 014515
- [121] Chou Y-Z, Liao Y and Foster M S 2017 Twisting Anderson pseudospins with light: quench dynamics in terahertz-pumped BCS superconductors *Phys. Rev. B* **95** 104507
- [122] Papenkort T, Kuhn T and Axt V M 2009 Nonequilibrium dynamics and coherent control of BCS superconductors driven by ultrashort THz pulses *J. Phys.: Conf. Ser.* **193** 012050
- [123] Smale S, He P, Olsen B A, Jackson K G, Sharum H, Trotzky S, Marino J, Rey A M and Thywissen J H 2019 Observation of a transition between dynamical phases in a quantum degenerate Fermi gas *Sci. Adv.* **5** eaax1568
- [124] Lewis-Swan R J, Barberena D, Cline J R K, Young D J, Thompson J K and Rey A M 2021 Cavity-QED quantum simulator of dynamical phases of a Bardeen–Cooper–Schrieffer superconductor *Phys. Rev. Lett.* **126** 173601
- [125] Yuzbashyan E A, Dzero M, Gurarie V and Foster M S 2015 Quantum quench phase diagrams of an s -wave BCS–BEC condensate *Phys. Rev. A* **91** 033628
- [126] Gurarie V and Radzihovsky L 2007 Resonantly paired fermionic superfluids *Ann. Phys., NY* **322** 2–119
- [127] Gurarie V 2009 Nonequilibrium dynamics of weakly and strongly paired superconductors *Phys. Rev. Lett.* **103** 075301
- [128] Dzero M, Khodas M and Levchenko A 2015 Amplitude modes and dynamic coexistence of competing orders in multicomponent superconductors *Phys. Rev. B* **91** 214505
- [129] Liao Y and Foster M S 2015 Spectroscopic probes of isolated nonequilibrium quantum matter: quantum quenches, Floquet states, and distribution functions *Phys. Rev. A* **92** 053620
- [130] Richardson R W and Sherman N 1964 Exact eigenstates of the pairing-force Hamiltonian *Nucl. Phys.* **52** 221–38
- [131] Richardson R W and Sherman N 1964 Pairing models of Pb^{206} , Pb^{204} and Pb^{202} *Nucl. Phys.* **52** 253–68
- [132] Gaudin M 2014 *The Bethe Wavefunction* (Cambridge: Cambridge University Press)
- [133] Dukelsky J, Pittel S and Sierra G 2004 Colloquium: exactly solvable Richardson–Gaudin models for many-body quantum systems *Rev. Mod. Phys.* **76** 643–62
- [134] Richardson R W 2002 *New Class of Solvable and Integrable Many-Body Models*
- [135] Skrypnik T 2009 Non-skew-symmetric classical r -matrices, algebraic Bethe ansatz, and Bardeen–Cooper–Schrieffer-type integrable systems *J. Math. Phys.* **50** 033504
- [136] Ibañez M, Links J, Sierra G and Zhao S-Y 2009 Exactly solvable pairing model for superconductors with $p_x + ip_y$ -wave symmetry *Phys. Rev. B* **79** 180501
- [137] Dunning C, Ibañez M, Links J, Sierra G and Zhao S-Y 2010 Exact solution of the $p + ip$ pairing Hamiltonian and a hierarchy of integrable models *J. Stat. Mech.* P08025
- [138] Rombouts S M A, Dukelsky J and Ortiz G 2010 Quantum phase diagram of the integrable $p_x + ip_y$ fermionic superfluid *Phys. Rev. B* **82** 224510
- [139] Yuzbashyan E A, Altshuler B L, Kuznetsov V B and Enolskii V Z 2005 Solution for the dynamics of the BCS and central spin problems *J. Phys. A: Math. Gen.* **38** 7831–49
- [140] Yuzbashyan E A, Altshuler B L, Kuznetsov V B and Enolskii V Z 2005 Nonequilibrium Cooper pairing in the nonadiabatic regime *Phys. Rev. B* **72** 220503
- [141] Dzero M, Yuzbashyan E A and Altshuler B L 2009 Cooper pair turbulence in atomic Fermi gases *Europhys. Lett.* **85** 20004
- [142] Chern G-W and Barros K 2019 Nonequilibrium dynamics of superconductivity in the attractive Hubbard model *Phys. Rev. B* **99** 035162
- [143] Barankov R A and Levitov L S 2007 *Excitation of the Dissipationless Higgs Mode in a Fermionic Condensate*
- [144] Yuzbashyan E A and Tsyplatyev O 2009 Dynamics of emergent Cooper pairing at finite temperatures *Phys. Rev. B* **79** 132504
- [145] Scaramazza J A, Smacchia P and Yuzbashyan E A 2019 Consequences of integrability breaking in quench dynamics of pairing Hamiltonians *Phys. Rev. B* **99** 054520
- [146] Lemonik Y and Mitra A 2017 Time-resolved spectral density of interacting fermions following a quench to a superconducting critical point *Phys. Rev. B* **96** 104506
- [147] Lemonik Y and Mitra A 2018 Model predictions for time-resolved transport measurements made near the superfluid

- critical points of cold atoms and K_3C_{60} films *Phys. Rev. Lett.* **121** 067001
- [148] Lemonik Y and Mitra A 2018 Quench dynamics of superconducting fluctuations and optical conductivity in a disordered system *Phys. Rev. B* **98** 214514
- [149] Lemonik Y and Mitra A 2019 Transport and spectral signatures of transient fluctuating superfluids in the absence of long-range order *Phys. Rev. B* **100** 094503
- [150] Oka T and Kitamura S 2019 Floquet engineering of quantum materials *Annu. Rev. Condens. Matter Phys.* **10** 387–408
- [151] Qi X-L and Zhang S-C 2011 Topological insulators and superconductors *Rev. Mod. Phys.* **83** 1057–110
- [152] Harper F, Roy R, Rudner M S and Sondhi S L 2020 Topology and broken symmetry in Floquet systems *Annu. Rev. Condens. Matter Phys.* **11** 345–68
- [153] Schrieffer J R 2018 *Theory of Superconductivity* (Boca Raton, FL: CRC Press)
- [154] Anderson P W 1958 Random-phase approximation in the theory of superconductivity *Phys. Rev.* **112** 1900
- [155] Instead of an N -fold spin product (spin coherent) state, one can also consider a state with $P \leq N$ ‘blocked’ levels. These are states that possess a single fermion occupying one state of a Cooper pair. For the reduced BCS Hamiltonian in equation (12), blocked levels completely decouple from the time-evolution of the pseudospins (which are superpositions of doubly empty and occupied states of a Cooper pair)
- [156] Altman E, Demler E and Lukin M D 2004 Probing many-body states of ultracold atoms via noise correlations *Phys. Rev. A* **70** 013603
- [157] Fölling S, Gerbier F, Widera A, Mandel O, Gericke T and Bloch I 2005 Spatial quantum noise interferometry in expanding ultracold atom clouds *Nature* **434** 481–4
- [158] Rom T, Best T, van Oosten D, Schneider U, Fölling S, Paredes B and Bloch I 2006 Free fermion antibunching in a degenerate atomic Fermi gas released from an optical lattice *Nature* **444** 733–6
- [159] Stahl C and Eckstein M 2019 Noise correlations in time- and angle-resolved photoemission spectroscopy *Phys. Rev. B* **99** 241111
- [160] Volkov A F and Kogan S M 1974 Collisionless relaxation of the energy gap in superconductors *JETP* **38** 1018
Volkov A F and Kogan S M 1973 *Zh. Eksp. Teor. Fiz.* **65** 2038 (Russian original)
- [161] Peronaci F, Schiró M and Capone M 2015 Transient dynamics of d -wave superconductors after a sudden excitation *Phys. Rev. Lett.* **115** 257001
- [162] Zhang X, Gurarie V, and Foster M S unpublished
- [163] Dzero M, Yuzbashyan E A, Altshuler B L and Coleman P 2007 Spectroscopic signatures of nonequilibrium pairing in atomic Fermi gases *Phys. Rev. Lett.* **99** 160402
- [164] Kennes D M, Wilner E Y, Reichman D R and Millis A J 2017 Nonequilibrium optical conductivity: general theory and application to transient phases *Phys. Rev. B* **96** 054506
- [165] Yuzbashyan E A 2008 Normal and anomalous solitons in the theory of dynamical Cooper pairing *Phys. Rev. B* **78** 184507
- [166] Mootz M, Wang J and Perakis I E 2020 Lightwave terahertz quantum manipulation of nonequilibrium superconductor phases and their collective modes *Phys. Rev. B* **102** 054517
- [167] Zhang J *et al* 2004 p -wave Feshbach resonances of ultracold ^6Li *Phys. Rev. A* **70** 030702
- [168] Jona-Lasinio M, Pricoupenko L and Castin Y 2008 Three fully polarized fermions close to a p -wave Feshbach resonance *Phys. Rev. A* **77** 043611
- [169] Levinsen J, Cooper N R and Gurarie V 2008 Stability of fermionic gases close to a p -wave Feshbach resonance *Phys. Rev. A* **78** 063616
- [170] Tinkham M 2004 *Introduction to Superconductivity* *Dover Books on Physics* 2nd edn (New York: Dover)
- [171] Nayak C, Simon S H, Stern A, Freedman M and Das Sarma S 2008 Non-abelian anyons and topological quantum computation *Rev. Mod. Phys.* **80** 1083–159
- [172] Volovik G E 2003 *The Universe in a Helium Droplet* *International Series of Monographs on Physics* (Oxford: Clarendon)
- [173] Mizushima T, Tsutsumi Y, Kawakami T, Sato M, Ichioka M and Machida K 2016 Symmetry-protected topological superfluids and superconductors—from the basics to ^3He — *J. Phys. Soc. Japan* **85** 022001
- [174] D’Alessio L and Rigol M 2015 Dynamical preparation of Floquet Chern insulators *Nat. Commun.* **6** 8336
- [175] Cao M D, Cooper N R and Bhaseen M J 2015 Quantum quenches in Chern insulators *Phys. Rev. Lett.* **115** 236403
- [176] Bermudez A, Amico L and Martin-Delgado M A 2010 Dynamical delocalization of Majorana edge states by sweeping across a quantum critical point *New J. Phys.* **12** 055014
- [177] Perfetto E 2013 Dynamical formation and manipulation of Majorana fermions in driven quantum wires in contact with a superconductor *Phys. Rev. Lett.* **110** 087001
- [178] Sacramento P D 2014 Fate of Majorana fermions and Chern numbers after a quantum quench *Phys. Rev. E* **90** 032138
- [179] Kells G, Sen D, Slingerland J K and Vishveshwara S 2014 Topological blocking in quantum quench dynamics *Phys. Rev. B* **89** 235130
- [180] Wilson J H, Song J C W and Refael G 2016 Remnant geometric hall response in a quantum quench *Phys. Rev. Lett.* **117** 235302
- [181] Hu Y, Zoller P and Budich J C 2016 Dynamical buildup of a quantized hall response from nontopological states *Phys. Rev. Lett.* **117** 126803
- [182] Sun W *et al* 2018 Uncover topology by quantum quench dynamics *Phys. Rev. Lett.* **121** 250403
- [183] Cooper N R, Dalibard J and Spielman I B 2019 Topological bands for ultracold atoms *Rev. Mod. Phys.* **91** 015005
- [184] Iyer D and Foster M S 2020 Topological quantum control: edge currents via Floquet depinning of skyrmions in the $\nu = 0$ graphene quantum hall antiferromagnet *Phys. Rev. B* **101** 241403
- [185] Dong Y, Dong L, Gong M and Pu H 2015 Dynamical phases in quenched spin-orbit-coupled degenerate Fermi gas *Nat. Commun.* **6** 6103
- [186] Dzero M, Kirmani A A and Yuzbashyan E A 2015 Nonadiabatic dynamics of superfluid spin-orbit-coupled degenerate Fermi gas *Phys. Rev. A* **92** 053626
- [187] Stouten E, Claeys P W, Caux J-S and Gritsev V 2019 Integrability and duality in spin chains *Phys. Rev. B* **99** 075111
- [188] Shankar A, Yuzbashyan E A, Gurarie V, Zoller P, Bollinger J J and Rey A M 2022 Simulating dynamical phases of chiral $p + ip$ superconductors with a trapped ion magnet (arXiv:2204.05671)
- [189] Zabalo A and Yuzbashyan E A 2021 *Time Reversal Symmetry Protected Chaotic Fixed Point in the Quench Dynamics of a Topological p -Wave Superfluid*
- [190] Polkovnikov A, Sengupta K, Silva A and Vengalattore M 2011 Colloquium: nonequilibrium dynamics of closed interacting quantum systems *Rev. Mod. Phys.* **83** 863–83
- [191] Metzner W and Vollhardt D 1989 Correlated lattice fermions in $d = \infty$ dimensions *Phys. Rev. Lett.* **62** 324–7
- [192] Alet F and Laflorencie N 2018 Many-body localization: an introduction and selected topics *C. R. Phys.* **19** 498–525
- [193] Nandkishore R and Huse D A 2015 Many-body localization and thermalization in quantum statistical mechanics *Annu. Rev. Condens. Matter Phys.* **6** 15–38
- [194] Abanin D A, Altman E, Bloch I and Serbyn M 2019 Colloquium: many-body localization, thermalization, and entanglement *Rev. Mod. Phys.* **91** 021001

- [195] Parameswaran S A, Potter A C and Vasseur R 2017 Eigenstate phase transitions and the emergence of universal dynamics in highly excited states *Ann. Phys. (Berlin)* **529** 1600302
- [196] Carleo G, Becca F, Schiró M and Fabrizio M 2012 Localization and glassy dynamics of many-body quantum systems *Sci. Rep.* **2** 243
- [197] Smith A, Knolle J, Moessner R and Kovrizhin D L 2017 Absence of ergodicity without quenched disorder: from quantum disentangled liquids to many-body localization *Phys. Rev. Lett.* **119** 176601
- [198] Smith A, Knolle J, Kovrizhin D L and Moessner R 2017 Disorder-free localization in a translation-invariant quantum glass model *Phys. Rev. Lett.* **118** 266601
- [199] Yao N Y, Laumann C R, Cirac J I, Lukin M D and Moore J E 2016 Quasi-many-body localization in translation-invariant systems *Phys. Rev. Lett.* **117** 240601
- [200] Michailidis A A, Žnidarič M, Medvedyeva M, Abanin D A, Prosen T Ž and Papić Z 2018 Slow dynamics in translation-invariant quantum lattice models *Phys. Rev. B* **97** 104307
- [201] Lan Z, van Horssen M, Powell S and Garrahan J P 2018 Quantum slow relaxation and metastability due to dynamical constraints *Phys. Rev. Lett.* **121** 040603
- [202] van Horssen M, Levi E and Garrahan J P 2015 Dynamics of many-body localization in a translation-invariant quantum glass model *Phys. Rev. B* **92** 100305
- [203] Scherg S, Kohlert T, Sala P, Pollmann F, Madhusudhana B H, Bloch I and Aidelsburger M 2021 Observing non-ergodicity due to kinetic constraints in tilted Fermi–Hubbard chains *Nat. Commun.* **12** 4490
- [204] Iadecola T and Žnidarič M 2019 Exact localized and ballistic eigenstates in disordered chaotic spin ladders and the Fermi–Hubbard model *Phys. Rev. Lett.* **123** 036403
- [205] Vafek O, Regnault N and Andrei Bernevig B 2017 Entanglement of exact excited eigenstates of the Hubbard model in arbitrary dimension *SciPost Phys.* **3** 043
- [206] Turner C J, Michailidis A A, Abanin D A, Serbyn M and Papić Z 2018 Weak ergodicity breaking from quantum many-body scars *Nat. Phys.* **14** 745–9
- [207] Choi S, Turner C J, Pichler H, Ho W W, Michailidis A A, Papić Z, Serbyn M, Lukin M D and Abanin D A 2019 Emergent $su(2)$ dynamics and perfect quantum many-body scars *Phys. Rev. Lett.* **122** 220603
- [208] Ho W W, Choi S, Pichler H and Lukin M D 2019 Periodic orbits, entanglement, and quantum many-body scars in constrained models: matrix product state approach *Phys. Rev. Lett.* **122** 040603
- [209] Müller-Hartmann E 1989 Correlated fermions on a lattice in high dimensions *Z. Phys. B* **74** 507–12
- [210] Georges A, Kotliar G, Krauth W and Rozenberg M J 1996 Dynamical mean-field theory of strongly correlated fermion systems and the limit of infinite dimensions *Rev. Mod. Phys.* **68** 13–125
- [211] Georges A and Kotliar G 1992 Hubbard model in infinite dimensions *Phys. Rev. B* **45** 6479–83
- [212] Schmidt P and Monien H Nonequilibrium Dynamical Mean-Field Theory of a Strongly Correlated System
- [213] Freericks J K, Turkowski V M and Zlatić V 2006 Nonequilibrium dynamical mean-field theory *Phys. Rev. Lett.* **97** 266408
- [214] Aoki H, Tsuji N, Eckstein M, Kollar M, Oka T and Werner P 2014 Nonequilibrium dynamical mean-field theory and its applications *Rev. Mod. Phys.* **86** 779–837
- [215] Arrighoni E, Knap M and von der Linden W 2013 Nonequilibrium dynamical mean-field theory: an auxiliary quantum master equation approach *Phys. Rev. Lett.* **110** 086403
- [216] Joura A V, Freericks J K and Pruschke T 2008 Steady-state nonequilibrium density of states of driven strongly correlated lattice models in infinite dimensions *Phys. Rev. Lett.* **101** 196401
- [217] Scarlatella O, Clerk A A, Fazio R and Schiró M 2021 Dynamical mean-field theory for Markovian open quantum many-body systems *Phys. Rev. X* **11** 031018
- [218] Tsuji N, Oka T and Aoki H 2008 Correlated electron systems periodically driven out of equilibrium: Floquet + DMFT formalism *Phys. Rev. B* **78** 235124
- [219] Werner P, Oka T and Millis A J 2009 Diagrammatic Monte Carlo simulation of nonequilibrium systems *Phys. Rev. B* **79** 035320
- [220] Alexander Wolf F, McCulloch I P and Schollwöck U 2014 Solving nonequilibrium dynamical mean-field theory using matrix product states *Phys. Rev. B* **90** 235131
- [221] Tsuji N and Werner P 2013 Nonequilibrium dynamical mean-field theory based on weak-coupling perturbation expansions: application to dynamical symmetry breaking in the Hubbard model *Phys. Rev. B* **88** 165115
- [222] Eckstein M and Werner P 2010 Nonequilibrium dynamical mean-field calculations based on the noncrossing approximation and its generalizations *Phys. Rev. B* **82** 115115
- [223] Tsuji N, Eckstein M and Werner P 2013 Nonthermal antiferromagnetic order and nonequilibrium criticality in the Hubbard model *Phys. Rev. Lett.* **110** 136404
- [224] Sandri M and Fabrizio M 2013 Nonequilibrium dynamics in the antiferromagnetic Hubbard model *Phys. Rev. B* **88** 165113
- [225] Berges J, Rothkopf A and Schmidt J 2008 Nonthermal fixed points: effective weak coupling for strongly correlated systems far from equilibrium *Phys. Rev. Lett.* **101** 041603
- [226] Nowak B, Schole J and Gasenzer T 2014 Universal dynamics on the way to thermalization *New J. Phys.* **16** 093052
- [227] Prüfer M, Kunkel P, Strobel H, Lannig S, Linnemann D, Schmied C-M, Berges J, Gasenzer T and Oberthaler M K 2018 Observation of universal dynamics in a spinor Bose gas far from equilibrium *Nature* **563** 217–20
- [228] Erne S, Bücken R, Gasenzer T, Berges J and Schmiedmayer J 2018 Universal dynamics in an isolated one-dimensional Bose gas far from equilibrium *Nature* **563** 225–9
- [229] Picano A and Eckstein M 2021 Accelerated gap collapse in a slater antiferromagnet *Phys. Rev. B* **103** 165118
- [230] Stark M and Kollar M 2013 Kinetic description of thermalization dynamics in weakly interacting quantum systems (arXiv:1308.1610)
- [231] D’Alessio L, Kafri Y, Polkovnikov A and Rigol M 2016 From quantum chaos and eigenstate thermalization to statistical mechanics and thermodynamics *Adv. Phys.* **65** 239–362
- [232] Mallayya K, Rigol M and De Roeck W 2019 Prethermalization and thermalization in isolated quantum systems *Phys. Rev. X* **9** 021027
- [233] Balzer K, Alexander Wolf F, McCulloch I P, Werner P and Eckstein M 2015 Nonthermal melting of Néel order in the Hubbard model *Phys. Rev. X* **5** 031039
- [234] Trotzky S, Chen Y-A, Flesch A, McCulloch I P, Schollwöck U, Eisert J and Bloch I 2012 Probing the relaxation towards equilibrium in an isolated strongly correlated one-dimensional Bose gas *Nat. Phys.* **8** 325–30
- [235] Kollath C, Läuchli A M and Altman E 2007 Quench dynamics and nonequilibrium phase diagram of the Bose–Hubbard model *Phys. Rev. Lett.* **98** 180601
- [236] Rosch A, Rasch D, Binz B and Vojta M 2008 Metastable superfluidity of repulsive fermionic atoms in optical lattices *Phys. Rev. Lett.* **101** 265301
- [237] Eckstein M and Werner P 2011 Thermalization of a pump-excited Mott insulator *Phys. Rev. B* **84** 035122
- [238] Sensarma R *et al* 2010 Lifetime of double occupancies in the Fermi–Hubbard model *Phys. Rev. B* **82** 224302
- [239] Strohmaier N *et al* 2010 Observation of elastic doublon decay in the Fermi–Hubbard model *Phys. Rev. Lett.* **104** 080401
- [240] Morong W, Muleady S R, Kimchi I, Xu W, Nandkishore R M, Rey A M and DeMarco B 2021 Disorder-controlled

- relaxation in a three-dimensional Hubbard model quantum simulator *Phys. Rev. Res.* **3** L012009
- [241] Yang C N 1989 η pairing and off-diagonal long-range order in a Hubbard model *Phys. Rev. Lett.* **63** 2144–7
- [242] Li J and Eckstein M 2020 *Nonequilibrium Steady-State Theory of Photodoped Mott Insulators*
- [243] Murakami Y, Takayoshi S, Kaneko T, Sun Z, Golež D, Millis A J and Werner P 2021 *Emergent Nonequilibrium Phases in the Photo-Doped One-Dimensional Mott Insulator*
- [244] Kaneko T, Shirakawa T, Sorella S and Yunoki S 2019 Photoinduced η pairing in the Hubbard model *Phys. Rev. Lett.* **122** 077002
- [245] Peronaci F, Parcollet O and Schiró M 2020 Enhancement of local pairing correlations in periodically driven Mott insulators *Phys. Rev. B* **101** 161101
- [246] Tindall J, Schlawin F, Buzzi M, Nicoletti D, Coulthard J R, Gao H, Cavalleri A, Sentef M A and Jaksch D 2020 Dynamical order and superconductivity in a frustrated many-body system *Phys. Rev. Lett.* **125** 137001
- [247] Werner P, Tsuji N and Eckstein M 2012 Nonthermal symmetry-broken states in the strongly interacting Hubbard model *Phys. Rev. B* **86** 205101
- [248] Eckstein M, Kollar M and Werner P 2009 Thermalization after an interaction quench in the Hubbard model *Phys. Rev. Lett.* **103** 056403
- [249] Uhrig G S 2009 Interaction quenches of Fermi gases *Phys. Rev. A* **80** 061602
- [250] Schiró M and Fabrizio M 2010 Time-dependent mean field theory for quench dynamics in correlated electron systems *Phys. Rev. Lett.* **105** 076401
- [251] Eckstein M, Kollar M and Werner P 2010 Interaction quench in the Hubbard model: relaxation of the spectral function and the optical conductivity *Phys. Rev. B* **81** 115131
- [252] Gunnarsson O, Rohringer G, Schäfer T, Sangiovanni G and Toschi A 2017 Breakdown of traditional many-body theories for correlated electrons *Phys. Rev. Lett.* **119** 056402
- [253] Schäfer T, Rohringer G, Gunnarsson O, Ciuchi S, Sangiovanni G and Toschi A 2013 Divergent precursors of the Mott–Hubbard transition at the two-particle level *Phys. Rev. Lett.* **110** 246405
- [254] Greiner M, Mandel O, Hänsch T W and Bloch I 2002 Collapse and revival of the matter wave field of a Bose–Einstein condensate *Nature* **419** 51–4
- [255] Will S, Best T, Schneider U, Hackermüller L, Lühmann D-S and Bloch I 2010 Time-resolved observation of coherent multi-body interactions in quantum phase revivals *Nature* **465** 197–201
- [256] Schiró M and Fabrizio M 2011 Quantum quenches in the Hubbard model: time-dependent mean-field theory and the role of quantum fluctuations *Phys. Rev. B* **83** 165105
- [257] Sandri M, Schiró M and Fabrizio M 2012 Linear ramps of interaction in the fermionic Hubbard model *Phys. Rev. B* **86** 075122
- [258] Hofmann F, Eckstein M and Potthoff M 2016 Nonequilibrium self-energy functional approach to the dynamical Mott transition *Phys. Rev. B* **93** 235104
- [259] Behrmann M, Fabrizio M and Lechermann F 2013 Extended dynamic Mott transition in the two-band Hubbard model out of equilibrium *Phys. Rev. B* **88** 035116
- [260] Hamerla S A and Uhrig G S 2013 Dynamical transition in interaction quenches of the one-dimensional Hubbard model *Phys. Rev. B* **87** 064304
- [261] Tsuji N, Barnettler P, Aoki H and Werner P 2014 Nonequilibrium dynamical cluster theory *Phys. Rev. B* **90** 075117
- [262] Sciolla B and Biroli G 2010 Quantum quenches and off-equilibrium dynamical transition in the infinite-dimensional Bose–Hubbard model *Phys. Rev. Lett.* **105** 220401
- [263] Strand H U R, Eckstein M and Werner P 2015 Nonequilibrium dynamical mean-field theory for bosonic lattice models *Phys. Rev. X* **5** 011038
- [264] Brandt U and Mielsch C 1989 Thermodynamics and correlation functions of the Falicov–Kimball model in large dimensions *Z. Phys. B* **75** 365–70
- [265] Freericks J K and Zlatić V 2003 Exact dynamical mean-field theory of the Falicov–Kimball model *Rev. Mod. Phys.* **75** 1333–82
- [266] Eckstein M and Kollar M 2008 Nonthermal steady states after an interaction quench in the Falicov–Kimball model *Phys. Rev. Lett.* **100** 120404
- [267] Eckstein M and Werner P 2011 Damping of Bloch oscillations in the Hubbard model *Phys. Rev. Lett.* **107** 186406
- [268] Fotso H, Mikelsons K and Freericks J K 2014 Thermalization of field driven quantum systems *Sci. Rep.* **4** 4699
- [269] Galaiko V P 1972 Kinetic equations for relaxation processes in superconductors *JETP* **34** 203
Galaiko V P 1971 *Zh. Eksp. Teor. Fiz.* **61** 382 (Russian original)
- [270] Yang X *et al* 2018 Terahertz-light quantum tuning of a metastable emergent phase hidden by superconductivity *Nat. Mater.* **17** 586–91
- [271] Yang X, Vaswani C, Sundahl C, Mootz M, Luo L, Kang J H, Perakis I E, Eom C B and Wang J 2019 Lightwave-driven gapless superconductivity and forbidden quantum beats by terahertz symmetry breaking *Nat. Photon.* **13** 707–13
- [272] Cui T, Yang X, Vaswani C, Wang J, Fernandes R M and Orth P P 2019 Impact of damping on the superconducting gap dynamics induced by intense terahertz pulses *Phys. Rev. B* **100** 054504
- [273] Fausti D *et al* 2011 Light-induced superconductivity in a stripe-ordered cuprate *Science* **331** 189–91
- [274] Hu W *et al* 2014 Optically enhanced coherent transport in $\text{YBa}_2\text{Cu}_3\text{O}_{6.5}$ by ultrafast redistribution of interlayer coupling *Nat. Mater.* **13** 705–11
- [275] Mitrano M *et al* 2016 Possible light-induced superconductivity in K_3C_{60} at high temperature *Nature* **530** 461–4
- [276] Knap M, Babadi M, Refael G, Martin I and Demler E 2016 Dynamical Cooper pairing in nonequilibrium electron–phonon systems *Phys. Rev. B* **94** 214504
- [277] Kennes D M, Wilner E Y, Reichman D R and Millis A J 2017 Transient superconductivity from electronic squeezing of optically pumped phonons *Nat. Phys.* **13** 479–83
- [278] Chiriaco G, Millis A J and Aleiner I L 2018 Transient superconductivity without superconductivity *Phys. Rev. B* **98** 220510
- [279] Buča B, Tindall J and Jaksch D 2019 Non-stationary coherent quantum many-body dynamics through dissipation *Nat. Commun.* **10** 1730
- [280] Tindall J, Buča B, Coulthard J R and Jaksch D 2019 Heating-induced long-range η pairing in the Hubbard model *Phys. Rev. Lett.* **123** 030603
- [281] Matsunaga R *et al* 2014 Light-induced collective pseudospin precession resonating with Higgs mode in a superconductor *Science* **345** 1145–9
- [282] Tsuji N and Aoki H 2015 Theory of Anderson pseudospin resonance with Higgs mode in superconductors *Phys. Rev. B* **92** 064508
- [283] Cea T, Castellani C and Benfatto L 2016 Nonlinear optical effects and third-harmonic generation in superconductors: cooper pairs versus Higgs mode contribution *Phys. Rev. B* **93** 180507
- [284] Fläschner N *et al* 2018 Observation of dynamical vortices after quenches in a system with topology *Nat. Phys.* **14** 265–8
- [285] Landig R, Hruby L, Dogra N, Landini M, Mottl R, Donner T and Esslinger T 2016 Quantum phases from competing short- and long-range interactions in an optical lattice *Nature* **532** 476–9

- [286] Landini M, Dogra N, Kroeger K, Hruby L, Donner T and Esslinger T 2018 Formation of a spin texture in a quantum gas coupled to a cavity *Phys. Rev. Lett.* **120** 223602
- [287] Kroeze R M, Guo Y, Vaidya V D, Keeling J and Lev B L 2018 Spinor self-ordering of a quantum gas in a cavity *Phys. Rev. Lett.* **121** 163601
- [288] Kroeze R M, Guo Y and Lev B L 2019 Dynamical spin-orbit coupling of a quantum gas *Phys. Rev. Lett.* **123** 160404
- [289] Baden M P, Arnold K J, Grimsmo A L, Parkins S and Barrett M D 2014 Realization of the Dicke model using cavity-assisted Raman transitions *Phys. Rev. Lett.* **113** 020408
- [290] Baumann K, Guerlin C, Brennecke F and Esslinger T 2010 Dicke quantum phase transition with a superfluid gas in an optical cavity *Nature* **464** 1301
- [291] Ritsch H, Domokos P, Brennecke F and Esslinger T 2013 Cold atoms in cavity-generated dynamical optical potentials *Rev. Mod. Phys.* **85** 553–601
- [292] Klinder J, Keßler H, Wolke M, Mathey L and Hemmerich A 2015 Dynamical phase transition in the open Dicke model *Proc. Natl Acad. Sci.* **112** 3290–5
- [293] Yang H-X *et al* 2019 Observation of dynamical quantum phase transitions in a spinor condensate *Phys. Rev. A* **100** 013622
- [294] Tian T, Yang H-X, Qiu L-Y, Liang H-Y, Yang Y-B, Xu Y and Duan L-M 2020 Observation of dynamical quantum phase transitions with correspondence in an excited state phase diagram *Phys. Rev. Lett.* **124** 043001
- [295] Rey A M *et al* 2014 Probing many-body interactions in an optical lattice clock *Ann. Phys.* **340** 311
- [296] Fuchs J N, Gangardt D M and Laloë F 2002 Internal state conversion in ultracold gases *Phys. Rev. Lett.* **88** 230404
- [297] Albiez M, Gati R, Fölling J, Hunsmann S, Cristiani M and Oberthaler M K 2005 Direct observation of tunneling and nonlinear self-trapping in a single bosonic Josephson junction *Phys. Rev. Lett.* **95** 010402
- [298] Anker T, Albiez M, Gati R, Hunsmann S, Eiermann B, Trombettoni A and Oberthaler M K 2005 Nonlinear self-trapping of matter waves in periodic potentials *Phys. Rev. Lett.* **94** 020403
- [299] Reinhard A, Riou J-F, Zundel L A, Weiss D S, Li S, Rey A M and Hipolito R 2013 Self-trapping in an array of coupled 1D Bose gases *Phys. Rev. Lett.* **110** 033001
- [300] Levy S, Lahoud E, Shomroni I and Steinhauer J 2007 The a.c. and d.c. Josephson effects in a Bose-Einstein condensate *Nature* **449** 579
- [301] Abbarchi M *et al* 2013 Macroscopic quantum self-trapping and Josephson oscillations of exciton polaritons *Nat. Phys.* **9** 275
- [302] Chin C, Grimm R, Julienne P and Tiesinga E 2010 Feshbach resonances in ultracold gases *Rev. Mod. Phys.* **82** 1225–86
- [303] Deutsch C *et al* 2010 Spin self-rephasing and very long coherence times in a trapped atomic ensemble *Phys. Rev. Lett.* **105** 020401
- [304] Solaro C, Bonnin A, Combes F, Lopez M, Alauze X, Fuchs J N, Piéchon F and Pereira Dos Santos F 2016 Competition between spin echo and spin self-rephasing in a trapped atom interferometer *Phys. Rev. Lett.* **117** 163003
- [305] Piéchon F, Fuchs J N and Laloë F 2009 Cumulative identical spin rotation effects in collisionless trapped atomic gases *Phys. Rev. Lett.* **102** 215301
- [306] Bernien H *et al* 2017 Probing many-body dynamics on a 51-atom quantum simulator *Nature* **551** 579–84
- [307] Ebadi S *et al* 2021 Quantum phases of matter on a 256-atom programmable quantum simulator *Nature* **595** 227–32
- [308] Serbyn M, Abanin D A and Papić Z 2021 Quantum many-body scars and weak breaking of ergodicity *Nat. Phys.* **17** 675–85
- [309] Kohlert T, Scherg S, Sala P, Pollmann F, Madhusudhana B H, Bloch I and Aidelsburger M 2021 Experimental realization of fragmented models in tilted Fermi-Hubbard chains (arXiv:2106.15586)
- [310] Guardado-Sanchez E, Spar B M, Schauss P, Belyansky R, Young J T, Bienias P, Gorshkov A V, Iadecola T and Bakr W S 2021 Quench dynamics of a Fermi gas with strong nonlocal interactions *Phys. Rev. X* **11** 021036
- [311] He P, Perlin M A, Muleady S R, Lewis-Swan R J, Hutson R B, Ye J and Rey A M 2019 Engineering spin squeezing in a 3D optical lattice with interacting spin-orbit-coupled fermions *Phys. Rev. Res.* **1** 033075
- [312] Foss-Feig M, Niroula P, Young J T, Hafezi M, Gorshkov A V, Wilson R M and Maghrebi M F 2017 Emergent equilibrium in many-body optical bistability *Phys. Rev. A* **95** 043826
- [313] Lewis-Swan R J, Muleady S R, Barberena D, Bollinger J J and Rey A M 2021 Characterizing the dynamical phase diagram of the Dicke model via classical and quantum probes *Phys. Rev. Res.* **3** L022020
- [314] Gross C and Bloch I 2017 Quantum simulations with ultracold atoms in optical lattices *Science* **357** 995–1001